FACIAL EXPRESSION RECOGNITION AND TRACKING BASED ON DISTRIBUTED LOCALLY LINEAR EMBEDDING AND EXPRESSION MOTION ENERGY

YANG YONG

(B.Eng., Xian Jiaotong University)

A THESIS SUBMITTED

FOR THE DEGREE OF MASTER OF ENGINEERING

DEPARTMENT OF ELECTRICAL AND COMPUTER ENGINEERING

NATIONAL UNIVERSITY OF SINGAPORE

2006

Acknowledgements

First and foremost, I would like to take this opportunity to express my sincere gratitude to my supervisors, Professor Shuzhi Sam Ge and Professor Lee Tong Heng, for their inspiration, encouragement, patient guidance and invaluable advice, especially for their selflessly sharing their invaluable experiences and philosophies, through the process of completing the whole project.

I would also like to extend my appreciation to Dr Chen Xiangdong, Dr Guan Feng, Dr Wang Zhuping, Mr Lai Xuecheng, Mr Fua Chengheng, Mr Yang Chenguang, Mr Han Xiaoyan and Mr Wang Liwang for their help and support.

I am very grateful to National University of Singapore for offering the research scholarship.

Finally, I would like to give my special thanks to my parents, Yang Guangping and Dong Shaoqin, my girl friend Chen Yang and all members of my family for their continuing support and encouragement during the past two years.

Yang Yong

September 2006

Contents

Summary

Facial expression plays an important role in our daily activities. It can provide sensitive and meaningful cues about emotional response and plays a major role in human interaction and nonverbal communication. Facial expression analysis and recognition presents a significant challenge to the pattern analysis and human-machine interface research community. This research aims to develop an automated and interactive computer vision system for human facial expression recognition and tracking based on the facial structure features and movement information. Our system utilizes a subset of Feature Points (FPs) for describing the facial expressions which is supported by the MPEG-4 standard. An unsupervised learning algorithm, Distributed Locally Linear Embedding (DLLE), is introduced to recover the inherent properties of scattered data lying on a manifold embedded in high-dimensional input facial images. The selected person-dependent facial expression images in a video are classified using DLLE. We also incorporate facial expression motion energy to describe the facial muscle's tension during the expressions for person-independent tracking. It takes advantage of the optical flow method which tracks the feature points' movement information. By further considering

different expressions' temporal transition characteristics, we are able to pin-point the actual occurrence of specific expressions with higher accuracy. A 3D realistic interactive head model is created to derive multiple virtual expression animations according to the recognition results. A virtual robotic talking head for human emotion understanding and intelligent human computer interface is realized.

List of Tables

List of Figures

Chapter 1

Introduction

Facial expression plays an important role in our daily activities. The human face is a rich and powerful source full of communicative information about human behavior and emotion. The most expressive way that humans display emotions is through facial expressions. Facial expression includes a lot of information about human emotion. It is one of the most important carriers of human emotion, and it is a significant way for understanding human emotion. It can provide sensitive and meaningful cues about emotional response and plays a major role in human interaction and nonverbal communication. Humans can detect faces and interpret facial expressions in a scene with little or no effort.

The origins of facial expression analysis go back into the 19th century, when Darwin proposed the concept of universal facial expressions in human and animals. In his book, "*The Expression of the Emotions in Man and Animals*" [1], he noted:

"*...the young and the old of widely different races, both with man and animals, express the same state of mind by the same movements.*"

In recent years there has been a growing interest in developing more intelligent interface between humans and computers, and improving all aspects of the interaction. This emerging field has attracted the attention of many researchers from several different scholastic tracks, i.e., computer science, engineering, psychology, and neuroscience. These studies focus not only on improving computer interfaces, but also on improving the actions the computer takes based on feedback from the user. There is a growing demand for multi-modal/media human computer interface (HCI). The main characteristics of human communication are: multiplicity and multi-modality of communication channels. A channel is a communication medium while a modality is a sense used to perceive signals from the outside world. Examples of human communication channels are: auditory channel that carries speech, auditory channel that carries vocal intonation, visual channel that carries facial expressions, and visual channel that carries body movements. Recent advances in image analysis and pattern recognition open up the possibility of automatic detection and classification of emotional and conversational facial signals. Automating facial expression analysis could bring facial expressions into man-machine interaction as a new modality and make the interaction tighter and more efficient. Facial expression analysis and recognition are essential for intelligent and natural HCI, which presents a significant challenge to the pattern analysis and human-machine interface research community. To realize natural and harmonious HCI, computer must have the capability for understanding human emotion and intention effectively. Facial expression recognition is a problem which must be overcome for future prospective application such as: emotional interaction, interactive video, synthetic face animation, intelligent home robotics, 3D games and entertainment. An automatic facial expression analysis system mainly include three important parts: face detection, facial feature points extraction and facial expression classification.

1.1 Facial Expression Recognition Methods

The development of an automated system which can detect faces and interpret facial expressions is rather difficult. There are several related problems that need to be solved: detection of an image segment as a face, extraction of the facial expression information, and classification of the expression into different emotion categories. A system that performs these operations accurately and in real-time would be a major step forward in achieving a human-like interaction between the man and computer. Fig. 1.1 shows the basic framework of facial expression recognition which includes the basic problems need to be solved and different approaches to solve these problem.

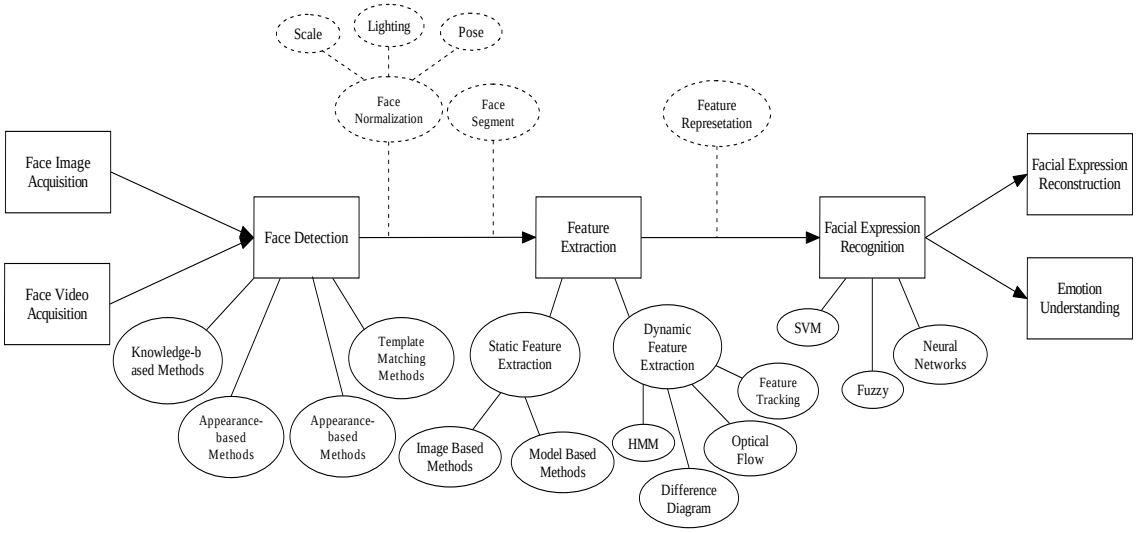

Figure 1.1: The basic facial expression recognition framework.

1.1.1 Face Detection Techniques

In various approaches that analyze and classify the emotional expression of faces, the first task is to detect the location of face area from a image. Face detection

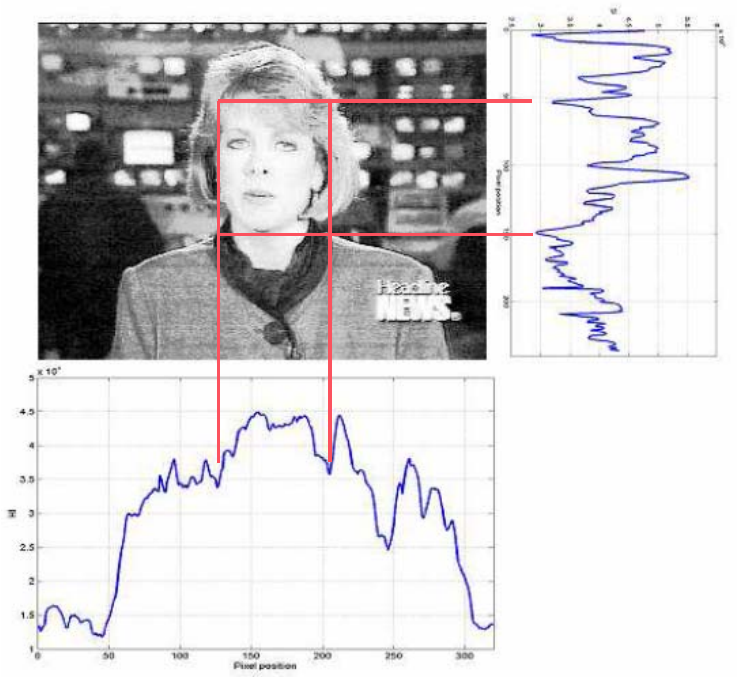

Figure 1.2: The horizontal and vertical signature used in [2]

is to determine whether or not there are any faces in a given arbitrary image. If there is any faces presented, determine the location and extent of each face in the image. The variations of the lighting directions, head pose and ordinations, facial expressions, facial occlusions, image orientation and image conditions make face detection from an image a challenging task.

Face detection can be viewed as a two-class recognition problem in which an image region is classified as being either a face or a non-face. Detecting face in a single image can be classified into the following approaches.

Knowledge-based methods These methods are rule-based that are derived from the researcher's knowledge what constitutes a typical face. A set of simple rules are predefined, e.g. the symmetry of eyes and the relative distance

between nose and eyes. The facial features are extracted and the face candidates are identified subsequently based on the predefined rules. In 1994, Yang and Huang presented a rule-based location method with a hierarchical structure consisting of three levels [3]. Kotropoulos and Pitas [2] presented a rule-based localization procedure which is similar to [3]. The facial boundary are located using the horizontal and vertical projections [4]. Fig. 1.2 shows an example where the boundaries of the face correspond to the local minimum of the histogram.

Feature invariant methods These approaches attempt to find out the facial structure features that are invariant to pose, viewpoint or lighting conditions. The human skin color has been widely used as an important cue and proven to be an effective feature for face area detection. The specific facial features include eyebrows, eyes, nose and mouth can be extracted using edge detectors. Sirohey presented a facial localization method which makes use of the edge map and generates an ellipse contour to fit the boundary of face [5]. Graf et al. proposed a method to locate the faces and facial features using gray scale images [6]. The histogram peaks and width are utilized to perform adoptive image segmentation by computing an adoptive threshold. The threshold is used to generate binarized images and connected area that are identified to locate the candidate facial features. These areas are combined and evaluated with classifier later to determine where the face is located. Sobottka and Pitas presented a method to locate skin-like region using shape and color information to perform color segmentation in the HSV color space [7]. By using the region growth method, the connected components are determined. For each connected components, the best-fit ellipse is computed and if it fits well, it is selected as a face candidate.

Template matching methods These methods detect the face area by computing the correlation between the standard patten template of a face and an input image. The standard face pattern is usually predefined or parameterized manually. The template is either independent for the eyes, nose and mouth, or for the entire face image. These methods include the predefined templates and deformable templates. Active Shape Model (ASM) are statistical models of the shape of objects which iteratively deform to fit to an example of the object in a new image [8]. The shapes are constrained by a statistical shape model to vary only in ways seen in a training set of labelled examples. Active Appearance Model (AAM) which was developed by Gareth Edwards et al. establishes a compact parameterizations of object variability to match any class of deformable objects [9]. It combines shape and gray-level variation in a single statistical appearance model. The parameter are learned from a set of training data by estimating a set of latent variables.

Appearance based methods The models used in these methods are learned from a set of training examples. In contrast to template matching, these methods rely on statistics analysis and machine learning to discover the characteristics of face and non-face images. The learned characteristics are consequently used for face detection in the form of distribution models or discriminant functions. Dimensionality reduction is an important aspect and usually carried out in these methods. These methods include: Eigenface [10], Neural Network [11], Supporting Vector Machine(SVM) [12], and Hidden Markov Model [13]. Most of these approaches can be viewed in a probabilistic framework using Bayesian or maximum likelihood classification method. Finding the discriminate functions between face and non-face classes has also been used in the appearance based methods. Image patterns are projected onto a low-dimensional space or using multi-layer neural networks to form a

nonlinear decision surface.

Face detection is the preparatory step for the following work. For example, it can fix a range of interests, decrease the searching range and initial approximation area for the feature selection. In our system, we assume and only consider the situation that there is only one face contained in one image. The face takes up a significant area in the image. Although the detection of multiple faces in one image is realizable, due to the image resolution, head pose variation, occlusion and other problems, it will greatly increase the difficulty of detecting facial expression if there are multiple faces in one image. The facial features will be more prominent if one face takes up a large area of image. The face location for expression recognition mainly deal with two problems: the head pose variation and the illumination variation since they can greatly affect the following feature extraction. Generally, facial image needs to be normalized first to remove the effect of head pose and illumination variation. The ideal head pose is that the facial plane is parallel to the project image. The obtained image from such pose has the least facial distortion. The illumination variation can greatly affect the brightness of the image and make it more difficult to extract features. Using a fixed lighting can avoid the illumination problem, but affect the robustness of the algorithm. The most common method to remove the illumination variation is using Gabor Filter on the input images [14]. Besides, there are some other work for removing the ununiformity of facial brightness caused by illumination and variation of reflection coefficient of different facial parts [15].

1.1.2 Facial Feature Points Extraction

The goal of facial feature points detection is to obtain the facial feature's variety and the face's movements. Under the assumption that there is only one face in an image, feature points extraction includes detecting the presence and locating of features, such as eyes, nose, nostrils, eyebrow, mouth, lips, ears, etc [16]. The face

feature detection method can be classified according to whether the operation is based on global movements or local movements. It could also be classified according to whether the extraction is based on the facial features's transformation or the whole face muscle's movement. Until now, there is no uniform solution. Each method has its advantages and is operated under certain conditions.

The facial features can be treated as permanent and temporary. The permanent ones are unremovable features existing on face. They will transform wrt. the face muscle's movement, e.g. the eyes, eyebrow, mouth and so on. The temporary features mainly include the temporary wrinkles. They will appear with the movement of the face and disappear when the movement is over. They are not constant features on the face.

The method based on global deformation is to extract all the permanent and temporary information. Most of the time, it is required to do background substraction to remove the effect of the background. The method based on local deformation is to decompose the face into several sub areas and find the local feature information. Feature extraction is done in each individual sub areas independently. The local features can be represented using Principal Components Analysis(PCA) and described using the intensity profiles or gradient analysis.

The method based on the image feature extraction does not depend on the priority knowledge. It extracts the features only based on the image information. It is fast and simple, but lack robustness and reliability. The method need to model the face features first according to priority knowledge. It is more complex and time consuming, but more reliable. This feature extraction method can be further divided according to the dimension of the model. The method is based on 2D information

to extract the features without considering the depth of the object. The method is based on 3D information considering the geometry information of the face. There are two typical 3D face models: face muscle model [17] and face movement model [18]. 3D face model is more complicated and time consuming compared to 2D face model. It is the muscle's movements that result in the appearance change of face, and the change of appearance is the reflection of muscle's movement.

Face movement detection method attempted to extract the displacement relative information from two adjacent temporal frames. These information is obtained by comparing the current facial expression and the neutral face. The neutral face is necessary for extracting the alteration information, but not always needed in the feature movement detection method. Most of the reference face used in this method is the previous frame. The classical optical flow method is to use the correlation of two adjacent frames for estimation [19]. The movement detection method can be only used in the video sequence while the deformation extraction can be adopted in either a single image or a video sequence. But the deformation extraction method could not get the detailed information such as each pixel's displacement information while the method based on facial movement can extract these information much easier.

Face deformation includes two aspects: the changes of face shape and texture. The change of texture will cause the change of gradient of the image. Most of the methods based on the shape distortion extract these gradient change caused by different facial expressions. High pass filter and Gabor filter [20] can be adopted to detect such gradient information. It has been proved that the Gabor filter is a powerful method used in image feature extraction. The texture could be easily affected by the illumination. The Gabor filter can remove the illumination variation effects

[21]. Active Appearance Model(AAM) were developed by Gareth Edwards et al. [9] which establishes a compact parameterizations of object variability to match any of a class of deformable objects. It combines shape and gray-level variation in a single statistical appearance model. The parameters learned are from a set of training data by estimating a set of latent variables.

In 1995, Essa et al. proposed two methods using dynamic model and motion energy to classify facial expressions [22]. One is based on the physical model where expression is classified by comparison of estimated muscle activations. The other is to use the spacial-temporal motion energy templates of the whole face for each facial expression. The motion energy is converted from the muscles activations. Both methods show substantially great recognition accuracy. However, the author did not give a clear definition of the motion energy. At the same time, they only used the spatial information in their recognition pattern. By considering different expressions' temporal transition characteristics, a higher recognition accuracy could be achieved.

1.1.3 Facial Expression Classification

According to the psychological and neurophysiological studies, there are six basic emotions-happiness, sadness, fear, disgust, surprise, and anger as shown in Fig. 1.3. Each basic emotion is associated with one unique facial expression.

Since 1970s, Ekman and Friesen have performed extensive studies on human facial expressions and developed an anatomically oriented coding system for describing all visually distinguishable facial movements, called the facial action coding system (FACS) [23]. It is used for analyzing and synthesizing facial expression based

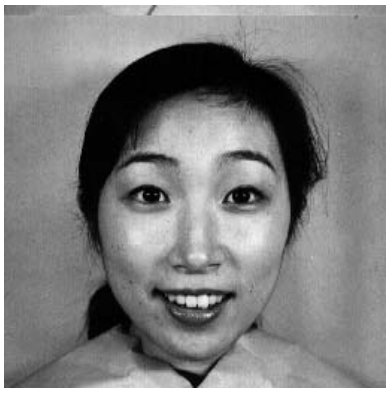

(a) happiness

(b) sadness

(c) fear

(d) disgust

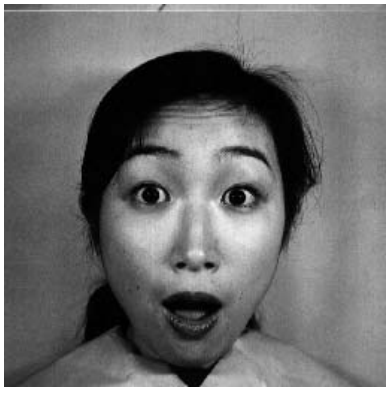

(e) surprise

(f) anger

Figure 1.3: Six universal facial expressions [14].

on 46 Action Units (AU) which describe basic facial movements. Each AU may correspond to several muscles' activities which are composed to a certain facial expression. FACS are used manually to describe the facial expressions, using still images when the facial expression is at its apex state. The FACS model has recently inspired interests to analyze facial expressions by tracking facial features or measuring the amount of facial movement. Its derivation of facial animation and definition parameters has been adopted in the framework of the ISO MPEG-4 standard. The MPEG-4 standardization effort grew out of the wish to create a video-coding standard more capable than previous versions [24].

Facial expression classification mainly deal with the task of categorizing active and spontaneous facial expressions to extract information of the underlying human emotional states. Based on the face detection and feature extraction results, the analysis of the emotional expression can be carried out. A large number of methods have been developed for facial expression analysis. These approaches could be divided into two main categories: target oriented and gesture oriented. The target oriented approaches [25, 26, 27] attempt to infer the human emotion and classify the facial expression from one single image containing one typical facial expression. The gesture oriented methods [28, 29] make use of the temporal information from a sequence of facial expression motion images. In particular, transitional approaches attempt to compute the facial expressions from the facial neural condition and expressions at the apex. Fully dynamic techniques extract facial emotions through a sequence of images.

The target oriented approaches can be subdivided into template matching methods and rule based methods. Tian et al. developed an anatomic face analysis system based on both permanent and transient facial features [30]. Multistate

facial component models such as lips and eyes are proposed for tracking. Template matching and neural networks are used in the system to recognize 16 AUs in nearly frontal-view face image sequences. Pantic et al. developed an automatic system to recognize facial gestures in static, frontal and profile view face images [31]. By making use of the action unions (AUs), a rule-based method is adopted which achieves 86 % recognition rate.

Facial expression is a dynamic process. How to fully make use of the dynamic information can be critical to the recognition result. There is a growing argument that the temporal information is a critical factor in the interpretation of facial expressions [32]. Essa et al. examined the temporal pattern of different expressions but did not account for temporal aspects of facial motion in their recognition feature vector [33]. Roivainen et al. developed a system using a 3D face mesh based on the FACS model [34]. The motion of the head and facial expressions is estimated in model-based facial image coding. An algorithm for recovering rigid and nonrigid motion of the face was derived based on two, or more frames. The facial images are analyzed for the purpose of re-synthesizing a 3D head model. Donato et al. used independent component analysis (IDA), optical flow estimation and Gabor wavelet representation methods that achieved 95.5% average recognition rate as reported in [35].

In transitional approaches, its focus is on computing motion of either facial muscles or facial features between neutral and apex instances of a face. Mase described two approaches–top-down and bottom-up–based on facial muscle's motion [36]. In the top-down method, the facial image is divided into muscle units that correspond to the AUs defined in FACS. Optical flow is computed within rectangles that include these muscle units, which in turn can be related to facial expressions. This

approach relies heavily on locating rectangles containing the appropriate muscles, which is a difficult image analysis problem. In the bottom-up method, the area of the face is tessellated with rectangular regions over which optical flow feature vectors are computed; a 15-dimensional feature space is considered, based on the mean and variance of the optical flow. Recognition of expressions is then based on k-nearest-neighbor voting rule.

The fully dynamic approaches make use of temporal and spatial information. The methods using both temporal and spatial are called spatial-time methods while the methods only using the spatial information are called spatial methods.

Optical flow approach is widely adopted using the dense motion fields computed frame by frame. It falls into two classes: global optical flow and local optical flow methods. The global method can extract information of the whole facial region's movements. However, it is computationally intensive and sensitive to the continuum of the movements. The local optical flow method can improve the speed by only computing the motion fields in selected regions and directions. The Lucas-Kanade optical flow algorithm [37], is capable of following and recovering the facial points lost due to lighting variations, rigid or non-rigid motion, or (to a certain extent) change of head orientation. It can achieve high efficiency and tracking accuracy.

In feature tracing approach, it could not track each pixel's movement like optical flow; motions are estimated only over a selected set of prominent features in the face image. Each image in the video sequence is first processed to detect the prominent facial features, such as edges, eyes, brows and mouth. The analysis of the image motion is carried out subsequently, in particular, tracked by Lucas-Kanade

algorithm. Yacoob used the local parameters to model the mouth, nose, eyebrows and eyelids and used dense sequences to capture expressions over time [28]. It was based on qualitative tracking of principal regions of the face and flow computation at high intensity gradient points.

Neural networks is a typical spatial method. It takes the whole raw image, or processed image such as: Gabor filtered, or eigen-image: such as PCA and ICA, as the input of the network. Most of the time, it is not easy to train the neural network for a good result.

Hidden markov models (HMM) is also used to extract facial feature vectors for its ability to deal with time sequences and to provide time scale invariance, as well as its learning capabilities. Ohya et al. assigned the condition of facial muscles to a hidden state of the model for each expression and used the wavelet transform to extract features from facial images [29]. A sequence of feature vectors were obtained in different frequency bands of the image, by averaging the power of these bands in the areas corresponding to the eyes and the mouth. Some other work also employ HMM to design classifier which can recognize different facial expressions successfully [38, 39].

1.2 Motivation of Thesis

The objective of our research is to develop an automated and interactive computer vision system for human facial expression recognition and tracking based on the facial structure features and movement information. Recent advances in the image processing and pattern analysis open up the possibility of automatic detection and classification of emotional and conversational facial signals. Most of the previous

work on the spatio-temporal analysis for facial expression understanding, however, suffer the following shortcomings:

- The facial motion information is obtained mostly by computing holistic dense flow between successive image frames. However, dense flow computing is quite time-consuming.

- Most of these technologies can not respond in real-time to the facial expressions of a user. The facial motion pattern has to be trained offline, whereas the trained model limits its reliability for realistic applications since facial expressions involve great interpersonal variations and a great number of possible facial AU combinations. For spontaneous behavior, the facial expressions are particularly difficult to be segmented by a neutral state in an observed image sequence.

- The approaches do not consider the intensity scale of the different facial expressions. Each individual has his/her own maximal intensity of displaying a particular facial action. A better description about the facial muscles's tension is needed.

- Facial expression is a dynamic processes. Most of the current technics adopt the facial texture information as the vectors for further recognition [8], or combined with the facial shape information [9]. There are more information stored in the facial expression sequence compared to the facial shape information. Its temporal information can be divided into three discrete expression states in an expression sequence: the beginning, the peak, and the ending of the expression. However, the existing approaches do not measure the facial movement itself and are not able to model the temporal evolution and the momentary intensity of an observed facial expression, which are indeed more informative in human behavior analysis.

- There is usually a huge amount of information in the captured images, which makes it difficult to analyze the human facial expressions. The raw data, facial expression images, can be viewed as that they define a manifold in the high-dimensional image space, which can be further used for facial expression analysis. Therefore, dimension reduction is critical for analyzing the images, to compress the information and to discover compact representations of variability.

- A facial expression consists of not only its temporal information, but also a great number of AU combinations and transient cues. The HMM can model uncertainties and time series, but it lacks the ability to represent induced and nontransitive dependencies. Other methods, e.g., NNs, lack the sufficient expressive power to capture the dependencies, uncertainties, and temporal behaviors exhibited by facial expressions. Spatio-temporal approaches allow for facial expression dynamics modeling by considering facial features extracted from each frame of a facial expression video sequence.

Compared with other existing approaches on facial expression recognition, the proposed method enjoys several favorable properties which overcome these shortcomings:

- Do not need to compute the holistic dense flow but rather after the key facial features are captured, optical flow are computed just for these features.

- One focus of our work is to address problems with previous solutions of their slowness and requirement for some degree of manual intervention. Automatically face detection and facial feature extraction are realized. Real-time processing for person-independent recognition are implemented in our system.

- Facial expression motion energy are defined to describe the individual's facial muscle's tension during the expressions for person independent tracking. It is proposed by analyzing different facial expression's unique spacial-temporal pattern.
- To compress the information and to discover compact representations, we proposed a new Distributed Locally Linear Embedding (DLLE) to discover the inherent properties of the input data.

Besides, there are several other characters in our system.

- Only one web camera is utilized
- Rigid head motions allowed.
- Variations in lighting conditions allowed
- Variation of background allowed

Our facial expression recognition research is conducted based on the following assumptions:

Assumption 1. *Using only vision camera, one can only detect and recognize the shown emotion that may or may not be the personal true emotions. It is assumed that the subject shows emotions through facial expressions as a mean to express emotion.*

Assumption 2. *Theories of psychology claim that there is a small set of basic expressions [23], even if it is not universally accepted. A recent cross-cultural study confirms that some emotions have a universal facial expression across the cultures and the set proposed by Ekman [40] is a very good choice. Six basic emotions-happiness, sadness, fear, disgust, surprise, and anger are considered in our research. Each basic emotion is assumed associated with one unique facial expression for each person.*

Assumption 3. *There is only one face contained in the captured image. The face takes up a significant area in the image. The image resolution should be sufficiently large to facilitate feature extraction and tracking.*

1.3 Thesis Structure

1.3.1 Framework

The objective of the facial recognition is for human emotion understanding and intelligent human computer interface. Our system is based on both deformation and motion information. Fig. 1.4 shows the framework of our recognition system. The structure of our system can be separated into four main parts. It starts with the facial image acquisition and ends with 3D facial expression animation.

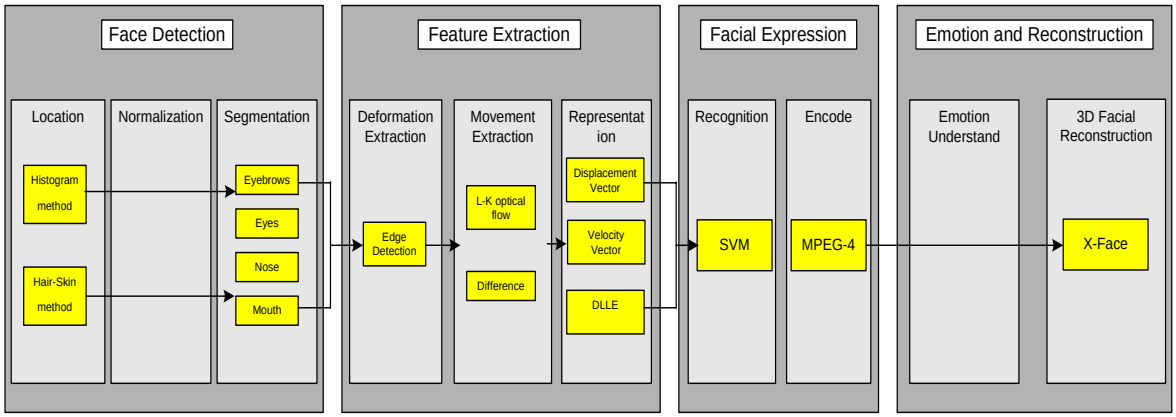

Figure 1.4: Overview of the system framework.

Static analysis

- Face detection and facial feature extraction. The facial image is obtained from a web camera. Robust and automated face detection system is carried out for the segmentation of face region. Facial feature extraction

include locating the position and shape of the eyebrows, eyes, nose, mouth, and extracting features related to them in a still image of human face. Image analysis techniques are utilized which can automatically extract meaningful information from facial expression motion without manual operation to construct feature vectors for recognition.

- Dimensionality reduction. In this stage, the dimension of the motion curve is reduced by analyzing with our proposed Distributed Locally Linear Embedding (DLLE). The goal of dimensionality reduction is to obtain a more compact representation of the original data, a representation that preservers all the information for further decision making.
- Perform classification using SVM. Once the facial data are transformed into a low-dimensional space, SVM is employed to classify the input facial pattern image into various emotion category.

Dynamic analysis

- The process is carried out using one web camera in real-time. It utilize the dynamics of features to identify expressions.
- Facial expression motion energy. It is used to describe the facial muscle's tension during the expressions for person-independent tracking.

3D virtual facial animation

- A 3D facial model is created based on MPEG-4 standard to derive multiple virtual character expressions in response to the user's expression.

1.3.2 Thesis Organization

The remainder of this thesis is organized as follows:

In Chapter 2, face detection and facial features extraction methods are discussed. Face detection can fix a range of interests, decrease the searching range and initial approximation area for the feature selection. Two methods, using vertical and horizontal projections and skin-hair information, are conducted to automatically detect and locate face area. A subset of Feature Points (FPs) is utilized in our system for describing the facial expressions which is supported by the MPEG-4 standard. Facial feature are extracted using deformable templates to get precise positions.

In Chapter 3, an unsupervised learning algorithm, distributed locally linear embedding (DLLE), is introduced which can recover the inherent properties of scattered data lying on a manifold embedded in high-dimensional input facial images. The input high-dimensional facial expression images are embeded into a low-dimensional space while the intrinsic structures are maintained and main characteristics of the facial expression are kept.

In Chapter 4, we propose facial expression motion energy to describe the facial muscle's tension during the expressions for person independent tracking. The facial expression motion energy is composed of potential energy and kinetic energy. It takes advantage of the optical flow method which tracks the feature points' movement information. For each expression we use the typical patterns of muscle actuation, as determined by a detailed physical analysis, to generate the typical pattern of motion energy associated with each facial expression. By further considering different expressions' temporal transition characteristics, we are able to pinpoint the actual occurrence of specific expressions with higher accuracy.

In Chapter 5, both static person dependent and dynamic person independent facial

expression recognition methods are discussed. For the person dependent recognition, we utilize the similarity of facial expressions appearance in low-dimensional embedding to classify different emotions. This method is based on the observation that facial expression images define a manifold in the high-dimensional image space, which can be further used for facial expression analysis. For the person independent facial expression classification, facial expression energy can be used by adjusting the general expression pattern to a particular individual according to the individual's successful expression recognition results.

In Chapter 6, a 3D virtual interactive expression model is created and applied into our face recognition and tracking system to derive multiple realistic character expressions. The 3D avatar model is parameterized according to the MPEG-4 facial animation standard. Realistic 3D virtual expressions are animated which can follow the object's facial expression.

In Chapters 7 and 8, we present the experimental results with our system and the conclusion of this thesis respectively.

Chapter 2

Face Detection and Feature Extraction

Human face detection has been researched extensively over the past decade, due to the recent emergence of applications such as security access control, visual surveillance, content-based information retrieval, and advanced human-to-computer interaction. It is also the first task performed in a face recognition system. To ensure good results in the subsequent recognition phase, face detection is a crucial procedure. In the last ten years, face and facial expression recognition have attracted much attention, though they truly have been studied for more than 20 years by psychophysicists, neuroscientists and engineers. Many research demonstrations and commercial applications have been developed from these efforts. The first step of any face processing system is to locate all faces that are present in a given image. However, face detection from a single image is a challenging task because of the high degree of spatial variability in scale, location and pose (rotated, frontal, profile). Facial expression, occlusion and lighting conditions also change the overall appearance of faces, as described in reference [41].

To build fully-automated systems that analyze the information contained in face

images, robust and efficient face detection algorithms are required. Such a problem is challenging, because faces are non-rigid objects that have a high degree of variability in size, shape, color and texture. Therefore, to obtain robust automated systems, one must be able to detect faces within images in an efficient and highly reproducible manner. In reference [41], the author gave a definition of face detection: "Given an arbitrary image, the goal of face detection is to determine whether or not there are any faces in the image and, if present, return the image location and extent of each face".

In this chapter, face detection and facial features extraction methods are discussed. Two methods of face detection, using vertical and horizontal histogram projections approach and skin-hair information approach, are discussed which can automatically detect face area. Face detection initializes the approximation area for the following feature selection. Facial feature are extracted using deformable templates to get precise positions. A subset of Feature Points (FPs), which is supported by the MPEG-4 standard, is described which are used in later section for expression modeling.

2.1 Projection Relations

Consider the points and coordinate frames as shown in Figure 2.1. The camera is placed in the top-middle of the screen that the image has the face in frontal view. The 3D point, $P_w = [x_w, y_w, z_w]^T$, in the world coordinate frame, Frame w, can be mapped to a 3D point, $P_i = [x_i, y_i, z_i]^T$, in the image frame, Frame i, by two frame transformation. By considering the pixel size and the image center parameter and using perspective projection with pinhole camera geometry, the transformation

from P_w to point $P_s = [x_s, y_s, 0]^T$ in the screen frame, Frame s, is given by [42]:

$$x_s = \frac{f}{s_x}\frac{x_w}{z_w} + o_x$$
$$y_s = \frac{f}{s_y}\frac{y_w}{z_w} + o_y \tag{2.1}$$

where s_x, s_y are the width and length of a pixel on the screen, o_x, o_y is the origin of Frame s, and the f is the focal length.

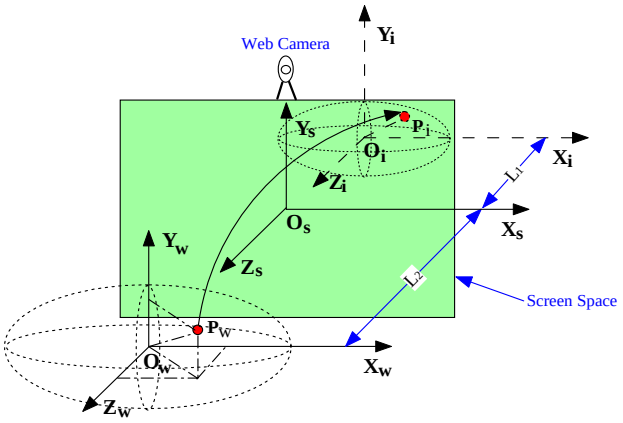

Figure 2.1: Projection relations between the real world and the virtual world.

The corresponding image point P_i can be expressed by a rigid body transformation:

$$P_i = R_s^i P_s + P_{sorg}^i \tag{2.2}$$

where $R_s^i \in \mathbb{R}^{3\times3}$ is the rotational matrix, $P_{sorg}^i \in \mathbb{R}^3$ is the origin of Frame s with respect to Frame i.

Fig. 2.2 illustrates the projection relationship of a real human head, a facial image and the 3D facial animation model.

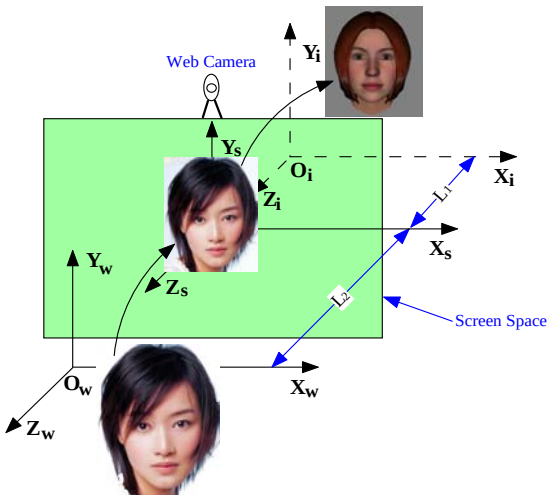

Figure 2.2: Projection relationship of a real head, a facial image on the screen and the corresponding 3D model

2.2 Face Detection and Location using Skin Information

In the literature, many different approaches are described in which skin color has been used as an important cue for reducing the search space [2, 43]. Human skin has a characteristic color, which indicate that the face region can be easily recognized. As indicated in many literatures, many different approaches make use of the skin color as an important cue for reducing the searching space.

2.2.1 Color Model

There are different ways of representing the same color in a computer, each with a different color space. Each color space has its own existing background and application areas. The main categories of the color models are listed below:

1. RGB model. A color image is a particular instance of multi-spectrogram

which corresponds to the three frequency band of the three visional base colors (i.e. Red, Green and Blue). It is popular to use RGB components as the format to represent colors. Most image acquisition equipment is based on CCD technology which perceives the RGB component of colors. Yet the method of RGB representation is very sensitive to perimeter light, making it difficult to segregate human skin from the background.

2. HSI(hue, saturation, intensity) model. This format reflects the way that people observe colors and is beneficial to image handling. The advantage of this format is its capability of segregating the two parameters that reflect the characteristics of colors C Hue and Saturation. When we are extracting the color characteristics of some object (e.g. face), we need to know its clustering characteristics in certain color space. Generally, the clustering characteristics are represented in the intrinsic characteristics of colors, and are often affected by illumination. The intensity component is directly influenced by illumination. So if we can extract an intensity component out from colors, and only use the hue and saturation that reflect the intrinsic characteristics of colors to carry out clustering analysis, we can achieve a better effect. This is the reason that a HSI format is frequently used in color image processing and computer vision.

3. YCbCr model. YCbCr model is widely applied in areas such as TV display and is also the representation format applied in many video frequency compression codes such as MPEG, JPEG standards. It has the following advantages: 1. Like HSI model, it can segregate the brightness component, but the calculation process and representation of space coordinates are relatively simple. 2. It has similar uses to the perception process of human vision. YCbCr can be achieved by RGB through linear transformation, the ITU.BT-601 transformation formula is as below.

2.2.2 Gaussian Mixed Model

We know that although the images are from different ethnicities, the skin distribution is relatively clustered in a small particular area [44]. It has been observed that skin colors differ more in intensity than in chrominance [45]. Hence, it is possible for us to remove brightness from the skin-color representation, while preserving an accurate, but low dimensional color information. We denote a class conditional probability as $P(x|\omega)$ which is the probability of likelihood of skin color x for each pixel of an image given its class ω. This gives an intensity normalized color vector x with two components. The definition of x is given in equation (2.3).

$$x = [r, b]^T \tag{2.3}$$

where

$$r = \frac{R}{R+G+B}, b = \frac{B}{R+G+B} \tag{2.4}$$

Thus, we project the 3D [R,G,B] model to a 2D [r,b] model. On this 2D plane, the skin color area is clustered in a small region. Hence, the skin-color distribution of different individuals can be modeled by a multivariate normal (Gaussian) distribution in normalized color space [46]. It is shown in Fig. 2.3. $P(x|\omega)$ can be treated as a Gauss distribution, and the equations of mean(μ) and covariance(C) are given:

$$\mu = E(x) \tag{2.5}$$

$$C = E(x - M)(x - M)^T \tag{2.6}$$

Finally, we calculate the probability that each pixel belongs to the skin tone through the Gaussian density function as shown in equation (2.7). Then we use Gaussian distribution to describe this kind of distribution

$$P(x|\omega) = \exp[-0.5(x - \mu)^T C^{-1}(x - \mu)] \tag{2.7}$$

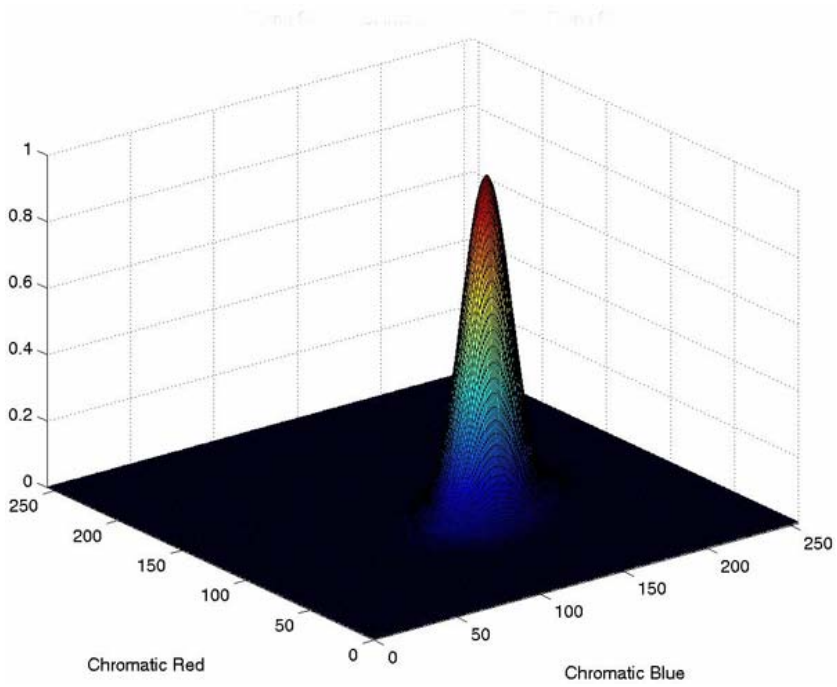

Figure 2.3: Fitting skin color into Gaussian distribution.

Through the distance between two pixels and the center we can get the information on how similar it is to skin and get a distribution histogram similar to the original image. The probability should be between 0 and 1, because we normalize the three components (R, G, B) of each pixel's color at the beginning. The probability of each pixel is multiplied by 255 in order to create a gray-level image $I(x, y)$. This image is also called a likelihood image. The computed likelihood image is shown in Fig. 2.4(c).

2.2.3 Threshold & Compute the Similarity

After obtaining the likelihood of skin $I(x, y)$, a binary image $B(x, y)$ can be obtained by thresholding each pixel's $I(x, y)$ with a threshold T according to

$$B(x,y) = \begin{cases} 0, & \text{if} \quad I(x,y) > T \\ 1, & \text{if} \quad I(x,y) \leq T \end{cases} \tag{2.8}$$

There is no definite criterion to determine a threshold. If the threshold value is too big, the false rate will increase. On the other hand, if the threshold is too small, the missed rate will increase. This detection threshold can be adjusted to trade-off between correct detections and false positives. According to the previous research work [47], we adopt the threshold value as 0.5. That is, when the skin probability of a certain pixel is larger or equal to 0.5, we will regard the pixel as skin. In Fig. 2.4(b), the binary image $B(x, y)$ is derived from the $I(x, y)$ according to the rule defined in equation (2.8). As observed from the experiments, if the background color is similar to skin, there will be more candidate regions, and the follow-up verifying time will increase.

2.2.4 Histogram Projection Method

We have used integral projections of the histogram map of the face image for facial area location [47]. The vertical and horizontal projection vectors in the image rectangle $[x1, x2] \times [y1, y2]$ are defined as:

$$V(x) = \sum_{y=y_1}^{y=y_2} B(x,y) \tag{2.9}$$

$$H(x) = \sum_{x=x_1}^{x=x_2} B(x,y) \tag{2.10}$$

The face area is located by applying sequentially the analysis of the vertical histogram and then the horizontal histogram. The peaks of the vertical histogram of

(a) The vertical histogram

(b) The binary image

(c) The likelihood image

(d) The horizontal histogram

Figure 2.4: Face detection using vertical and horizontal histogram method

the head box correspond with the border between the hair and the forehead, the eyes, the nostrils, the mouth and the boundary between the chin and the neck.

The horizontal line going through the eyes goes through the local maximum of the second peak. The x axis of the vertical line going between the eyes and through the nose is chosen as the absolute minimum of the contrast differences found along the horizontal line going through the eyes. By performing the analysis of the vertical and the horizontal histogram, the eyes' area is reduced so that it contains just the

(b) Face and hair color segment

(c) The hair histogram

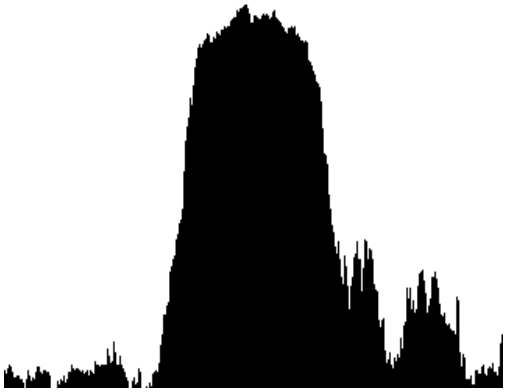

(d) The face histogram

Figure 2.5: Face detection using hair and face skin method.

local maximums of the histograms. The same procedure is applied to define the box that bounds the right eye. The initial box bounding the mouth is set around the horizontal line going through the mouth, under the horizontal line going through the nostrils and above the horizontal line representing the border between the chin and the neck. By analyzing the vertical and the horizontal histogram of an initial box containing the face, facial feature can be tracked.

Fig. 2.5 shows the face detection process using hair-skin method. It can be seen

from Fig. 2.5(b) that the skin(red) and hair(blue) area are successfully and clearly segmented into different colors.

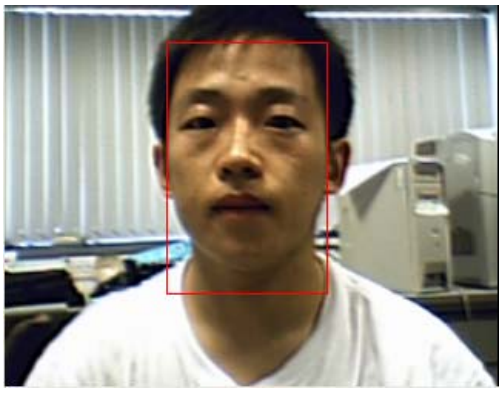

(a) Using vertical and horizontal histogram method

(b) Using hair and face skin method.

Figure 2.6: The detected rectangle face boundary.

2.2.5 Skin & Hair Method

The distribution of skin color across different ethnic groups under controlled conditions of illumination has been shown to be quite compact. Researches have shown that given skin and non-skin histogram models, a skin pixel classifier can be constructed. The distribution of skin and non-skin colors can be separated accurately accordingly[47].

The face detection step can provide us a rectangle head boundary, in which the whole face region is included. Subsequently, the face area can be segmented roughly using static anthropometric rules into several rectangular feature-candidate areas of interest which is shown in Fig. 2.8, including the eyes, the eyebrows, the mouth and the nose. These areas are utilized to initialize the feature extraction process.

As illustrated in Fig. 2.6, both methods can detect the face region successfully. There is a bit variations in the detected rectangles. As long as the main facial area is included, the following feature detection won't be affected. However, sometimes both method may fail to locate the facial region when the illusion is too dark or the background is similar to skin color.

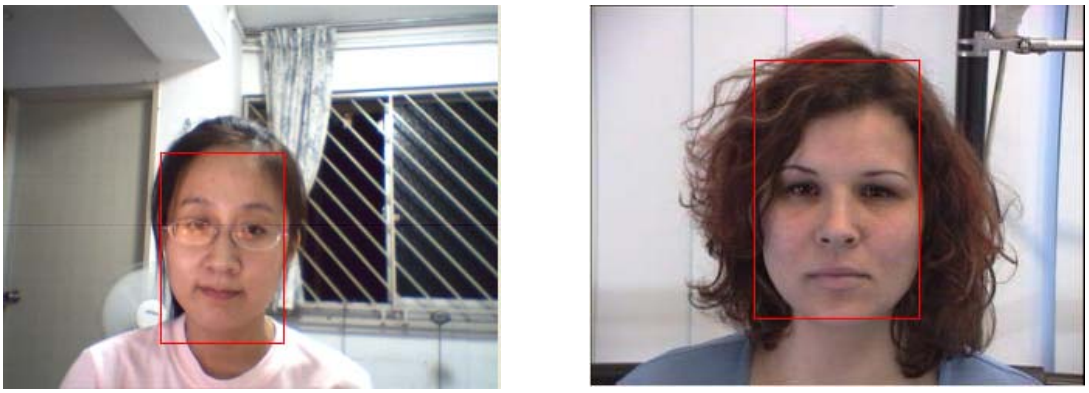

(a) Test image 1 (b) Test image 2

Figure 2.7: Sample experimental face detection results.

As can be seen from Fig. 2.7, faces can be successfully detected in different surroundings in these images where each detected face is shown with an enclosing window.

2.3 Facial Features Extraction

A facial expression involves simultaneous changes of facial features on multiple facial regions. Facial expression states vary over time in an image sequence and so do the facial visual cues. Facial feature extraction include locating the position and shape of the eyebrows, eyes, eyelids, mouth, wrinkles, and extracting features related to them in a still image of human face. For a particular facial activity, there

is a subset of facial features that are the most informative and maximally reduces the ambiguity of classification. Therefore we actively and purposefully select 21 facial visual cues to achieve a desirable result in a timely and efficient manner while reducing the ambiguity of classification to a minimum. In our system, features are extracted using deformable templates with details given below.

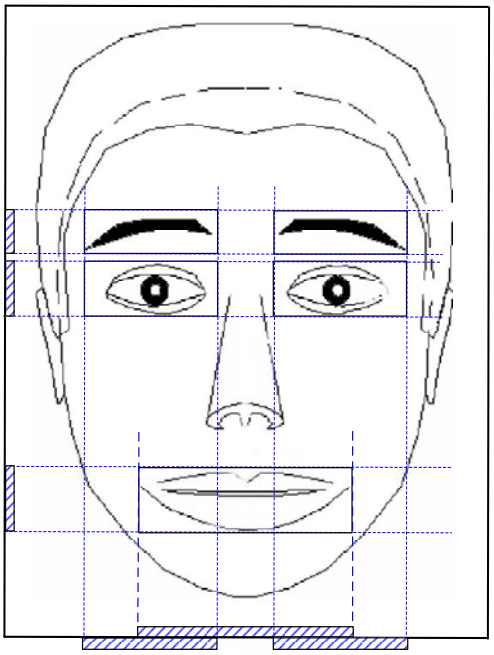

Figure 2.8: The rectangular feature-candidate areas of interest.

2.3.1 Eyebrow Detection

The segmentation algorithm cannot give bounding box for the eyebrow exclusively. Brunelli suggests use of template matching for extracting the eye, but we use another approach as described below. Eyebrow is segmented from eye using the fact that the eye occurs below eyebrow and its edges form closed contours, obtained by applying Laplacian of Gaussian operator at zero threshold. These contours are filled and the resulting image containing masks of eyebrow and eye. From the two

largest filled regions, the region with higher centroid is chosen to be the mask of eyebrow.

2.3.2 Eyes Detection

The positions of eyes are determined by searching for minima in the topographic grey level relief. The contour of the eyes can be precisely found. Since the real images are always affected by the lighting and noises, it is not robust and often require expert supervision using the general local detection method such as corner detection [48]. The Snake algorithm is much more robust, but rely much on the image itself and there may be too many details in the result [49]. We can make full use of the priority knowledge of human face which describes the eyes as piece-wise polynomial. A more precise contour can be obtained by making use of the deformable template.

The eye's contour model can be composed by four second order polynomials which are given below:

$$\begin{cases} y = h_1(1 - \frac{x^2}{w_1^2}) & -w_1 \leq x \leq 0 \\ y = h_1(1 - \frac{x^2}{w_2^2}) & 0 < x \leq -w_2 \\ y = h_2(\frac{(x+w_1-w_3)^2}{w_3^2} - 1) & -w_1 \leq x \leq w_3 - w_1 \\ y = h_2(\frac{(x+w_1-w_3)^2}{(w_1+w_2-w_3)^2} - 1) & 0 < x \leq -w_2 \end{cases} \tag{2.11}$$

where (x_0, y_0) is the center of the eye, h_1 and h_2 are the heights of the upper half eye and the lower half eye, respectively.

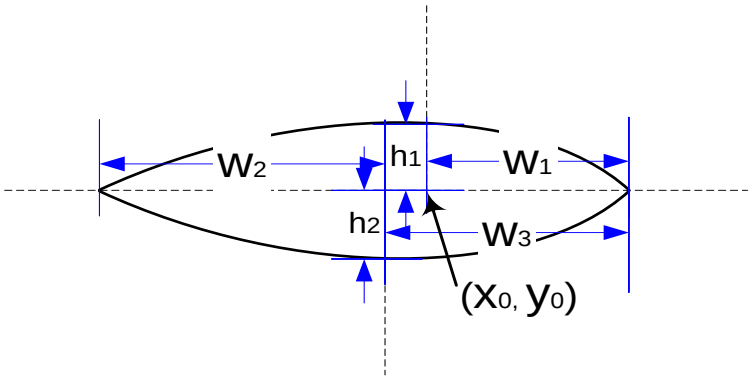

Figure 2.9: The outline model of the left eye.

Since the eyes's color are not accordant and the edge information is abundant, we can do edge detection with a closed operation followed. The inner part of the eye becomes high-luminance while the outer part of the eye becomes low-luminance. The evaluation function we choose is:

$$\min C = \oint_{\partial} D^{+} I(\mathrm{x}) d\mathrm{x} - \oint_{\partial} D^{-} I(\mathrm{x}) d\mathrm{x} \tag{2.12}$$

where D represent the eye's area, ∂D^{+} denotes the outer part and ∂D^{-} denotes the inner part of the eye.

2.3.3 Nose Detection

After the eyes' position is fixed, it will be much easier to locate the nose position. The nose is at the center area of the face rectangle. As indicated in Fig. 2.16(b), if the ES0 is set as one unit, the ENS0 is about 07 to 1.0 of ES0. We can search this area for the light color region. Thus the two nostrils can be approximated by finding the dark area. Then the nose can be located above the two nostrils at the brightest point.

2.3.4 Mouth Detection

Similar to the eye's model, the lips can be modeled by two pieces of fourth order polynomials which are given below:

$$\begin{cases} y = h_1(1 - \frac{x^2}{w^2}) + q_1(\frac{x^2}{w^2} - \frac{x^4}{w^4}) & -w \le x \le 0 \\ y = h_2(\frac{x^2}{w^2} - 1) + q_2(\frac{x^2}{w^2} - \frac{x^4}{w^4}) & 0 \le x \le w \end{cases} \tag{2.13}$$

where (x_0, y_0) is the lip center position, h_1 and h_2 are the heights of the upper half and the lower half of the lip respectively.

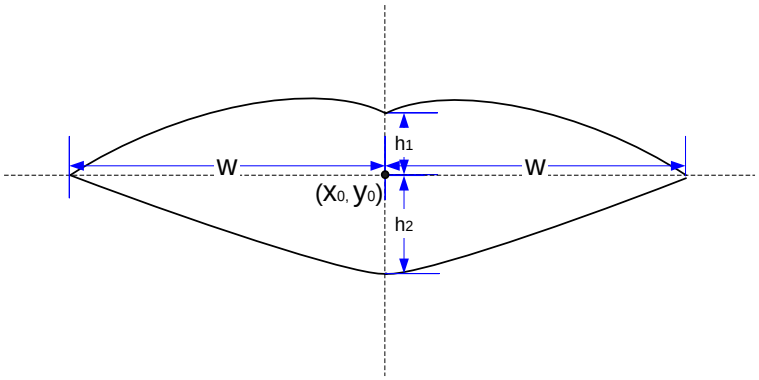

Figure 2.10: The outline model of the mouth.

The mouth's evaluation function is much easier to confirm since the color of the mouth is uniform. The mouth could be easily separated by the different color of mouth and skin. The position of mouth can be determined by searching for minima in the topographic grey level relief. The formation of the evaluation function is similar to equation (2.12).

2.3.5 Feature Extraction Results

Fig. 2.11(a) shows the results of edge detection of human face. It can be seen from Fig. 2.11(b) that all the facial features are successfully marked. Fig. 2.12

(a) The contour of the face (b) The marked features

Figure 2.11: Feature label

illustrates the feature extraction results on different testers. As we can see from these test images, the required facial features are correctly detected and marked under different conditions. With these corrected marked features, facial movement information can be traced.

2.3.6 Illusion & Occlusion

Glasses, scarves and beards would change the facial appearance which make it difficult for face detection and feature extraction. Some previous work has addressed the problem of partial occlusion [50]. The method they proposed could detect a face wearing sunglasses or scarf but is conducted under restrained conditions. The people with glasses can be somehow detected but it may fail sometimes. Fig. 2.13 shows the face detection and feature extraction results with glasses. In this paper, we did not consider the occlusion problem such as scarf or purposive occlusion. Such occlusion may cover some of the feature points, and the face feature extraction can not be conducted subsequently.

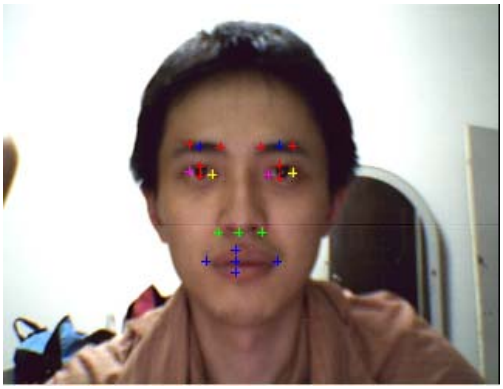

(a) Test image 1

(b) Test image 2

(c) Test image 3

(d) Test image 4

Figure 2.12: Sample experimental facial feature extraction results.

2.4 Facial Features Representation

A facial expression is composed of simultaneous changes of multiple feature regions. To efficiently analyze and correctly classify different facial expressions, it is crucial to detect and track the facial movements. Several facial features can be employed to assist this process. The MPEG-4 defines a standard face model using facial definition parameters (FDP). These proposed parameters can be used directly to deform the face model.

Figure 2.13: The feature extraction results with glasses.

The combination of these parameters can result in a set of possible facial expressions. The proposed system uses a subset of Feature Points (FPs) for describing the facial expressions which is supported by the MPEG-4 standard. The 21 visual features used in our system are carefully selected from the FPs 2.16(a). Their dynamic movements are more prominent compared to other points defined by FPs. They are more informative for the goal of reducing ambiguity of classification. At the same time, the movements of these feature points are significant while a expression occur which could be detected for further recognition. These features are selected by considering their suitability for a real-time video system. They can give a satisfactory recognition results while meeting the time constraints.

As shown in Fig. 2.16(a), these features are: For the mouth portion: LeftMouthCorner, RightMouthCorner, UpperMouth, LowerMouth; For the nose portion,

LeftNostril, RightNostril, NoseTip; for the eye portion: LeftEyeInnerCorner, LeftEyeOuterCorner, LeftEyeUpper, LeftEyeLower, RightEyeInnerCorner, RightEyeOuterCorner, RightEyeUpper, RightEyeLower; for the eyebrow portion: LeftEyeBrowInner, LeftEyeBrowOuter, LeftEyeBrowMiddle, RightEyeBrowInner, RightEyeBrowOuter, RightEyeBrowMiddle.

The facial expression is controlled by these facial muscles. Fig. 2.14 is the anatomy image of the face muscles. From this image, we can see clearly that there are quite a number of facial muscles which may result in a great variation of facial expressions. It is hard to give a simple description of the comprehensive facial muscle movements and the facial expression. The MPEG-4 standard defines a set of efficient rules for facial description which has been widely used.

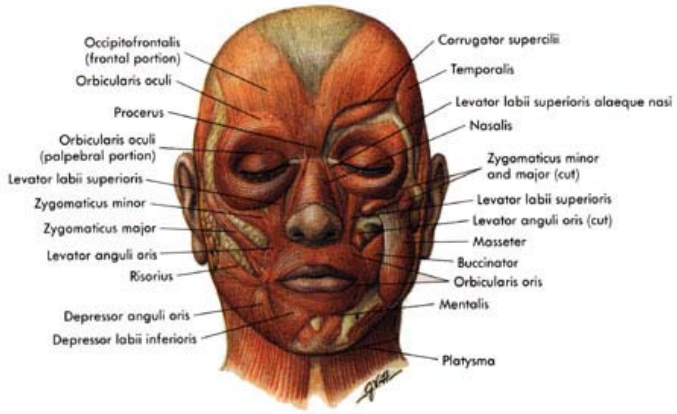

Figure 2.14: Anatomy image of face muscles.

2.4.1 MPEG-4 Face Model Specification

A feature point represents a key-point in a human face, like the corner of the mouth or the tip of the nose. MPEG-4 has defined a set of 84 feature points, described in Fig. 2.15 with white and black spots, used both for the calibration and the

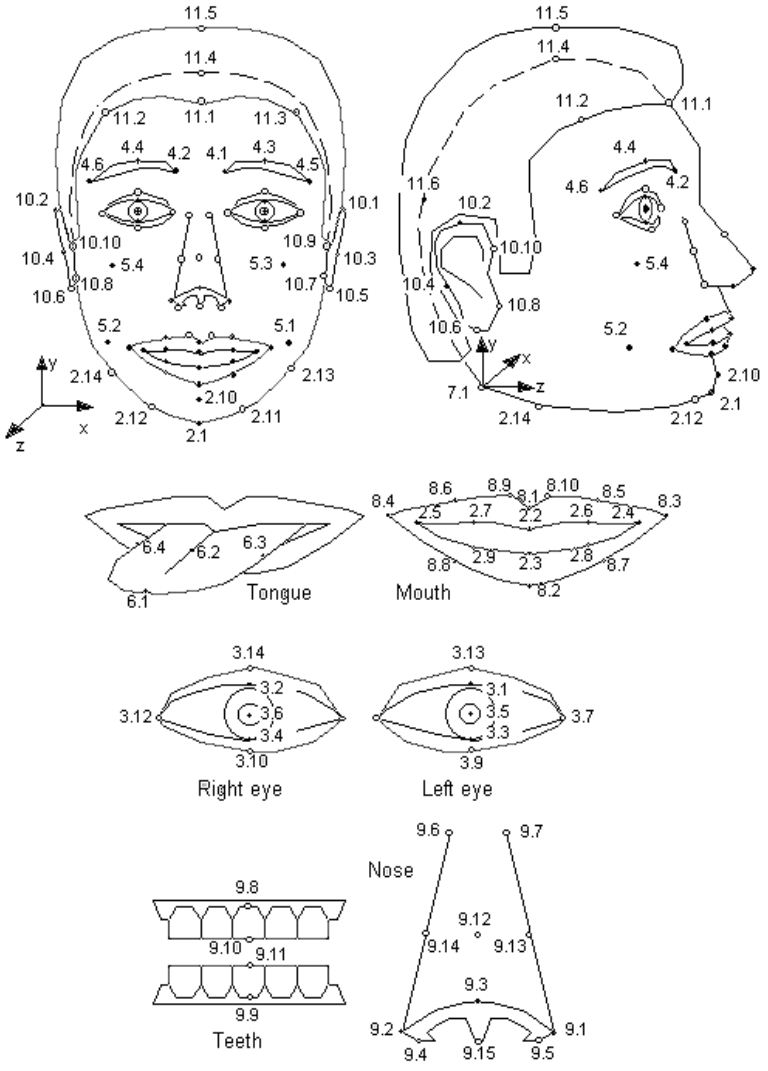

Figure 2.15: The facial feature points [24].

animation of a synthetic face. More precisely, all the feature points can be used for the calibration of a face, while only the black ones are used also for the animation. Feature points are subdivided in groups according to the region of the face they belong to, and numbered accordingly.

In order to define FAPs for arbitrary face models, MPEG-4 defines FAPUs that serve to scale FAPs for any face model. FAPUs are defined as fractions of distances between key facial features as shown in Fig. 2.16. These features, such as eye separation are defined on a face model which is in the neutral state. The FAPU allows interpretation of the FAPs on any facial model in a consistent way producing reasonable results in terms of expression and speech pronunciation.

Although FAPs provide all the necessary elements for MPEG-4 compatible animation, they cannot be directly used for the analysis of expressions from video sequences, due to the absence of a clear quantitative definition. In order to measure the FAPs in real image sequences, we adopt the mapping between them and the movement of specific FDP feature points(FPs), which correspond to salient points on human face. As shown in Fig. 2.16(b), some of these points can be used as reference points in neutral face. Distances between these points are used for normalization purposes [51]. The quantitative modeling of FAPs are shown in Table 2.1 and 2.2.

The MPEG-4 standard defines 68 FAPs. They are divided into ten groups, which describe the movement of the face. These parameters are either high level parameter, that is, parameters that describe visemes and facial expressions, or low-level parameters which describe displacement of the specific single point of the face.

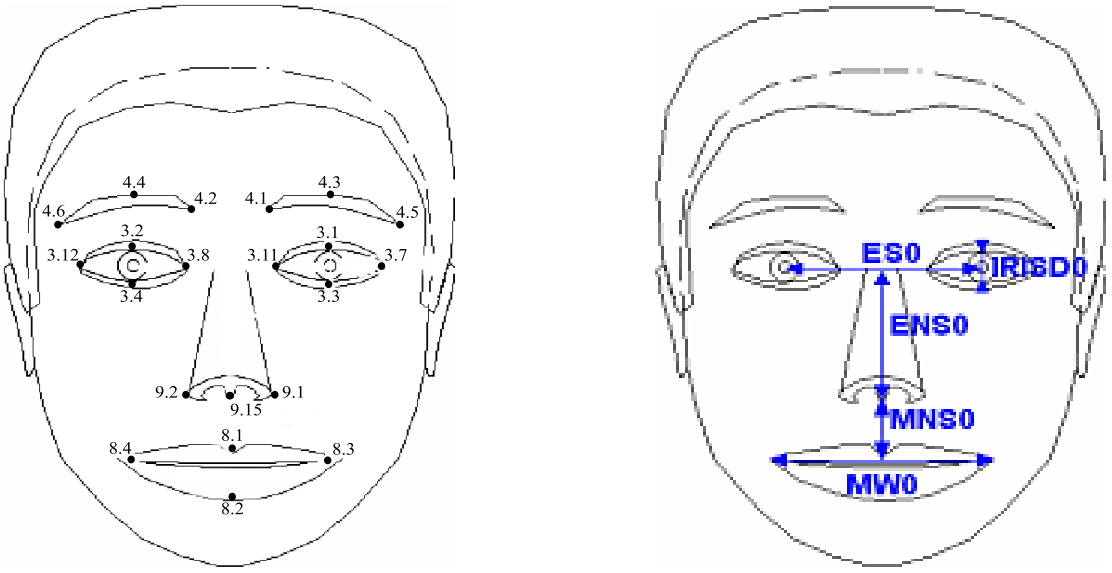

(a) Feature points used in our system.

(b) Facial animation parameters units (FAPUs)

Figure 2.16: Feature points (FPs) and facial animation parameters units (FAPUs). (from ISO/IEC IS 14496-2 Visual, 1999 [24]).

Table 2.1: Facial animation parameter units and their definitions

IRISD0	Iris diameter in neutral face	IRISD = IRISD0/1024
ES0	Eye separation	ES = ES0/1024
ENS0	Eye-nose separation	ENS = ENS0/1024
MNS0	Mouth-nose separation	MNS = MNS0/1024
MW0	Mouth width	MW = MW0/1024
AU	Angle unit	10E-5rad

FAPs control the key features of the model of a head, and can be used to animate facial movements and expressions. Facial expression analysis using FAPs has

several advantages. One of these is that it secures compliance with the MPEG-4 standard. Another is that existing FAP extraction systems or available FAPs can be utilized to perform automatic facial expression recognition. In addition, FAPs are expressed in terms of facial animation parameter units (FAPUs). These units are normalized by important facial feature distances, such as mouth width, mouth-nose, eye-nose, or eye separation, in order to give an accurate and consistent representation. This is particularly useful for facial expression recognition, since normalizing facial features corresponding to different subjects enables better modeling of facial expressions.

Table 2.2: Quantitative FAPs modeling

FAP name	Feature for the discription	Utilized features
squeeze_l_eyebrow	D_1 = d(4.6, 3.8)	$f_1 = D_1$-Neutral - D_1
squeeze_r_eyebrow	D_2 = d(4.5, 3.11)	$f_2 = D_2$-Neutral - D_2
low_t_midlip	D_3 = d(9.3, 8.1)	$f_3 = D_3$-Neutral - D_3
raise_b_midlip	D_4 = d(9.3, 8.2)	$f_4 = D_4$-Neutral - D_4
raise_l_i_eyebrow	D_5 = d(4.2, 3.8)	$f_5 = D_5$-Neutral - D_5
raise_r_i_eyebrow	D_6 = d(4.1, 3.11)	$f_6 = D_6$-Neutral - D_6
raise_l_o_eyebrow	D_7 = d(4.6, 3.12)	$f_7 = D_7$-Neutral - D_7
raise_r_o_eyebrow	D_8 = d(4.5, 3.7)	$f_8 = D_8$-Neutral - D_8
raise_l_m_eyebrow	D_9 = d(4.4, 3.12)	$f_9 = D_9$-Neutral - D_9
raise_r_m_eyebrow	D_{10} = d(4.3, 3.7)	$f_{10} = D_{10}$-Neutral - D_{10}
stretch_l_cornerlip	D_{11} = d(8.4, 8.3)	$f_{11} = D_{11}$-Neutral - D_{11}
close_t_l_eyelid	D_{12} = d(3.2, 3.4)	$f_{12} = D_{12}$-Neutral - D_{12}
close_t_r_eyelid	D_{13} = d(3.1, 3.3)	$f_{13} = D_{13}$-Neutral - D_{13}

In order to understand facial animation based on MPEG-4 standard, we give a

brief description of some keywords of the parameters system.

FAPU(Facial Animation Parameters Units) All animation parameters are described in FAPU units. This unit is based on face model proportions and computed based on a few key points of the face (like eye distance or mouth size).

FDP(Facial Definition Parameters) This acronym describes a set of 88 feature points of the face model. FAPU and facial animation parameters are based on these feature points.

FAP(Facial Animation Parameters) It is a set of values decomposed in high level and low level parameters that represent the displacement of some features points (FP) according to a specific direction.

We select the feature displacement and velocity approach due to its suitability for a real-time video system, in which motion is inherent and which places a strict upper bound on the computational complexity of methods used in order to meet time constraints.

Although FAPs are practical and very useful for animation purpose, they are inadequate for analyzing facial expressions from video scenes or still images. The main reason is the absence of quantitative definitions for FAPs as well as their nonadditive nature. In order to measure facial related FAPs in real images and video sequences, it is necessary to define a way of describing them through the movement of points that lie in the facial area and that can be automatically detected. Quantitative description of FAPs based on particular FDPs points, which correspond to movement of protuberant facial points, provides the means of bridging the gap between expression analysis and animation. In the expression analysis case, the

FAPs can be addressed by a fuzzy rule system.

Quantitive modeling of FAPs is implemented using the features labeled as f_i. The features set employs FDP points that lie in the facial area and under some constraints, can be automatically detected and tracked. It consists of distances, noted as $d(p_i, p_j)$ where p_i and p_j correspond to FDP points, between these protuberant points. Some of the points are constant during expressions and can be used as the reference points. Distances between reference points are used for normalization.

2.4.2 Facial Movement Pattern for Different Emotions

The various facial expressions are driven by the muscular activities which are the direct results of emotion state and mental condition of the individual. Facial expressions are the visually detectable changes in appearance which represent the change in neuromuscular activity. In 1979, Bassili observed and verified that facial expressions could be identified by facial motion cues without any facial texture and complexion information [52]. As illustrated in Fig. 2.18, the principal facial motions provide powerful cues for facial expression recognition. This observed motion patterns of expression have been explicitly or implicitly employed by a lot of researchers [28].

From Table 2.3 and 2.4, we can summarize the movement pattern of different facial expressions.

- When a person is happy, e.g. smiling or laughing, the main facial movement occurs at the lower half portion while the upper facial portion is kept still. The most significant feature is that both the mouth corners will move outward

Table 2.3: The facial movements cues for six emotions.

Emotion	Forehead & eyebrow	Eyes	Mouth & Nose
Happiness	Eyebrows are relaxed	Raise upper and lower lids slightly	Pull back and up lip corners toward the ears
Sadness	Bend together and upward the inner eyebrows	Drop down upper lids Raise lower lids slightly	Extend mouth
Fear	Raise brows and pull together Bent upward inner eyebrows	Eyes are tense and alert	Slightly tense mouth and draw back May open mouth
Disgust	Lower the eyebrows	Push up lids without tense	Lips are curled and often asymmetrical
Surprise	Raise eyebrows Horizontal wrinkles	Drawn down lower eyelid Raise upper eyelid	Drop jaw, Open mouth No tension or stretching of the mouth
Anger	Lower and draw together eyebrows Vertical wrinkles between eyebrows	Eyes have a hard stare Tense upper and lower lids	Mouth firmly pressed Nostrils may be dilated

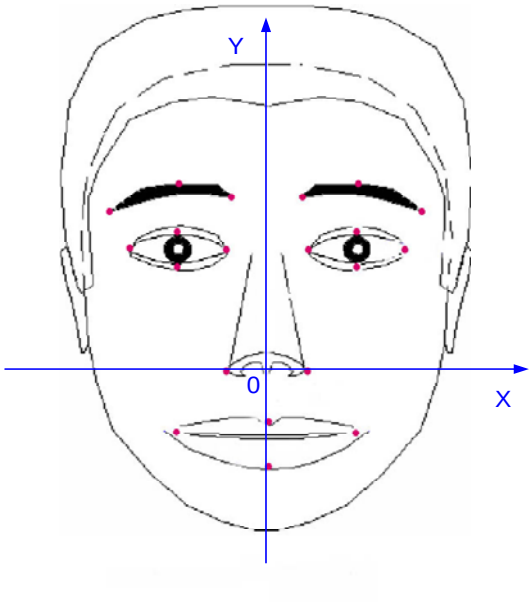

Figure 2.17: The facial coordinates.

and toward the ear. Sometimes, when laughing, the jaw will drop and mouth will be open.

- When a sad expression occur, the eyebrows will bend together and upward a bit at the inner parts. The mouth will extend. At the same time, the upper lids may drop down and lower lids may raise slightly.

- The facial moving features of the fear expression mainly occur at the eye and mouth portion. The eyebrows may raise and pull together. The eyes will become tense and alert. The mouth will also tend to be tense and may draw back and open.

- When a person is disgusted about something, the lips will be curled and often asymmetrical.

- The surprise expression has the most widely spread features. The whole eyebrows will bend upward and horizontal wrinkles may occur as a result

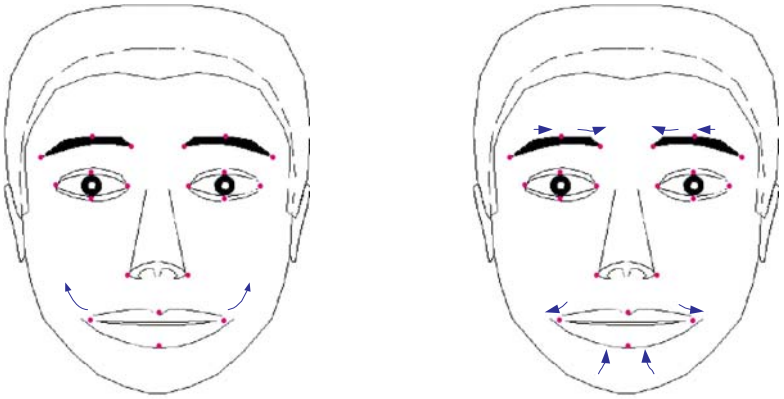

(a) happiness

(b) sadness

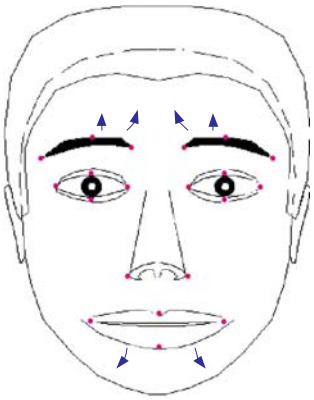

(c) fear

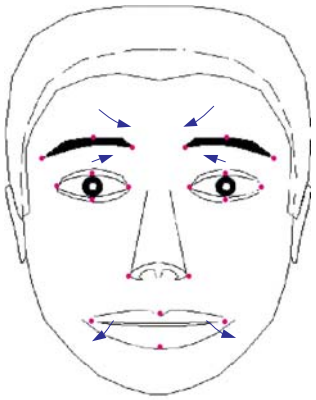

(d) disgust

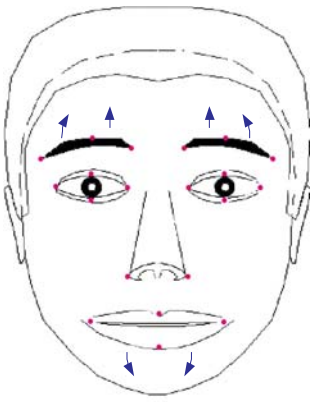

(e) surprise

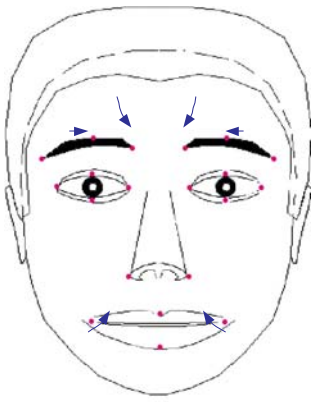

(f) anger

Figure 2.18: Facial muscle movements for six emotions suggested by Bassili.

of the eyebrow raise. The eyelids will move oppositely and the eyes will be open. Jaw will drop and mouth may open largely.

- When a person is in anger, the eyebrows are lowered and drawn together. Vertical wrinkles may appear between eyebrows. The eyes have a hard stare and both lids are tense. The mouth may be firmly pressed.

Table 2.4: The movements clues of facial features for six emotions

Features Points	Happiness	Sadness	Fear	Anger	Surprise	Disgust
LeftEyeBrowInner	↑	→	↑	→	↑	→
LeftEyeBrowOuter			↑		↑	→
LeftEyeBrowMiddle	↑	↓	↑	↓	↑	
RightEyeBrowInner	↑	←	↑	←	↑	←
RightEyeBrowOuter			↑		↑	←
RightEyeBrowMiddle	↑	↓	↑	↓	↑	
LeftEyeInnerCorner						
LeftEyeOuterCorner	←					
LeftEyeUpper	↑	↓	↑	↓	↑	
LeftEyeLower		↓	↓	↑	↓	
RightEyeInnerCorner						
RightEyeOuterCorner	→					
RightEyeUpper	↑	↓	↑	↓	↑	
RightEyeLower		↓	↓	↑	↓	
LeftMouthCorner	↖	↙				↙
RightMouthCorner	↗	↘				↘
UpperMouth	↑		↑	↑	↑	
LowerMouth	↓		↓	↑	↓	

Chapter 3

Nonlinear Dimension Reduction (NDR) Methods

To analyze faces in images efficiently, dimensionality reduction is an important and necessary operation for multi-dimensional image data. The goal of dimensionality reduction is to discover the intrinsic property of the expression data. A more compact representation of the original data can be obtained which nonetheless captures all the information necessary for higher-level decision-making. The reasons for reducing the dimensionality can be summarized as: (i) To reduce storage requirements; (ii) To eliminate noise; (iii) To extract features from data for face detection; and (iv) To project data to a lower-dimensional space, especially a visualized space, so as to be able to discern data distribution [53]. For facial expression analysis, classical dimensionality reduction methods have included Eigenfaces [10], Principal Component Analysis (PCA) [5], Independent Component Analysis (ICA) [54], Multidimensional Scaling (MDS) [55] and Linear Discriminate Analysis (LDA) [56]. However, these methods all have serious drawbacks, such as being unable to reveal the intrinsic distribution of a given data set, or inaccuracies in detecting faces that exhibit variations in head pose, facial expression or illumination.

The facial image data are always high-dimensional and require considerable computing time for classification. Face images are regarded as a nonlinear manifold in high-dimensional space. PCA and LDA are two powerful tools utilized for data reduction and feature extraction in face recognition approaches. Linear methods like PCA and LDA are bounds to ignore essential nonlinear structures that are contained in the manifold. Nonlinear dimension reduction methods, such as ISOMAP [57], Locally Linear Embedding (LLE) [58] method etc. are presented in recent years.

The high dimensionality of the raw data would be an obstacle for direct analysis. Therefore, dimension reduction is critical for analyzing the images, to compress the information and to discover compact representations of variability. In this chapter, we modify the LLE algorithm and propose a new Distributed Locally Linear Embedding (DLLE) to discover the inherent properties of the input data. By estimating the probability density function of the input data, an exponential neighbor finding method is proposed. Then the input data are mapped to low dimension where not only the local neighborhood relationship but also global distribution are preserved [59]. Because the DLLE can preserve the neighborhood relationships among input samples, after embedded in low-dimensional space, the 2D embedding could be much easier for higher-level decision-making.

3.1 Image Vector Space

The human face image can be seen as a set of high dimensional values. A movement of facial muscle will result in different images. The similarity between two images can be extracted by comparing the pixel values. An image of a subject's facial

expressions with $M \times N$ pixels can be thought of a point in an $M \times N$ dimensional image space with each input dimension corresponding to the brightness of each pixel in the image which is shown in Fig. 3.1. The variability of expressions can be represented as low-dimensional manifolds embedded in image space. Since people change facial expression continuously over time, it is reasonable to assume that video sequences of a person undergoing different facial expressions define a smooth and relatively low dimensional manifold in the $M \times N$ dimensional image space. Although the input dimensionality may be quite high (e.g., 76800 pixels for a 320 $\times$ 240 image), the perceptually meaningful structure of these images has many fewer independent degrees of freedom. The intrinsic dimension of the manifold is much lower than $M \times N$. If other factors of image variation are considered, such as illumination and face pose, the intrinsic dimensionality of the manifold of expression would increase accordingly. In the next section, we will describe how to discover compact representations of high-dimensional data.

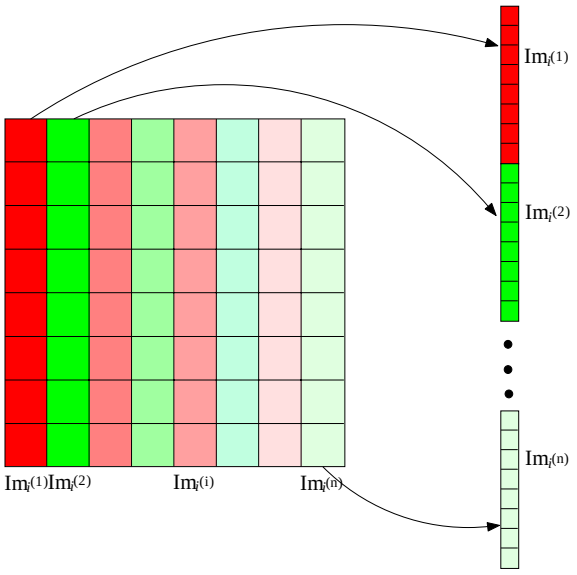

Figure 3.1: An image with $M \times N$ pixels can be thought of a high-dimensional point vector.

3.2 LLE and NLE

For ease of the forthcoming discussion, we first introduce the main features of LLE and NLE methods. LLE is an unsupervised learning algorithm that attempts to map high-dimensional data to low-dimensional space while preserving the neighborhood relationship. Compared to principle component analysis (PCA) and multidimensional scaling (MDS), LLE is for nonlinear dimensionality reduction. It is based on simple geometric intuitions: (i) each high dimensional data point and its neighbors lie on or close to a locally linear patch of a manifold, and (ii) the local geometric characterization in original data space is unchanged in the output data space. The neighbor finding process of each data point of LLE is: for each data point in the given data set, using the group technique such as K nearest neighbors based on the Euclidean distance, the neighborhood for any given point can be found. A weighted graph is set up with K nodes, one for each neighbor point, and a set of edges connecting neighbor points. These neighbors are then used to reconstruct the given point by linear coefficients.

In order to provide a better basis for structure discovery, NLE [60] is proposed. It is an adaptive scheme that selects neighbors according to the inherent properties of the input data substructures. The neighbor finding procedure of NLE for a given point x_i, by defining d_{ij} the Euclidean distance from node x_j to x_i and $\mathbf{S}_i$ the data set containing all the neighbor indices of x_i, can be summarized as follows:

- *If* $d_{ij} = min\{d_{im}\}$, $\forall\ m \in$ *1, 2,..., N, then* x_j *is regarded as a neighbor of the node* x_i. *Initial* $\boldsymbol{S}_i = \{x_j\}$
- *Provided that* x_k *is the second nearest node to node* x_i, x_k *is a neighbor of*

node x_i if the following two inequations is satisfied.

$$\boldsymbol{S}_i = \begin{cases} \boldsymbol{S}_i \cup \{x_k\}, & if \;\; d_{jk} > d_{ik} \\ \boldsymbol{S}_i, & otherwise \end{cases}$$

- *If $\boldsymbol{S}_i$ contains two or more elements, that is card($\boldsymbol{S}_i$) $\geq$ 2, if $\forall\, m \in \boldsymbol{S}_i$, the following two inequations hold:*

$$\begin{cases} d_{jm} > d_{ji} \\ d_{jm} > d_{mi} \end{cases}$$

then $\boldsymbol{S}_i = \boldsymbol{S}_i \cup \{x_m\}$"

Both LLE and NLE methods can find the inherent embedding in low dimension. According to the LLE algorithm, each point x_i is only reconstructed from its K nearest neighbors by linear coefficients. However, due to the complexity, nonlinearity and variety of high dimensional input data, it is difficult to use a fixed K for all the input data to find the intrinsic structure [61]. The proper choice of K affects an acceptable level of redundancy and overlapping. If K is too small or too large, the K-nearest neighborhood method cannot properly approximate the embedding of the manifold. The size of range depends on various features of the data, such as the sampling density and the manifold geometry. An improvement can be done by adaptively selecting neighbor number according to the density of the sample points.

Another problem of using K nearest neighbors is the information redundancy. As illustrated in Fig. 3.2, e.g., for a certain manifold, we choose $K(K = 8)$ nearest neighbors to reconstruct x_i. However, the selected neighbors in the dashed circle are closely gathered. Obviously, if we use all of samples in the circle as the neighbors of x_i, the information captured in that direction will have somewhat redundancy. A better straightforward way is to use one or several samples to represent a group

of closely related data points.

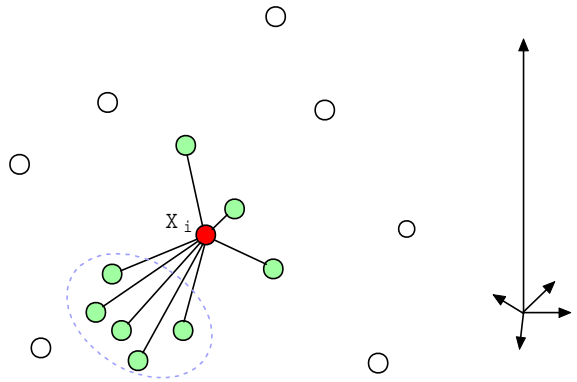

Figure 3.2: Select $K(K = 8)$ nearest neighbors using LLE. The samples in the dashed circle cause the information redundancy problem.

According to NLE's neighborhood selection criterion, the number of neighbor selected to be used is small. For example, according to our experiment on Twopeaks data sample, the average number of neighbors for NLE for 1000 samples are 3.74. The reconstruction information may not be enough for an embedding.

By carefully considering the LLE and NLE's neighbor selection criterion, we propose a new algorithm by estimating the probability density function from the input data and using an exponential neighbor finding method to automatically obtain the embedding.

3.3 Distributed Locally Linear Embedding (DLLE)

3.3.1 Estimation of Distribution Density Function

In most cases, a prior knowledge of the distribution of the samples in high dimension space is not available. However, we can estimate a density function of the given data. Consider a data set with N elements in m dimensional space, for each sample x_i, the approximated distribution density function $\hat{p}_{x_i}$ around point x_i can be calculated as:

$$\hat{p}_{x_i} = \frac{k_i}{\sum_1^N k_i} \tag{3.1}$$

where k_i is number of the points within a hypersphere kernel of fixed radius around point x_i.

Let $\hat{P} = \{\hat{p}_{x_1}, \hat{p}_{x_2}, \cdots, \hat{p}_{x_N}\}$ denote the set of estimated distribution density function, $\hat{p}_{\max}$=max$(\hat{P})$ and $\hat{p}_{\min}$=min$(\hat{P})$.

3.3.2 Compute the Neighbors of Each Data Point

Suppose that a data set $\mathcal{X} = \{x_1, x_2, \cdots, x_n\}$, $x_i \in \mathbb{R}^m$ is globally mapped to a data set $\mathcal{Y} = \{y_1, y_2, \cdots, y_n\}$, $y_i \in \mathbb{R}^l$, $m \gg l$. For the given data set, each data point and its neighbors lie on or close to a locally linear patch of the manifold. The neighborhood set of x_i, $\mathbf{S}_i$ $(i = 1, ..., N)$ can be constructed by making use of the neighborhood information.

Assumption 4. *Suppose that the input data set $\mathcal{X}$ contains sufficient data in $\mathbb{R}^m$ sampled from a smooth parameter space Φ. Each data point x_i and its neighbors e.g. x_j, to lie on or close to a roughly linear patch on the manifold. The range of this linear patch is subject to the estimated sampling density $\hat{p}$ and mean distances*

$\bar{d}$ from other points in the input space.

Based on above geometry conditions, the local geometry in the neighborhood of each data point can be reconstructed from its neighbors by linear coefficients. At the same time, the mutual reconstruction information depends on the distance between the points. The larger the distance between points, the little mutual reconstruction information between them.

Assumption 5. *The parameter space Φ is a convex subset of $\mathbb{R}^m$. If x_i and x_j is a pair of points in $\mathbb{R}^m$, ϕ_i and ϕ_j is the corresponding points in Φ, then all the points defined by $\{(1-t)\phi_i + t\phi_j : t \in (0,1)\}$ lies in Φ.*

In view of the above observations, the following procedure is conducted making use of the neighbor information to construct the reconstruction data set of x_i, $\mathbf{S}_i$ $(i = 1, ..., N)$. To better sample the near neighbor and the outer data points, we propose an algorithm using an exponential format to gradually enlarge the range to find the reconstruction sample.

For a given point x_i, we can compute the distances from all other points around it. According to the distribution density function around x_i estimated before, we introduce α_i to describe the normalized density of the sample point x_i and is used to control the increment of the segment according to the sample points density for neighbor selection. We first give the definition of α_i by normalizing $\hat{p}_{x_i}$ using the estimated distribution density function computed by equation (3.1):

$$\alpha_i = \beta \cdot \frac{\hat{p}_{\max} - \hat{p}_{x_i}}{\hat{p}_{\max} - \hat{p}_{\min}} + \alpha_0 \tag{3.2}$$

where β is scaling constant, default value is set to 1.0; α_0 is the constant to be set.

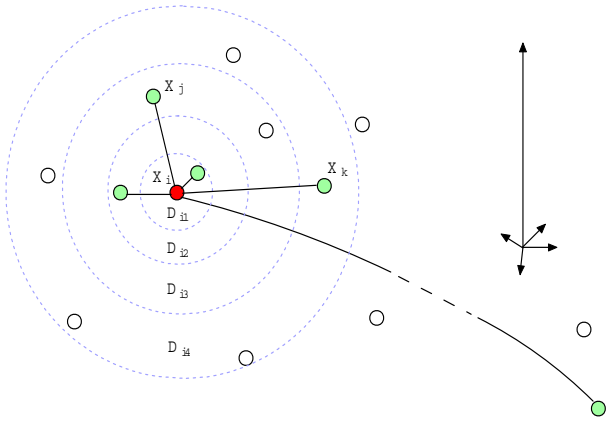

Figure 3.3: The neighbor selection process.

The discussion of this definition is given later.

According to the distances values from all other points to x_i, these points are rearranged in ascending order and stored in $\mathbb{R}_i$. Based on the estimated distribution density function, $\mathbb{R}_i$ is separated into several segments, where $\mathbb{R}_i = R_{i1} \cup R_{i2} \cup R_{i3} \ldots \cup R_{ik} \ldots \cup R_{iK}$. The range of each segment is given following an exponential format:

$$\begin{cases} \min(R_{ik}) = \ulcorner \alpha_i^k \urcorner \\ \max(R_{ik}) = \ulcorner \alpha_i^{k+1} \urcorner \end{cases} \tag{3.3}$$

where k is the index of segment and $\ulcorner \alpha_i^k \urcorner$ denotes the least upper bound integer when α_i^k is not an integer. A suitable range of α_i is set from 1.0 to 2.0 by setting $\alpha_0 = 1.0$.

For each segment R_{ik}, the mean distance from all points in this segment to x_i is calculated by:

$$\overline{d}_{ik} = \frac{1}{\max(R_{ik}) - \min(R_{ik})} \sum_j \|x_i - x_j\|^2, \forall\ j \in R_{ik} \tag{3.4}$$

To overcome the information redundancy problem, using the mean distance computed by equation (3.4), we find the most suitable point in R_{ik} to represent the contribution of all points in R_{ik} by minimizing the following cost equation:

$$\varepsilon(d) = \min\|\overline{d}_{ik} - x_j\|^2, \quad \forall\ j \in R_{ik} \tag{3.5}$$

To determine the number of neighbors to be used for further reconstruction and achieve adaptive neighbor selection, we can compute the mean distance from all other samples to x_i

$$\overline{d}_i = \frac{1}{N}\sum_{j=1}^{N}\|x_i - x_j\|^2, \quad i \neq j \tag{3.6}$$

Starting with the $\mathbf{S}_i$ computed above at given point x_i, from the largest element in $\mathbf{S}_i$, remove the element one by one until all elements in $\mathbf{S}_i$ is less than the mean distance $\overline{d}_i$ computed by equation (3.6). Then the neighbor set $\mathbf{S}_i$ for point x_i is fixed.

3.3.3 Calculate the Reconstruction Weights

The reconstruction weight W is used to rebuild the given point. To store the neighborhood relationship and reciprocal contributions to each other, the sets $\mathbf{S}_i$ (i = 1, 2, ..., N) are converted to a weight matrix $W = w_{ij}$ (i, j = 1, 2, ..., N). The construction weight W that best represents the given point x_i from its neighbor x_j is computed by minimizing the cost function given below:

$$\varepsilon(W) = \sum_{i}^{N}\|x_i - \sum_{j=\mathbf{S}_{i(1)}}^{\mathbf{S}_{i(n_j)}} w_{ij}x_j\|^2, \quad i \neq j \tag{3.7}$$

where the reconstruction weight w_{ij} represents the contribution of the jth data point to the ith point's reconstruction. The reconstruction weight w_{ij} is subjected to two constraints. First, each data point x_i is reconstructed only from its neighborhood set points, enforcing $w_{ij} = 0$ if x_j is not its neighbor. Second, the rows of

the weight matrix sum to one.

To compute W row by row, equation (3.7) can be further written as:

$$\begin{aligned}\varepsilon(W_i) &= \|x_i - \sum_{j=\mathbf{S}_{i(1)}}^{\mathbf{S}_{i(n_i)}} w_{ij}x_j\|^2, \quad i \neq j \\ &= \|\sum_{j=\mathbf{S}_{i(1)}}^{\mathbf{S}_{i(n_i)}} w_{ij}x_i - \sum_{j=\mathbf{S}_{i(1)}}^{\mathbf{S}_{i(n_i)}} w_{ij}x_j\|^2 \\ &= \sum_{j=\mathbf{S}_{i(1)}}^{\mathbf{S}_{i(n_i)}} w_{ij} \sum_{k=\mathbf{S}_{i(1)}}^{\mathbf{S}_{i(n_i)}} w_{ik}(x_i - x_j)^T(x_i - x_j) \end{aligned} \tag{3.8}$$

where W_i is the ith row of W. By defining a local covariance

$$C_i(j,k) = (x_i - x_j)(x_i - x_k)$$

combined with the constraint of W, we can apply Lagrange multiplier and have [60]:

$$\varepsilon(W_i) = \sum_{j=\mathbf{S}_{i(1)}}^{\mathbf{S}_{i(n_i)}} w_{ij} \sum_{k=\mathbf{S}_{i(1)}}^{\mathbf{S}_{i(n_i)}} w_{ik}C_i(j,k) + \eta_i(\sum_{j=\mathbf{S}_{i(1)}}^{\mathbf{S}_{i(n_i)}} w_{ij} - 1) \tag{3.9}$$

where η_i is the Lagrange coefficient. To obtain the minimum of ε, we can find the partial differentiation with respect to each weight and set it to zero

$$\frac{\partial\varepsilon(W_i)}{\partial w_{ij}} = 2\sum_{k=\mathbf{S}_{i(1)}}^{\mathbf{S}_{i(n_i)}} w_{ik}C_i(\mathbf{S}_i(j),k) + \eta_i = 0, \quad \forall j \in u_i \tag{3.10}$$

Rewrite equation (3.10) as

$$C \cdot W_i^T = q \tag{3.11}$$

where $C = \{C_{jk}\}(j,k = 1,...,n_i)$ is a symmetric matrix with dimension $n_i \times n_i$, $C_{jk} = C_i(\mathbf{S}_i(j), \mathbf{S}_i(k))$, and

$$W_i = [w_{i\mathbf{S}_i(1)}, w_{i\mathbf{S}_i(2)}, \cdots, w_{i\mathbf{S}_i(n_i)}], \tag{3.12}$$

$q = [q_1, q_2, \ldots, q_{n_i}]$ and $q_i = \eta_i/2$. If $n_i > l$, the covariance matrix C might be singular. When in such situation, we can modify the C a bit by $C = C + \mu I$, where μ is a small positive constant. Therefore, W_i can be obtained from equation (3.12)

$$W_i^T = C^{-1}q \tag{3.13}$$

The constrained weights of equation obey an important symmetry that they are invariant to rotation, resealing, and translation for any particular data point and its neighbors. Thus, W is a sparse matrix that contains the information about the neighborhood relationship represented spatially by the position of the non-zero elements in the weight matrix and the contribution of one node to another represented numerically by their values. The construction of $\mathbf{S}_i$ and W is detailed in Algorithm 1.

3.3.4 Computative Embedding of Coordinates

Finally, we find the embedding of the original data set in the low-dimensional space, e.g. l dimension. Because of the invariance property of reconstruction weights w_{ij}, the weights reconstructing the ith data point in m dimensional space should also reconstruct the ith data point in l dimensional space. Similarly, this is done by trying to preserve the geometric properties of the original space by selecting l dimensional coordinates y_i to minimize the embedding function given below:

$$\begin{aligned}
\Phi(Y) &= \sum_{i}^{N} \|y_i - \sum_{j=\mathbf{S}_{i(1)}}^{\mathbf{S}_{i(n_i)}} w_{ij} y_j\|^2 \\
&= \sum_{i}^{N} \|Y(I_i - W_i)\|^2 \\
&= \mathrm{tr}(Y(I_i - W_i)(Y(I_i - W_i))^T) \\
&= \mathrm{tr}(YMY^T)
\end{aligned} \tag{3.14}$$

Algorithm 1 W = NeighborFind(X)

Compute $\mathbf{D}$ from $\mathbf{X}$ ▷ $\mathbf{D}$=$\{d_{ij}\}$ is the distance matrix
Sort $\mathbf{D}$ along each column to form $\mathbb{D}$
for $i \leftarrow 1, N$ **do**
    for $k \leftarrow 1, K$ **do**
        if $\alpha^k < N$ **then**
            $\min(D_{ik}) = \ulcorner \alpha^k \urcorner + k - 1$
            $\max(D_{ik}) = \ulcorner \alpha^{k+1} \urcorner + k$
        else $\alpha^k > N$
            break
        end if
        $\overline{d}_{ik} \leftarrow \alpha, k, D_{ik}$ ▷ by solving equation(3.4)
        $x_j = \arg\min_{x_j \in D_{ik}} \|\overline{d}_{ik} - x_j\|^2$
        $\mathbf{S}_i = \mathbf{S}_i \cup \{x_j\}$
        $n_i = n_i + 1$
    end for
    $\overline{d}_i = \frac{1}{N} D_i$
    if $x_j > \overline{d}_i$ **then**
        $\mathbf{S}_i = \mathbf{S}_i - \{x_j\}$
        $n_i = n_i - 1$
    end if
end for

where w_{ij} are the reconstruction weights computed in Section 3.3.3, y_i and y_j are the coordinates of the point x_i and its neighbor x_j in the embedded space.

Equation (3.14) can be rearranged as the inner products, $(y_i \cdot y_j)$, we rewrite it as the quadratic form:

$$\Phi(Y) = \sum_{ij} m_{ij}(y_i \cdot y_j) \tag{3.15}$$

where $M = \{m_{ij}\}$ is an $N \times N$ matrix given by

$$m_{ij} = \delta_{ij} - w_{ij} - w_{ji} + \sum_k w_{ki} w_{kj} \tag{3.16}$$

and δ_{ij} is the Kronecker delta.

Equation (3.16) can be solved as an eigenvector problem by forcing the embedding outputs to be centered at the origin with the following constraint:

$$\sum_i y_i = 0 \tag{3.17}$$

To force the embedding coordinates to have unit covariance by removing rotational degree of freedom, the out products must satisfy:

$$\frac{1}{N} \sum_i y_i y_i^T = I \tag{3.18}$$

where I is the $d \times d$ identity matrix. Optimal embedding coordinates are given by the bottom $d + 1$ nonzero eigenvectors of M for the desired dimensionality.

The lower complexity of the embedded motion curve allows a rather simple geometric tool to analyze the curve in order to disclose significant points. In the next section, we explore the space of expression through the manifold of expression. The analysis of the relationships between different facial expressions will be facilitated on the manifold.

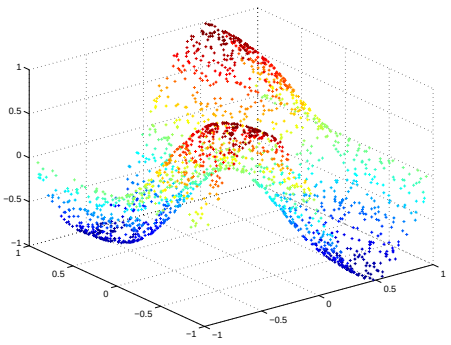

(a) Twopeaks

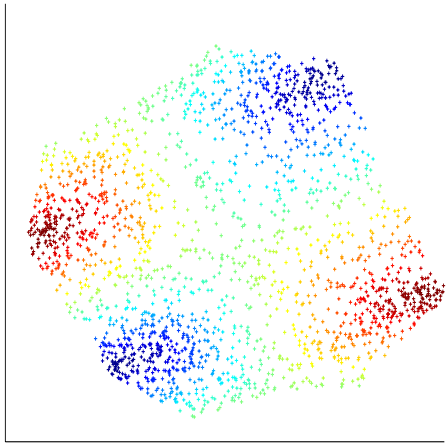

(b) LLE

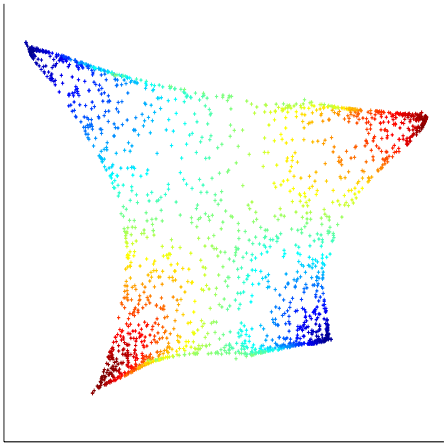

(c) NLE

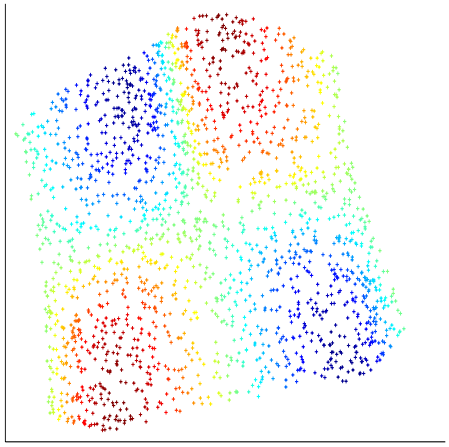

(d) DLLE

Figure 3.4: Twopeaks

3.4 LLE, NLE and DLLE comparison

For the comparison of the embedding property, we have conducted several manifold learning algorithms as well as several testing examples. Here we mainly illustrate three algorithms LLE, NLE and DLLE graphicly using two classical data sets: two peaks and punched sphere. For each data set, each method was used to obtain

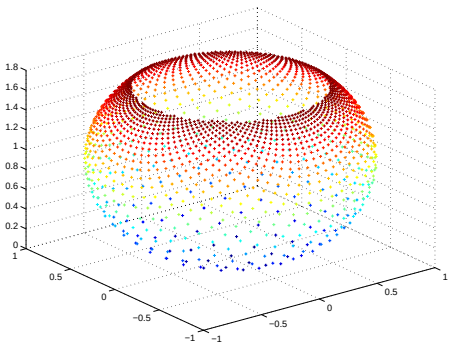

(a) Punched Sphere

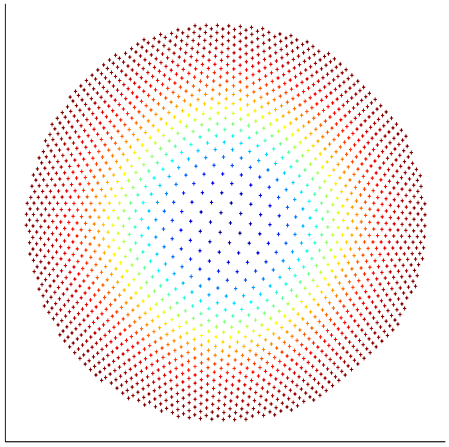

(b) LLE

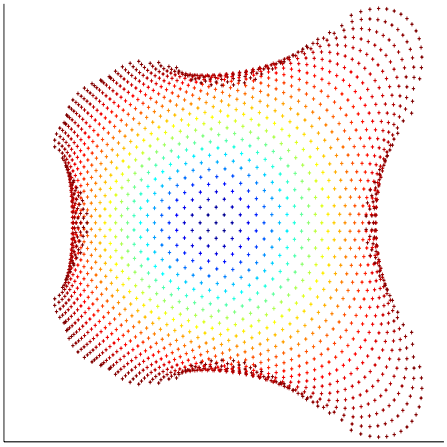

(c) NLE

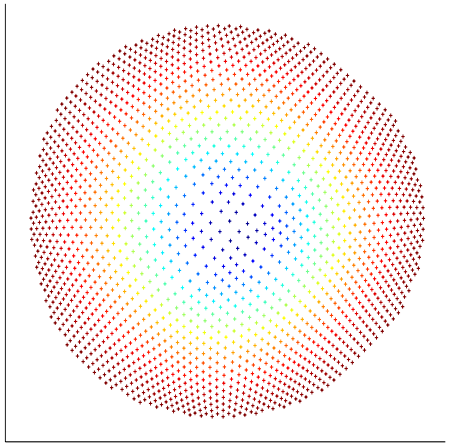

(d) DLLE

Figure 3.5: Punched sphere

a 2D embedding of the points. Figs. 3.4 and 3.5 summaries the results of these embedding results. The data set is shown at the top left, in a 3D representation. For the two peaks data set, two corners of a rectangular plane are bent up. Its 2D embedding should show a roughly rectangular shape with blue and red in opposite corners. The punched sphere is the bottom 3/4 of a sphere which is sampled non-uniformly. The sampling is densest along the top rim and sparsest on the bottom

of the sphere. Its intrinsic structure should be 2D concentric circles. Both the sample data sets were constructed by sampling 2000 points.

In Fig. 3.4, as expected, all the three algorithms can correctly embed the blue and red samples in opposite corners. However, the outline shape of the embedding using NLE is distorted when projected in 2D. DLLE can give a better preservation of the global shape of the original rectangle compared to LLE. At the same time, the green samples perform as the inner and outer boundary are also well kept using DLLE.

As can be seen in Fig. 3.5, both DLLE and LLE are successful in flattening the punched sphere and recover all the original concentric circles. NLE seems to be confused about the heavy point density around the rim. It can preserve the inner circles well but fails on the outer circle because of its neighbors selection criterion.

Chapter 4

Facial Expression Energy

Each person has his/her own maximal intensity of displaying a particular expression. There is a maximal energy pattern for each person for their respective facial expression. Therefore, facial expression energy can be used for classification by adjusting the general expression pattern to a particular individual according to the individual's successful expression recognition results.

Matsuno et al. presented a method from an overall pattern of the face which is represented in a potential field activated by edges in the image for recognition [62]. In [22], Essa et al. proposed motion energy template where the authors use the physics-based model to generate spatio-temporal motion energy template for each expression. The motion energy is converted from muscles activations. However, the authors did not provide a definition for motion energy. At the same time, they only used the spatial information in their recognition pattern. In this thesis, we firstly give out a complete definition of facial expression potential energy and kinetic energy based on the facial features' movements information. A facial expression energy system is built up to describe the muscles' tension in facial expression for classification. By further considering different expressions' temporal

transition characteristics, we are able to pin-point the actual occurrence of specific expressions with higher accuracy.

4.1 Physical Model of Facial Muscle

Muscles are a kind of soft tissues that possess contractile properties. Facial surface deformation during an expression is triggered by the contractions of the synthetic facial muscles. The muscle forces are propagated through the skin layer and finally deform the facial surface. A muscle can contract more forcefully when it is slightly stretched. Muscle generates maximal concentric tension beyond its physiological range-at a length 1.2 times its resting length. Beyond this length, active tension decreases due to insufficient sarcomere overlap. To simulate muscle forces and the dynamics of muscle contraction, mass-spring model is typically utilized [63, 64, 65]. Waters and Frisble [66] proposed a two-dimensional mass-spring model of the mouth with the muscles represented as bands.

A mass-spring model used to construct a face mask is shown in Fig. 4.1 [67]. Each node in the model is regarded as a particle with mass. The connection between two nodes is modeled by a spring. The spring force is proportional to the change of spring length according to the Hooke's law. The node in the model can move to the position until it arrives at the equilibrium point.

The facial expression energy is computed by "compiling" the detailed, physical model of facial feature movements into a set of biologically motion energy. This

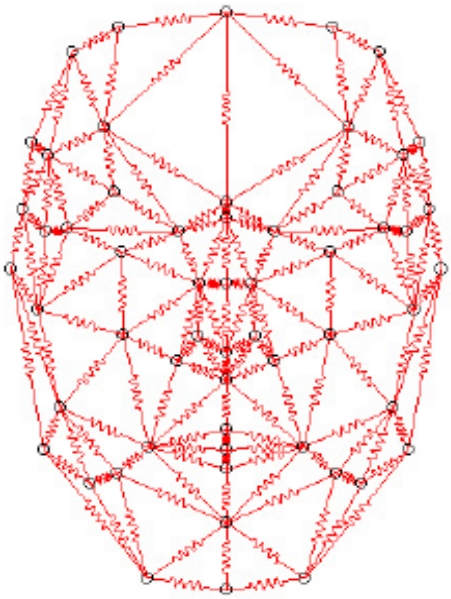

Figure 4.1: The mass spring face model [67].

method takes advantage of the optical flow which tracks the feature points' movements information. For each expression, we use the facial feature movements information to compute the typical pattern of motion energy. These patterns are subsequently used for expression recognition.

4.2 Emotion Dynamics

Fig. 4.2 shows some preprocessed and cropped example images for a happy expression. As illustrated in the example, all acquired sequences start from the neutral state passing into the emotional state and end with a neutral state.

One common limitation of the existing works is that the recognition is performed by using static cues from still face images without considering the temporal behavior of facial expressions. The psychological experiments by Bassili [52] have suggested that facial expressions are more accurately recognized from a dynamic

(a) Frame 1 (b) Frame 4 (c) Frame 7

(d) Frame 10 (e) Frame 13 (f) Frame 16

(g) Frame 19 (h) Frame 22 (i) Frame 25

(j) Frame 28 (k) Frame 31 (l) Frame 34

Figure 4.2: Smile expression motion starting from the neutral state passing into the emotional state

image than from a single static image. The temporal information often reveals information about the underlying emotional states. For this purpose, our work concentrates on modeling the temporal behavior of facial expressions from their dynamic appearances in an image sequence.

The facial expression occurs in three distinct phases which can be interpreted as the beginning of the expression, the apex and the ending period. Different facial expressions have their unique spacial temporal patterns at these three phases. These movement vectors are good features for recognition.

Fig. 4.3 shows the temporal curve of one mouth point of smile expression. According to the curve shape, there are three distinct phrases: starting, apex and ending. Notice that the boundary of the these three stages are not so distinct in some cases. When there is a prominent change in the curve, we can set that as the boundary of a phrase.

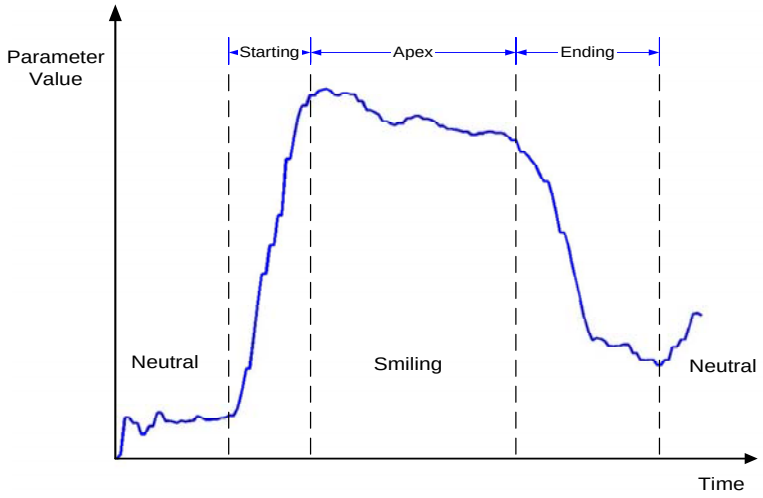

Figure 4.3: The temporal curve of one mouth point in smile expression. Three distinct phases: starting, apex and ending.

4.3 Potential Energy

Expression potential energy is the energy that is stored as a result of deformation of a set of muscles. It would be released if a facial expression in a facial potential field was allowed to go back from its current position to an equilibrium position (such as the neutral position of the feature points). The potential energy may be defined as the work that must be done in the facial expression, the muscles' force so as to achieve that configuration. Equivalently, it is the energy required to move the feature point from the equilibrium position to the given position. Considering the contractile properties of muscles, this definition is similar to the elastic potential energy. It is defined as the work done by the muscle's elastic force. For example, the mouth corner extended at the extreme position has greater facial potential energy than the same corner extended a bit. To move the mouth corner to the extreme position, work must be done, with energy supplied. Assuming perfect efficiency (no energy losses), the energy supplied to extend the mouth corner is exactly the same as the increase of its facial potential energy. The mouth corner's potential energy can be released by relaxing the facial muscle when the expression is to the end. As the facial expression fades out, its potential energy is converted to kinetic energy.

For each expression, there is a typical pattern of muscle actuation. The corresponding feature movement pattern can be tracked and determined using optical flow analysis. Typical pattern of motion energy can be generated and associated with each facial expression. This results in a set of simple expression "detectors" each of which looks for the particular space-time pattern of motion energy associated with each facial expression.

According to the captured features' displacements using Lucas and Kanade(L-K)

optical flow method, we can define potential energy E_p at time t as:

$$\begin{aligned} E_p(p_i, t) &= \frac{1}{2}\, k_i\, f_i(t)^2 \\ &= \frac{1}{2}\, k_i\, (D_{iNeutral} - D_i(t))^2 \end{aligned} \tag{4.1}$$

- $f_i(t)$ is the distance between p_i and p_j at time t defined in Table 2.3, expressed in **m**.

- $k_{i,j}$ is the the muscle's constant parameter (a measure of the stiffness of the muscle) linking p_i and p_j, expressed in **N/m**.

The nature of facial potential energy is that the equilibrium point can be set like the origin of a coordinate system. That is not to say that it is insignificant; once the zero of potential energy is set, then every value of potential energy is measured with respect to that zero. Another way of saying it is that it is the change in potential energy which has physical significance. Typically, the neutral position of a feature point is considered to be an equilibrium position. The potential energy is proportional to the distance from the neutral position. Since the force required to stretch a muscle changes with distance, the calculation of the work involves an integral. The equation (4.1) can be further written as follows with $E_p(p_i) = 0$ at the neutral position:

$$\begin{aligned} E_p(p_i, t) &= -\int_{\vec{r}=0}^{\vec{r}} -k_i \vec{r}\, d\vec{r} \\ &= -\left(\int_0^x -k_i x\, dx + \int_0^y -k_i y\, dy \right) \end{aligned} \tag{4.2}$$

Potential energy is energy which depends on mutual positions of feature points. The energy is defined as a work against an elastic force of a muscle. When the face is at the neutral state and all the facial features are located at its neutral state, the potential energy is defined as zero. With the change of displacements of the

feature points, the potential energy will change accordingly.

The potential energy can be viewed as a description of the muscle's tension state. The facial potential energy is defined with an upper-bound. That means there is a maximum value when the feature points reach their extreme positions. It is natural to understand because there is an extreme for the facial muscles's tension. When the muscle's tension reaches the apex, the potential energy of the point associated with the muscle will reach its upper-bound. For each person, the facial muscle's extreme tension is different. The potential motion energy varies accordingly.

Each person has his/her own maximal intensity to display a particular expression. Our system can start with a generic expression classification and then adapt to a particular individual according to the individual's successful expression recognition results.

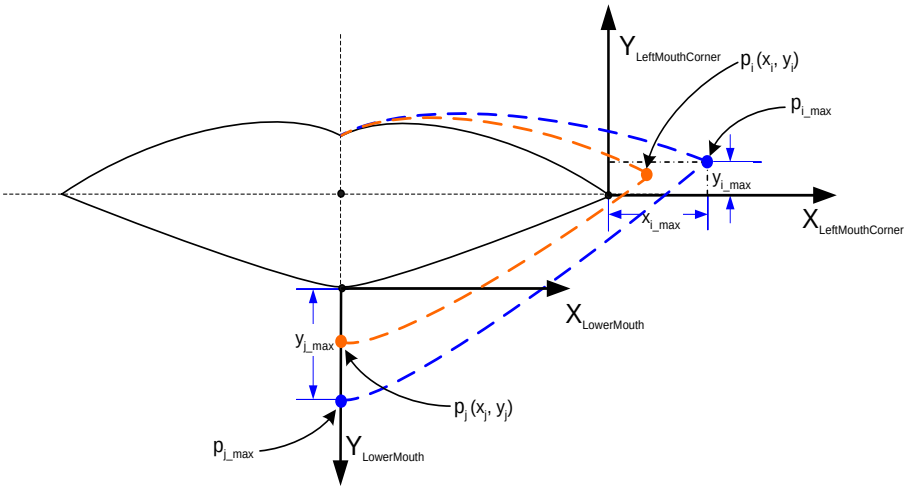

Figure 4.4: The potential energy of mouth points.

Fig. 4.4 shows the potential energy of two points: the left mouth corner and the

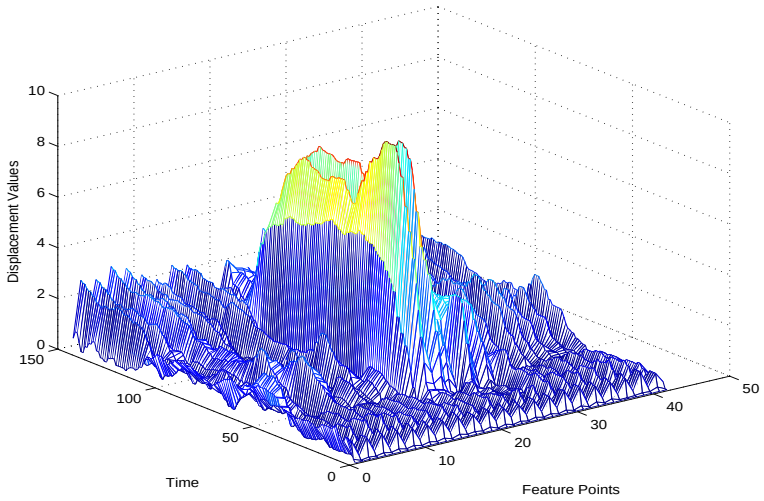

Figure 4.5: The 3D spatio-temporal potential motion energy mesh of the smile expression.

lower mouth. The black contour represents the mouth at its neutral position, the blue dash line represents mouth's extreme contour while the orange dash line is mouth contour at some expression. For the left mouth corner, we define a local coordinate that could be used for the computation of potential energy. The extreme point of the muscle tension is represented by E_{pi_max}. At this position, this feature point E_{pi} has the largest potential energy computed along the X-axis and Y-axis. When this feature point located between the neutral position and the extreme position, as illustrated of E_{pi}, its corresponding potential energy can be computed following equation (4.2). The same rule can also applied to the lower mouth point. According to the nature of human month structure, the movement of this feature point is mostly limited along the Y-axis.

At the neutral state, all the facial features are located at their equilibrium positions. Therefore, the potential energy is equal to zero. When one facial expression reaches its apex state, its potential energy reaches the largest value. When the

expression is at the ending state, the potential energy will decrease accordingly. Fig. 4.5 shows the 3D spatio-temporal potential motion energy mesh of the smile expression.

For each facial expression pattern, there are great varieties in the feature points' movements. Therefore, the potential energy value varies spatially and temporally. When an expression reaches its apex state, the potential value will also reach its maximum. Therefore, the pattern can be classified accordingly.

4.4 Kinetic Energy

Kinetic energy is defined as a work of the force accelerating a facial feature points. It is the energy that a feature point possesses as a result of facial motion. It is a description energy.

Our system not only considers the displacement of the feature points in one direction, but also takes the velocity into account as movements pattern for analysis. The velocity of each feature points is computed frame by frame. It is natural that the feature points remain nearly static in the initial and apex state. During the change of the facial expressions, the related feature points' movements are fast. By analyzing the moving features' velocity, we can find the cue of a certain emotion.

According to the velocity obtained from equation (5.16), we can define kinetic energy E_k as:

$$E_k(p_i, t) = \frac{1}{2} w_i \|v_i\|^2 \tag{4.3}$$

where w_i denote the i^{th} feature point's weight, v_i is the velocity for point i.

For each facial expression pattern, it will occur from the starting, translation and vanishing. At the neutral state, since the face is static, the kinetic energy is nearly zero. When the facial expression is at the starting state, the feature points are moving fast, the kinetic energy will vary temporally–increase first and decrease later. During this state, the muscle's biological energy is converted to feature points' kinetic energy. The kinetic energy is converted to feature points' potential energy. When an expression reaches its apex state, the kinetic energy will decrease to a stable state. If the facial muscle is still then, the kinetic energy will decrease to zero. At this time, the potential energy will reach to its apex. When the expression is at the ending state, feature points will move back to the neutral positions. Therefore, the kinetic energy will increase first and decrease later again. By analyzing and setting a set of rules, associated with the potential energy value, the pattern can be classified accordingly.

At the same time, the feature points' movement may temporally differ a lot when an expression occur, e.g. when someone is angry, he may frown first and then extend his mouth. Therefore, the kinetic energy for each feature points may not reach the apex concurrently.

We use a normalized dot product similarity metric to compare the differences between facial expressions. A simple form of similarity metric is the dot product between two vectors. We employ a normalized dot product as a similarity metric. Let X_i be the ith feature of the facial expression vector for expression X. Let the normalized feature vector, be defined as

$$\bar{X}_i = \frac{X_i}{\sqrt{\sum_j^m X_j^2}} \tag{4.4}$$

where m is the number of elements in each expression vector. The similarity between two facial expression vectors, X and Y, for the normalized dot product is defined to be $\bar{X} \cdot \bar{Y}$, the dot product on the normalized feature vectors.

Chapter 5

Facial Expression Recognition

Most of the researches on automated expression analysis perform an emotional classification. Once the face and its features have been perceived, the next step of an automated expression analysis system is to recognize the facial expression conveyed by the face. A set of categories of facial expression, defined by Ekman, is referred as the six basic emotions [23]. It is based on the cross culture study on existence of "universal categories of emotional expressions", the most known and most commonly used study on the facial expression classification.

To achieve automating facial expression emotional classification is difficult for a number of reasons. Firstly, there is no uniquely defined description either in terms of facial actions or in terms of some other universally defined facial codes. Secondly, it should be feasible to classify the multiple facial expressions. FACS is the well known study on describing all visually distinguishable facial movements [23].

Based on the selected person-dependent facial expression images in a video, DLLE is utilized to project the high dimensional data into the low dimensional embedding. After the embedding of input images are represented in a lower dimension,

SVM is employed for static person-dependent expression classification.

For the person independent expression recognition, facial expression motion energy is introduced to describe the facial muscle's tension during the expressions. This method takes advantage of the L-K optical flow which tracks the feature points' movement information.

5.1 Person Dependent Recognition

In this section, we make use of the similarity of facial expressions appearance in low-dimensional embedding to classify different emotions. This method is based on the observation(arguments) that facial expression images define a manifold in the high-dimensional image space, which can be further used for facial expression analysis. On the manifold of expression, similar expressions are points in the local neighborhood while different expressions separate apart. The similarity of expressions depends greatly on the appearance of the input images. Since different people have great varieties in their appearances, the difference of facial appearance will overcome the discrimination caused by different expressions. It is a formidable task to group the same expression among different people by several static input images. However, for a certain person, the difference caused by different expressions can be used as the cues for classification.

As a result of the process, for each expression motion sequence, only one image during the apex of expression is selected for the corresponding reference set. These selected images of different expressions are used as inputs of a nonlinear dimension reduction algorithm. Static images taken at the expressions can also be employed. Fig. 5.2 shows the result of projecting our training data (set of facial shapes) in

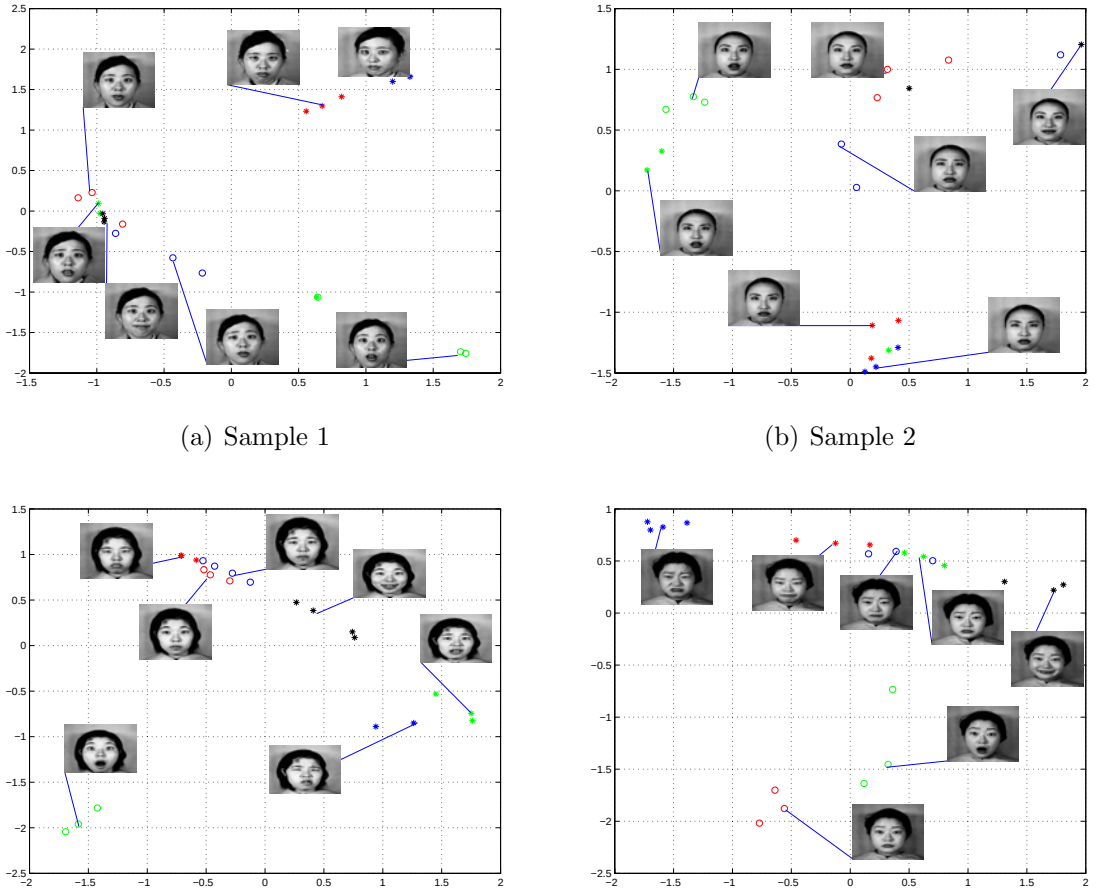

(a) Sample 1

(b) Sample 2

(c) Sample 3

(d) Sample 4

Figure 5.1: The first two coordinates of DLLE of some samples of the JAFFE database.

a two dimensional space using DLLE, NLE and LLE embedding. In this space, images which are similar are projected with a small distance while the images that differ greatly are projected with a large distance. The facial expressions are roughly clustered. The classifier works on a low-dimensional facial expression space which is obtained by DLLE, LLE and NLE respectively. Each image is projected to a six dimensional space. For the purpose of visualization, we can map the manifold onto its first two and three dimensional space.

As illustrated in Fig. 5.1, according to the DLLE algorithm, neighborhood relationship and global distribution can be preserved in the low dimension data set. The distances between the projected data points in low dimension space depend on the similarity of the input images. Therefore, images of the same expression are comparatively closer than images of different expressions in low dimension space. At this time, the training samples of the same expressions are "half clustered" and only a few of them may be apart from their corresponding cluster. This makes it easier for the classifier to categorize different emotions. Seven different expressions are represented by: anger, red star; disgust, blue star; fear, green star; happiness, black star; neutral, red circle; sadness, blue circle; surprise, green circle.

In Fig. 5.2, we compare the property of the DLLE, NLE and LLE after the sample images are mapped to low dimension. The projected low dimension data should keep the separating features of the original images. Images of the same expression should cluster together while different ones should be apart. Fig. 5.2 compares the two dimensional embeddings obtained by DLLE, NLE and LLE for 23 samples of one person from seven expressions respectively. We can see from Fig. 5.2(a) that for $d = 2$, the embedding of DLLE separates the seven expressions well. Samples of the same gesture clustered together while only a few different gesture samples are overlapped. Fig. 5.2(b) shows that the embedding of NLE can achieve similar result as DLLE. The LLE is very sensitive to the selection of number of nearest neighbors. The images of different expressions become mixed up easily when we increase the number of nearest neighbors as shown in Fig. 5.2(c) and Fig. 5.2(d).

Fig. 5.3 compares the three dimensional embeddings obtained by DLLE, NLE and LLE for 22 samples of one person from seven expressions respectively. From Fig. 5.3(a) we can see that for $d = 3$, the embedding of DLLE can keep the similarity of

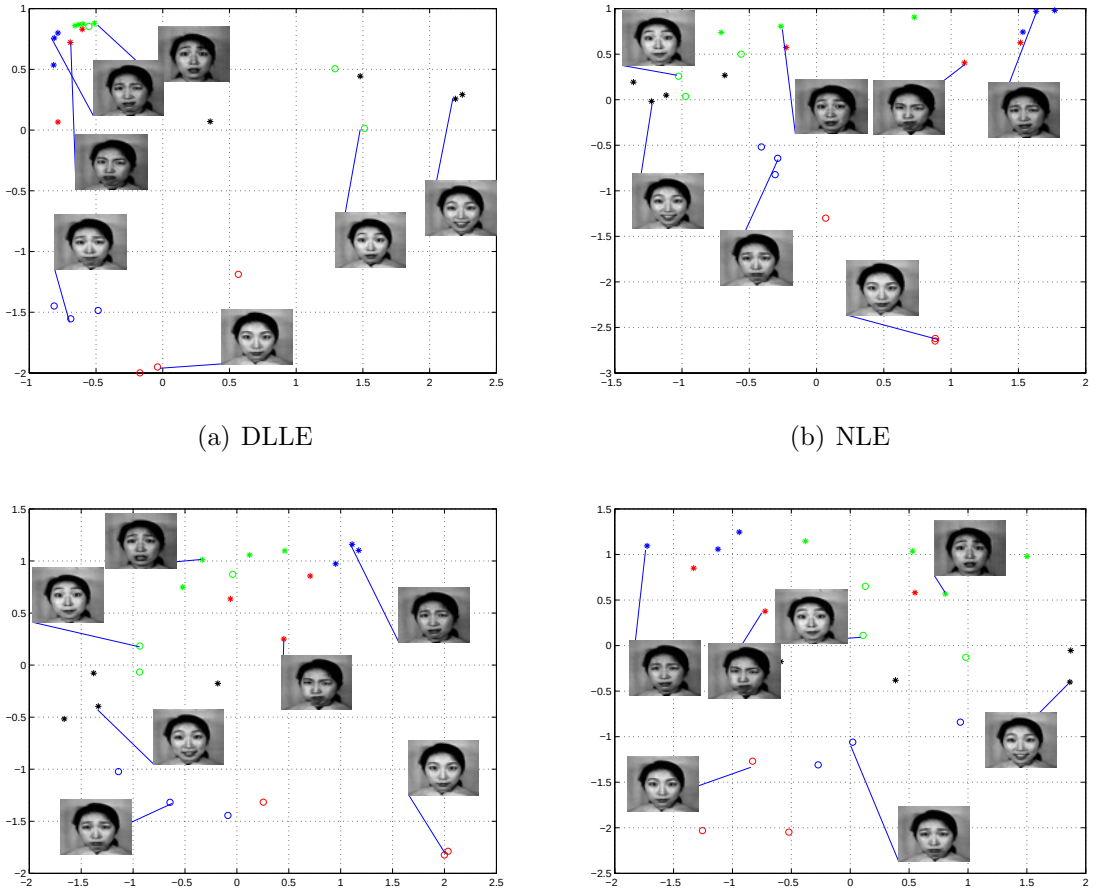

(a) DLLE (b) NLE

(c) LLE (K=6) (d) LLE (K=8)

Figure 5.2: 2D projection using different NDR methods.

each expression samples and preserve the seven expressions clusters well in three dimensional space. As seen in Fig. 5.3(b), some classes of the projected samples points by NLE are not as wide spread as DLLE. As shown in Fig. 5.3(c), some classes are mixed up when K = 6 in the LLE embedding. The embedding of LLE is similar as DLLE when K = 8 as shown in Fig. 5.3(d).

Based on the distances computed in low-dimensional space, we can use the neural network to classify different gesture images. SVM, KNN and PNN can be then

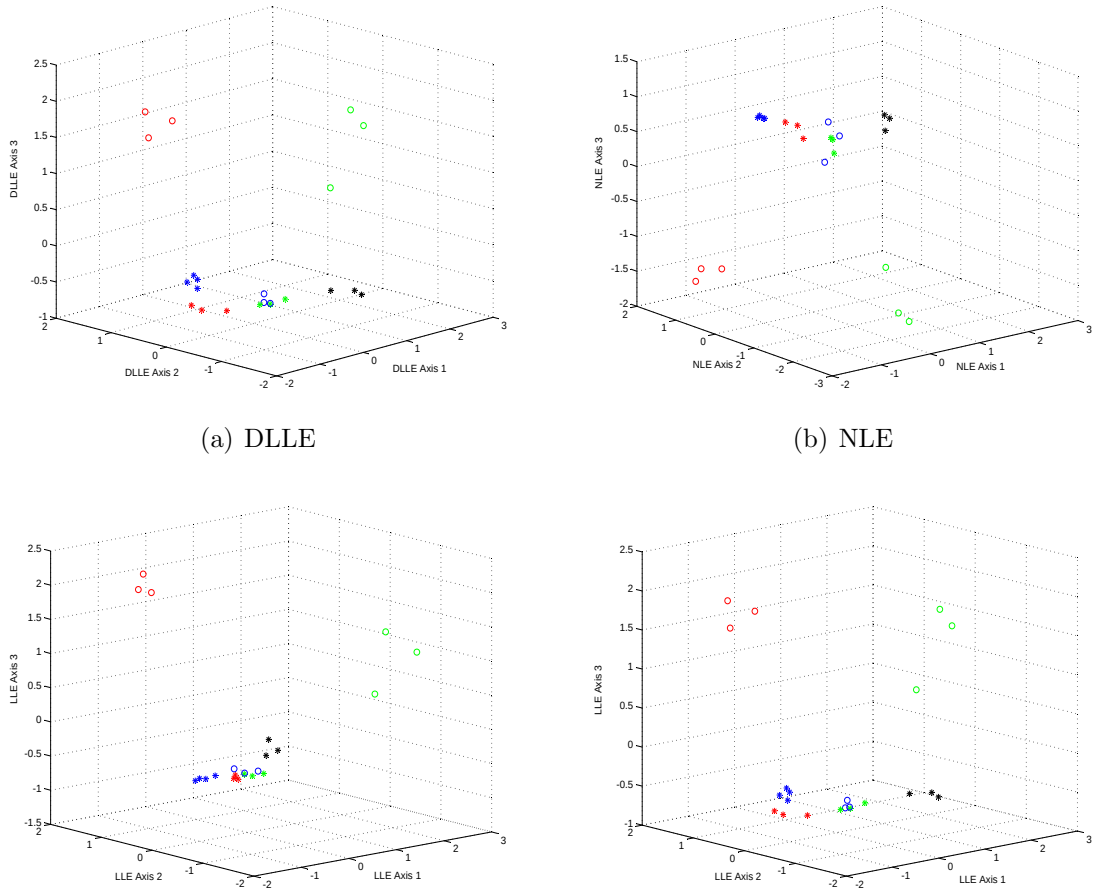

(a) DLLE (b) NLE

(c) LLE (K=6) (d) LLE (K=8)

Figure 5.3: 3D projection using different NDR methods.

employed as the classifier to group the samples. SVM is selected in our system as the classifier because of its rapid training speed and good accuracy.

5.1.1 Support Vector Machine

Support vector machines (SVM), which is a very effective method for general purpose pattern recognition, has been developed by Vapnik and is gaining popularity due to many attractive features, and promising empirical performance [68]. It is particularly a good tool to classify a set of points which belong to two or more

classes. It is based on statistical learning theory and attempts to maximize the margin to separate different classes. SVM uses the hyperplane that separates the largest possible fraction of points of the same class on the same side, while it maximizes the distance of either class from the hyper-plane. Hence there is only the inner product involved in SVM, learning and predicting is much faster than a multilayer neural network. Compared with traditional methods, SVM has advantages in selecting model, overcoming over-fitting and local minimum, etc. SVM is based on the Structural Risk Minimization (SRM) principle that minimizes an upper bound on the expected risk.

When a linear boundary is inappropriate in low dimensional space, SVM can map the input vector into a high dimensional feature space by defining a non-linear mapping. SVM can construct an optimal linear separating hyperplane in this higher dimensional space. Since our DLLE is a nonlinear dimension reduction method, there is no need to perform the mapping into high dimensional feature space. It can be simply achieved by increasing the projected low dimension.

The classification problem can be restricted to consideration of the two-class problem without loss of generality. Multi-class classification problem can be solved by a decomposition into several binary problems.

Consider the problem of separating the set of training vectors belonging to two separate classes, $\mathcal{D} = \{(x^1, y^1), \cdots, (x^l, y^l)\}$, $x^i \in \mathbb{R}^N, y^i \in \{-1, 1\}$ with a hyperplane

$$\mathbf{w} \cdot x + b = 0 \tag{5.1}$$

which satisfies the following constraints,

$$\begin{cases} \mathbf{w} \cdot x^i + b \geq 1, & y^i = 1 \\ \mathbf{w} \cdot x^i + b \leq 1, & y^i = -1 \end{cases} \tag{5.2}$$

These constraints can be combined into one set of inequalities:

$$y^i(\mathbf{w} \cdot x^i + b) \geq 1, i = 1, 2, \cdots, l. \tag{5.3}$$

The distance $d(w, b; x^j)$ of a point x^j from the hyperplane (w, b) is,

$$d(w, b; x^j) = \frac{|\mathbf{w} \cdot x^j + b|}{\|w\|} \tag{5.4}$$

The optimal hyperplane separating the data is given by maximizing the margin, ρ, subject to the constraints of equation (5.3). That is minimizing the reciprocal of the margin. The margin is given by,

$$\rho(w, b) = \frac{2}{\|w\|} \tag{5.5}$$

The problem now is a quadratic programming optimization problem.

$$\begin{aligned} & \min \frac{1}{2}\|w\|^2 \\ s.t. \quad & y^i(\mathbf{w} \cdot x^i + b) \geq 1, i = 1, 2, \cdots, l. \end{aligned} \tag{5.6}$$

If there exists no hyperplane that can split the "yes" and "no" examples, the Soft Margin method will choose a hyperplane that splits the examples as clean as possible, while still maximizing the distance to the nearest cleanly split examples. This method introduces non-negative slack variables and the equation (5.6) now transforms to

$$\begin{aligned} & \min \frac{1}{2}\|w\|^2 + C\sum_{i=1}^{l} \xi_i \\ s.t. \quad & y^i(\mathbf{w} \cdot x^i + b) \geq 1 - \xi_i, \quad \xi_i \geq 0, \quad i = 1, 2, \cdots, l. \end{aligned} \tag{5.7}$$

where C is a penalty parameter. This quadratic programming optimization can be solved using Lagrange multipliers.

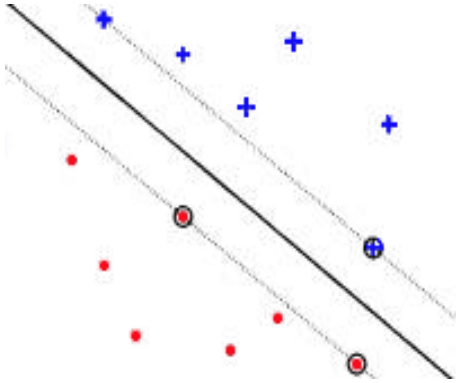

Figure 5.4: Optimal separating hyperplane.

The set of vectors is said to be optimally separated by the hyperplane if it is separated without error and the distance between the closest vector to the hyperplane is maximal.

The multi-class classification problem can be solved by a decomposition where the multi-class problem is decomposed into several binary problems. Several binary classifiers have to be constructed or a larger optimization problem is needed. It is computationally more expensive to solve a multi-class problem than a binary problem with the same number of samples. Vapnik proposed a one-against-rest (1-a-r) algorithm [68]. The basic idea for the formulation to solve multi-class SVM problem can be expressed differently: the problem can be written as "class A against the rest, class B against the rest, and ...". It is equivalent for each class that "class n against the rest" for the N binary classification problem. The reduction to binary problems can be interpreted geometrically as searching N separating hyperplanes.

The ith SVM is trained with all of the examples in the ith class with positive labels while all other examples with negative labels. Given N training data $(x_1, y_1), (x_2, y_2), \ldots, (x_N, y_N)$, where $x_i \in R^n$, $i = 1, 2, \ldots, N$ and $y_i \in 1, 2, \ldots, k$ is the class of x_i, the ith SVM solves the following problem:

$$\begin{aligned} \min_{w^i, b^i, \xi^i} \quad & \frac{1}{2}\|w\|^2 + C\sum_{i=1}^{l} \xi_i^j \\ s.t. \quad & y^i(\mathbf{w} \cdot x^i + b^i) \geq 1 - \xi_i^j, \text{if} \;\; y^i = j \\ & y^i(\mathbf{w} \cdot x^i + b^i) \leq -1 + \xi_i^j, \text{if} \;\; y^i \neq j \\ & \xi_i^j \geq 0, \quad i = 1, 2, \cdots, l. \end{aligned} \tag{5.8}$$

When the data set is not separable, the penalty term $C\sum_{i=1}^{l} \xi_i^j$ is used to reduce the training errors. As the solution of equation (5.8), there will be k decision functions listed below:

$$\begin{aligned} & y^1(\mathbf{w} \cdot x^1 + b^1) \\ & \vdots \\ & y^k(\mathbf{w} \cdot x^k + b^k) \end{aligned} \tag{5.9}$$

If class i has the largest value computed by the following decision function with x, x is classified into class i.

$$\text{class of } x = \arg\max_{i=1,2,\ldots,k} y^i(\mathbf{w} \cdot x^i + b^i) \tag{5.10}$$

The dual problem of equation (5.8) can be solved when the variables are the same as the number of data. A more detailed description of SVM can be found at [69]. Therefore, after the SVM is conducted, the data set can be classified into several classes. As shown in the experiments, the SVMs can be effectively utilized for facial expression recognition.

5.2 Person Independent Recognition

Although person dependent method can reach satisfactory results, it required a set of pre-captured expression samples. It is conducted off-line, which is hard to apply on real-time on-line classification. Most of the existing methods are not conducted in real-time [43, 70]. A general method is needed which can recognize facial expressions of different individuals without the training sample images. By analysis of facial movements pattern captured by optical flow tracker, a recognition system based on facial expression motion energy is set up to recognize expressions in real-time.

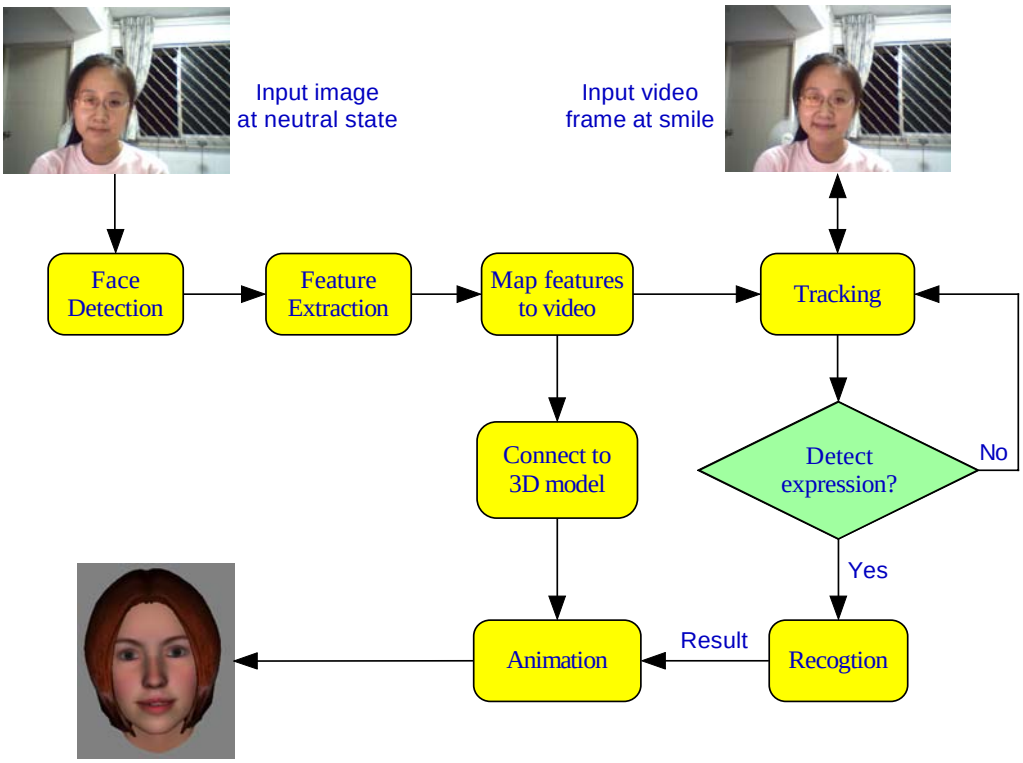

Figure 5.5: The framework of our tracking system.

5.2.1 System Framework

Fig. 5.5 shows the framework of our recognition system. At the initiation stage, the face image at neutral state is captured. This image is processed in our system to do face detection, facial features extraction. After the facial features are detected, they are mapped back to the real-time video. The tester's face should keep static during this process. At the same time, the connection with the 3D animation window is set up. These facial features are tracked by L-K optical flow in real-time. The captured information is processed frame by frame. Once a facial expression is detected, either the recognition result or the FAP stream is sent to the animation part. The 3D virtual avatar will display the recognized expression accordingly.

5.2.2 Optical Flow Tracker

Once a face has been located and the facial features are extracted in the scene by the face tracker, we adopt the optical flow algorithm to determine the motion of the face. The face motion information can be used for the purposes of classification. Firstly, expressions are inherently dynamic events. Secondly, by using motion information, the task is simplified as it ignores variations in the texture of different people's faces. Hence, the facial motion patterns is independent of person who is expressing the emotion. At the same time, facial motion alone has already been shown to be a useful cue in the field of human face recognition. There is a growing argument that the temporal information is a critical factor in the interpretation of facial expressions [32]. Essa et al. examined the temporal pattern tracked by optical flow of different expressions but did not account for temporal aspects of facial motion in their recognition feature vector [33].

The optical flow methods attempt to calculate the motion between two adjacent image frames which are taken at times t and $t + \delta t$ at every pixel position. The tracker, based on the Lucas-Kanade tracker [37], is capable of following and recovering any of the 21 facial points lost due to lighting variations, rigid or non-rigid motion, or (to a certain extent) change of head orientation. Automatic recovery, which uses the nostrils as a reference, is performed based on some heuristics exploiting the configuration and visual properties of faces.

As a pixel at location (x, y, z) at time t with intensity $I(x, y, z, t)$ will have moved by $\delta x, \delta y, \delta z$ after time slide δt between the two frames, a translational model of motion can be given:

$$I_1(x) = I_2(x + \delta x) \tag{5.11}$$

Let Δt be a small increment in time. Let t be the time at which the first image is taken, and at time $t + \Delta t$ the second image is taken. Then for the first image, we have $I_1(\mathbf{x}) = I(\mathbf{x}(t), t)$, and for the second image, we have $I_2(\mathbf{x}) = I(\mathbf{x}(t + \Delta t), t + \Delta t)$. Following image constraint equation, it can be given:

$$I(\mathbf{x}(t), t) = I(\mathbf{x}(t) + \Delta\mathbf{x}(t), t + \Delta t) \tag{5.12}$$

Note that we have removed the subscripts from the expression and have expressed it purely in terms of displacements in space and time. Assuming the movement to be small enough, we can develop the image constraint at $I(\mathbf{x}(t), t)$ with Taylor series to get:

$$I(\mathbf{x}(t) + \Delta\mathbf{x}(t), t + \Delta t) = I(\mathbf{x}(t), t) + \Delta x \frac{\partial I}{\partial x} + \Delta y \frac{\partial I}{\partial y} + \Delta t \frac{\partial I}{\partial t} + H.O.T$$

where H.O.T. means higher order terms, which are small enough to be ignored. Since we have assumed brightness constancy, the first order Taylor series terms

must vanish:

$$\Delta x \frac{\partial I}{\partial x} + \Delta y \frac{\partial I}{\partial y} + \Delta t \frac{\partial I}{\partial t} = 0 \tag{5.13}$$

Dividing equation (5.13) by an instant of time Δt, we have

$$\frac{\Delta x}{\Delta t}\frac{\partial I}{\partial x} + \frac{\Delta y}{\Delta t}\frac{\partial I}{\partial y} + \frac{\Delta t}{\Delta t}\frac{\partial I}{\partial t} = 0 \tag{5.14}$$

which results in:

$$u \frac{\partial I}{\partial x} + v \frac{\partial I}{\partial x} + I_t = 0 \tag{5.15}$$

or

$$(\nabla I)^\top \mathbf{u} + I_t = 0 \tag{5.16}$$

where $\mathbf{u} = (u, v)^\top$ denotes the velocity.

Equation (5.16) is known as the Horn-Schunck (H-S) equation. The H-S equation holds for every pixel of an image. The two key entities in the H-S equation are the spatial gradient of the image, and the temporal change in the image. These can be calculated from the image, and are hence known. From these two vectors, we want to find the velocity vector which, when dotted with the gradient, is cancelled out by the temporal derivative. In this sense, the velocity vector "explains" the temporal difference measured in I_t in terms of the spatial gradient. Unfortunately this equation has two unknowns but we have only one equation per pixel. So we cannot solve the H-S equation uniquely at one pixel.

We will now consider a least squares solution proposed by Lucas and Kanade (1981) (L-K). They assume a translational model and solve for a single velocity vector $\mathbf{u}$ that approximately satisfies the H-S equation for all the pixels in a small neighborhood $\mathcal{N}$ of size $N \times N$. In this way, we obtain a highly over-constrained system of equations, where we only have 2 unknowns and N^2 equations.

Let $\mathcal{N}$ denote a $N \times N$ patch around a pixel $\mathbf{p}_i$. For each point $\mathbf{p}_i \in \mathcal{N}$, we can write:

$$\nabla I(\mathbf{p}_i)^\top \mathbf{u} + I_t(\mathbf{p}_i) = 0 \tag{5.17}$$

Thus we arrive at the over-constrained least squares problem, to find the $\mathbf{u}$ that minimizes $\Psi(\mathbf{u})$:

$$\Psi(\mathbf{u}) = \sum_{\mathbf{p}_i \in \mathcal{N}} [\nabla I(\mathbf{p}_i)^\top \mathbf{u} + I_t(\mathbf{p}_i)]^2 \tag{5.18}$$

Due to the presence of noise and other factors (like, hardly ever all points pixels move with the same velocity), the residual will not in general be zero. The least squares solution will be the one which minimizes the residual. To solve the over-determined system of equations we use the least squares method:

$$A^\top A\mathbf{u} = A^\top \mathbf{b} \quad or \tag{5.19}$$

$$\mathbf{u} = (A^\top A)^{-1} A^\top \mathbf{b} \tag{5.20}$$

where $A \in \mathbb{R}^{N^2 \times 2}$ and $\mathbf{b} \in \mathbb{R}^{N^2}$ are given by:

$$A = \begin{bmatrix} \nabla I(\mathbf{p}_1)^\top \\ \nabla I(\mathbf{p}_2)^\top \\ \vdots \\ \nabla I(\mathbf{p}_{N^2})^\top \end{bmatrix} \tag{5.21}$$

$$\mathbf{b} = \begin{bmatrix} I_t(\mathbf{p}_1) \\ I_t(\mathbf{p}_2) \\ \vdots \\ I_t(\mathbf{p}_{N^2}) \end{bmatrix} \tag{5.22}$$

This means that the optical flow can be found by calculating the derivatives of the image in all four dimensions.

One of the characteristics of the Lucas-Kanade algorithm, and that of other local optical flow algorithms, is that it does not yield a very high density of flow

vectors, i.e. the flow information fades out quickly across motion boundaries and the inner parts of large homogenous areas show little motion. Its advantage is the comparative robustness in presence of noise.

5.2.3 Recognition Results

Fig. 5.6 shows the facial features points(green spots) traced by optical flow method during a surprise expression. It is cut from a recorded video and illustrated frame by frame. It can greatly reduce the computation time to track of the specified limited number of feature points compared to track the holistic dense flow between successive image frames. As we can seen from these images, the feature points are tracked closely frame by frame using the L-K optical flow method. With these tracked position and velocity parameters, expression motion energy can be computed out and expression patterns can be recognized in real-time.

The results of real-time expression recognition are given in Fig. 5.7. The pictures are captured while the expression occurs. The recognition results are displayed in real-time in red at the up-left corner of the window. From these pictures, we can see that the proposed system can effectively detect the facial expressions.

(a) Frame 56 (b) Frame 57 (c) Frame 58

(d) Frame 59 (e) Frame 60 (f) Frame 61

(g) Frame 62 (h) Frame 63 (i) Frame 64

(j) Frame 65 (k) Frame 66 (l) Frame 67

(m) Frame 68 (n) Frame 69 (o) Frame 70

Figure 5.6: Feature tracked using optical flow method during a surprise expression

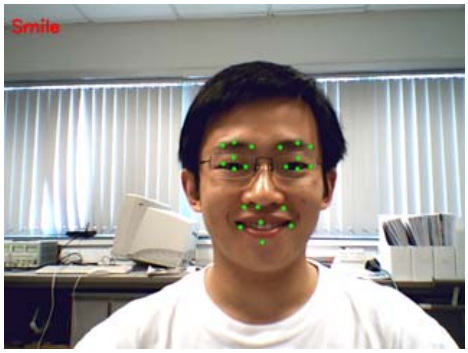

(a) happiness

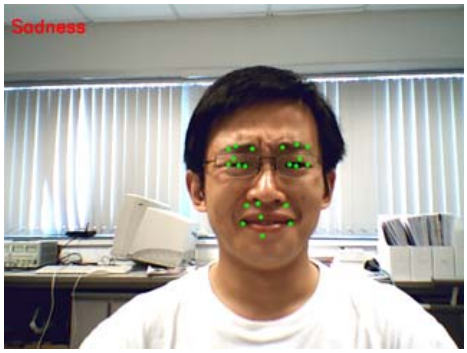

(b) sadness

(c) fear

(d) disgust

(e) surprise

(f) anger

Figure 5.7: Real-time video tracking results.

Chapter 6

3D Facial Expression Animation

In recent years, 3D talking heads have attracted the attention in both research and industry domains for developing intelligent human computer interaction system. In our system, a 3D morphable model, Xface, is applied to our face recognition system to derive multiple virtual character expressions. It is an open source, platform independent toolkit, which is developed using C++ programming language incorporating object oriented techniques, for developing 3D talking agents. It relies on MPEG-4 Face Animation (FA) standard. A 3D morphable head model is utilized to generate multiple facial expressions. When one facial expression occurs, the movements of tracked feature points are translated to MPEG-4 FAPs. The FAPs can describe the observed motion in a high level. The virtual model can follow the human's expressions naturally. The virtual head also can talk using speech synthesis, another open source tool, Festival [71]. A full-automatic MPEG-4 compliant facial expression animation and talking pipeline was developed.

6.1 3D Morphable Models–Xface

The Xface open source toolkit [72] offers the XfaceEd tool for defining the influence zone of each FP. More specifically, each FP is associated with a group of points (non-FPs) in terms of animated movements. Xface also supports the definition of a deformation function for each influence zone and this function computes the displacement of a point as influenced by its associated FP during animation. Hence, a given MPEG-4 FAP values stream, together with corresponding FAP durations can be rendered as influence zones of animated position coordinates in a talking avatar.

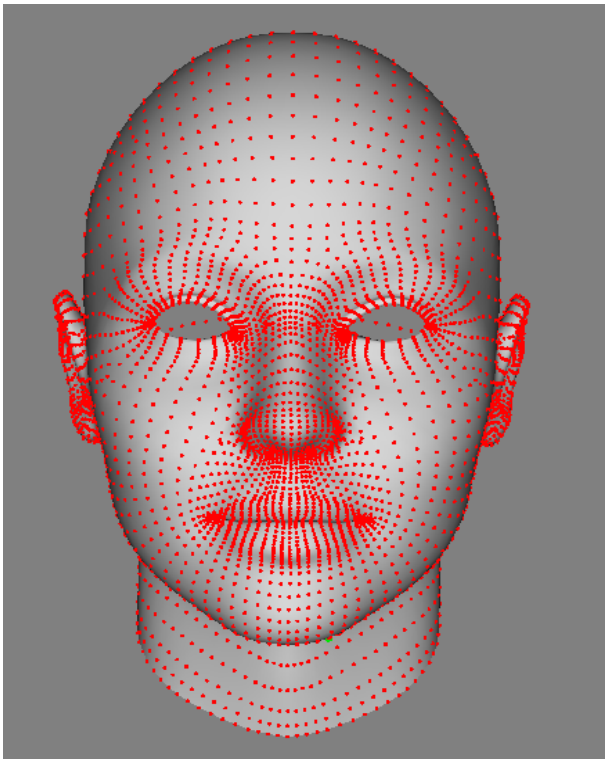

Figure 6.1: 3D head model.

6.1.1 3D Avatar Model

We created a 3D avatar model with the image of a young man using the software 3D Studio Max. The avatar model specifies the 3D positional coordinates for animation and rendering, normal coordinates for lighting effects as well as texture coordinates for texture mapping. Both lighting and texture enhance the appearance of the avatar. The positional coordinates are connected to form a mesh of triangles that determine the neutral coordinates of the model.

Fig. 6.1 shows the wire frame of the head model. The outlook of the head model can be changed easily by changing the textures.

6.1.2 Definition of Influence Zone and Deformation Function

Each FAP corresponds to a set of FP and in turn, each FP corresponds to an influence zone of non-FP points. We utilize the XfaceEd tool to define influence zones for each FP in the eyes, eyebrows, and mouth regions. For example, FP 8.4 (Right corner of outer lip contour) is directly affected by FAP 54 (Horizontal displacement of right outer lip corner) and FAP 60 (Vertical displacement of right outer lip corner). FP 8.4 is shown as the yellow cross in Fig. 6.2(a) and its influence zone is shown in terms of big blue dots. Similarly, FP4.1 (left inner eyebrow) is related to FAP31 (raise left inner eyebrow) and FAP37 (squeeze left inner eyebrow). FP4.1 is shown as the yellow cross in Fig. 6.2(b) and its influence zone as the group of big blue dots.

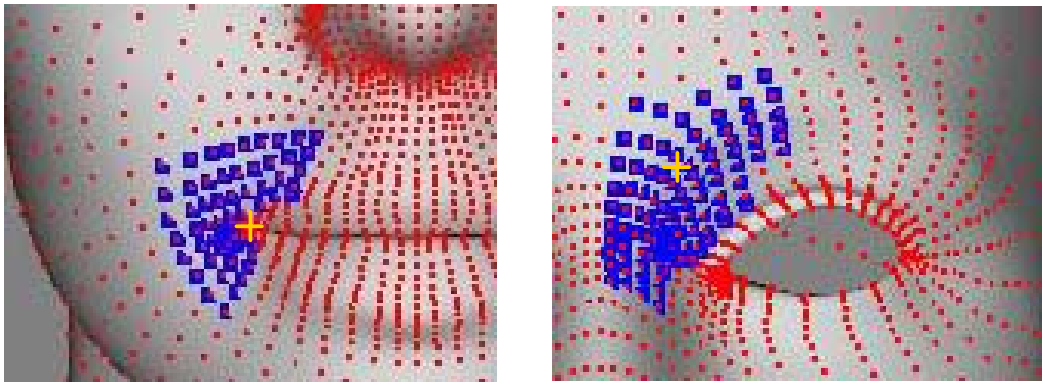

(a) Influence zone of FP 8.4.

(b) Influence zone of FP 4.1.

Figure 6.2: Influence zone of FP 8.4 (left point of lip) and FP4.1 (left inner eyebrow).

6.2 3D Facial Expression Animation

6.2.1 Facial Motion Clone Method

To automatically copy a whole set of morph targets from a real face to face model, we develop a methodology for facial motion clone. The inputs includes two face, one is in neutral position and the other is in a position containing some motions that we want to copy, e.g. in a laughing expression. The target face model exists only at the neutral state. The goal is to obtain the target face model with the motion copied from the source face–the animated target face model. Fig. 6.3 shows the synthesized smile facial expression obtained using an MPEG-4 compliant avatar and FAPs.

The facial expression of the 3D virtual model is changed according to the input signal, which indicates the emotion to be carried out in the current frame. There are two alternative methods to animate the facial expressions:

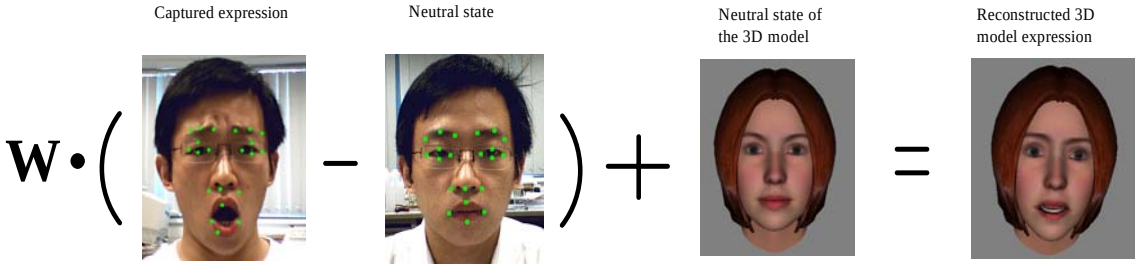

Figure 6.3: The facial motion clone method illustration.

Using the recognition results Using a series of techniques described before, after the face detection, feature points location, feature points tracking and motion energy pattern identification, the tester's facial expression can be recognized. The recognition result is transferred to the 3D virtual model module. The morphable model can act according to the recognition result. Using the predefined the facial expression sequence, the model will act naturally as the tester's facial expression.

Using the feature points' movement This method relies much on the real-time video tracking result. After the initiation section is done, the feature points are tracked by Lucas-Kanade optical flow method. The displacements and velocities of the MPEG-4 compatible feature points are recorded and transmitted to the 3D virtual model module frame by frame. The corresponding points in the victual model will move accordingly. Therefore, the facial expressions are animated vividly. To make more comedic and exaggerated facial expressions, different weights can be added to the facial features. Once a facial expression occur, the displacements and velocity will multiply different weights which can give more comprehensive diversiform virtual expressions.

Chapter 7

System and Experiments

In this section we present the results of simulation using the proposed static person dependent and dynamic person independent facial expression recognition methods. In our system, resolution of the acquired images is 320×240 pixels. Any captured images that are in other formats are converted first before further processing. Our system is developed under Microsoft Visual Studio .NET 2003 using VC++. The Intel's Open Source Computer Vision Library (OpenCV) is employed in our system [73]. The OpenCV Library is developed mainly aimed at real-time computer vision. It provides a wide variety of tools for image interpretation. The system is executed on a PC with Pentium IV 2.8G CPU and 512M RAM running Microsoft XP. Our experiments are carried out under the following assumptions:

- There is only one face contained in one image. The face takes up a significant area in the image.
- The image resolution should be sufficiently large to facilitate feature extraction and tracking.
- The user's face is stationary during the time when the initialization or re-initialization takes place.

Table 7.1: Conditions under which our system can operate

Conditions	Tolerance
Illumination	Lighting from above and front
Scale	± 30% from optimal scale
Roll	Head ± 10^o from vertical
Yaw	Head ± 30^o from view around horizontal plane
Tilt	Head ± 10^o from frontal view around vertical plane

- While tracking, the user should avoid fast global movement. Sudden, jerky face movements should also be avoided. There should be not an excessive amount of rigid motion of the face.

The face tracking method does not require that the hand gesture must be centered in the image. It is able to detect frontal views of human faces under a range of lighting conditions. It can also handle limited changes in scale, yaw, roll and tilt. Table 7.1 summaries the conditions under which face tracker operates.

7.1 System Description

Fig. 7.1 shows the interface of our tracking system. It contains seven modules: The menu of the system, the camera function module, the face detection module, the facial features' extraction module, 3D animation module, initiation neutral facial image display module and real-time video display module.

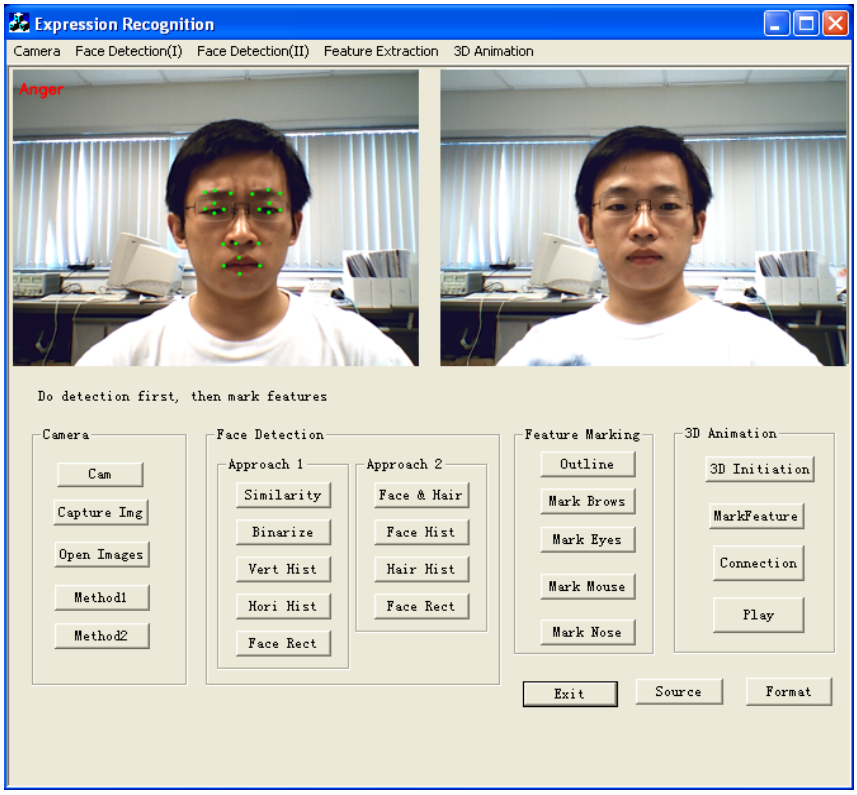

Figure 7.1: The interface of the our system.

The top right image is the captured image at the neutral state for initialization. Face detection and facial features extraction are carried out based on this image. After the features are detected, they are mapped to the real-time video on the left. One can either do this step by step to see the step result, or just click the button [$Method1$](Histogram method) or the button [$Method2$](Hair and face skin method) to realize entire functions at one time. The top right image is the real-time video display. The facial features are marked with green dots which can follow the features' movements based on L-K optical flow method. The recognition results of facial expression is displayed on the top right corner of the video window in red.

The 3D virtual head model interface is illustrated in Fig. 7.2. This animation

window will be opened when the "3D Initiation" button in the main interface is clicked. When the "Connection" button is pressed, a connection is set up using server-client architecture between two applications. The virtual model will change her expression according to the input signal–either using the real-time recognition results of the captured video or using the feature points' movement(FAP stream) frame by frame.

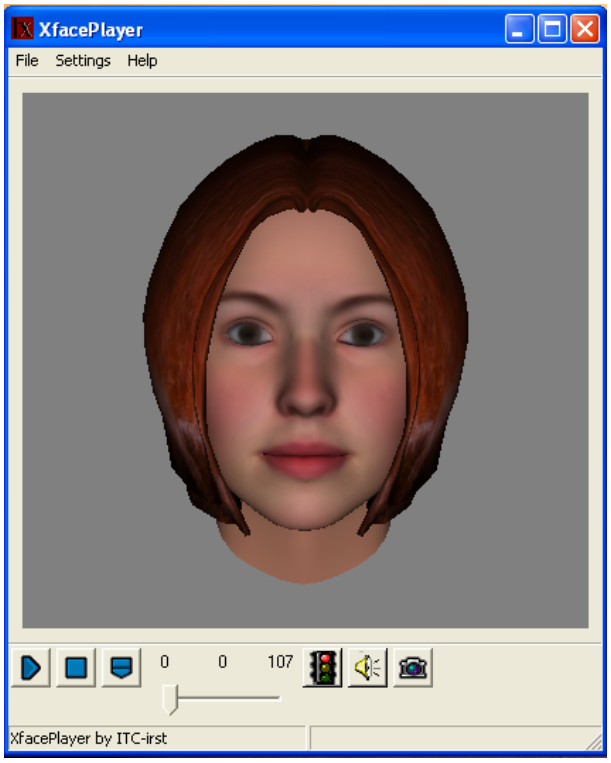

Figure 7.2: The 3D head model interface for expression animation.

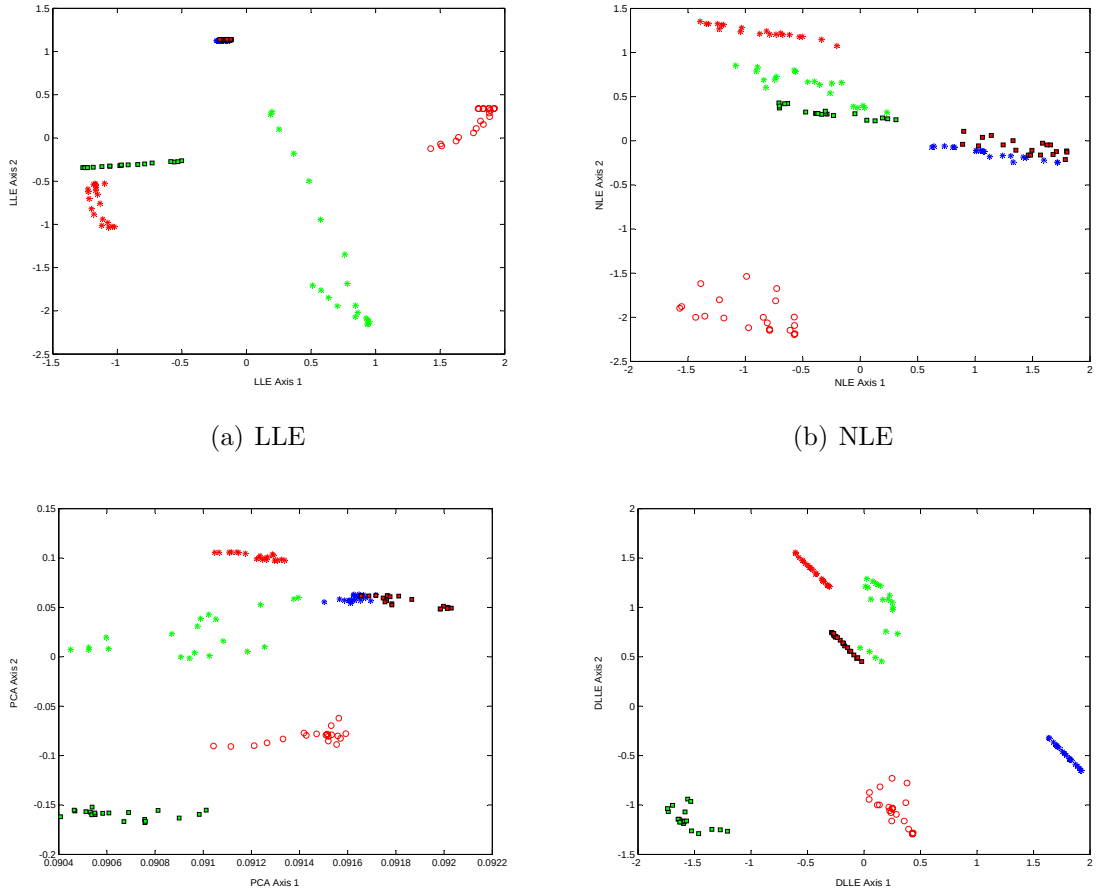

(a) LLE (b) NLE

(c) PCA (d) DLLE

Figure 7.3: 2D projection using different NDR methods.

7.2 Person Dependent Recognition Results

7.2.1 Embedding Discovery

In Fig. 7.3, we compare the properties of the LLE, NLE, PCA and DLLE after the sample images are mapped to 2D dimension using the feedtum database [74]. Six different expressions are represented by: anger, blue star; disgust, red star; fear, green star; happiness, green square; sadness, black square; surprise, red circle. The

projected low dimension data should keep the separating features of the original images. Images of the same expression should cluster together while different should be apart. There are 120 samples of one person from six expressions respectively (20 samples per expression). These samples are manually selected after the automatic selection described in chapter 3. We can see from Fig. 7.3(d) that for $d = 2$, different expressions' embedding of LLE are separated. However, the red and blue points are overlapped and not separatable in 2D dimension. Fig. 7.3(b) shows the embedding of NLE. It can be seen that in general they are separated, but the boundary between different groups are not clear. PCA achieves similar result as NLE which is shown in Fig. 7.3(c). The samples of the same expression are not so centralized and the red and blue star samples are mixed up. As illustrated in Fig. 7.3(d), we can see that DLLE can separate the six expressions well. Samples of the same expression cluster together while different expression samples are clearly separated.

Fig. 7.4 shows 3D embeddings obtained by LLE, NLE, PCA and DLLE. As illustrated in the four images, DLLE can give a better separated embedding compared to other methods-same expressions are more centralized while different expressions separated apart. Different expressions can be easily separated by linear separator. As illustrated in Fig. 7.4(a) and Fig. 7.4(c), LLE and PCA both have some overlaps.

The reason is that LLE is an unsupervised learning algorithm. It selects the nearest neighbors to reconstruct the manifold in the low dimensional space. There are two types of variations in the data set: the different kinds of facial expressions and the varying intensity for every kind of facial expression. Generally, LLE can catch the second type of variation-an image sequence is mapped in a "line", and LLE can keep the sequences with different expressions distinctive when there is

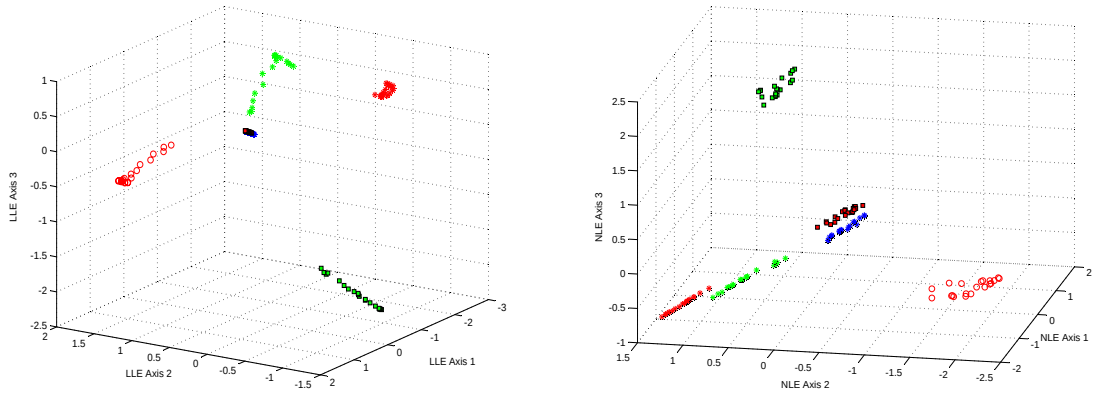

(a) LLE

(b) NLE

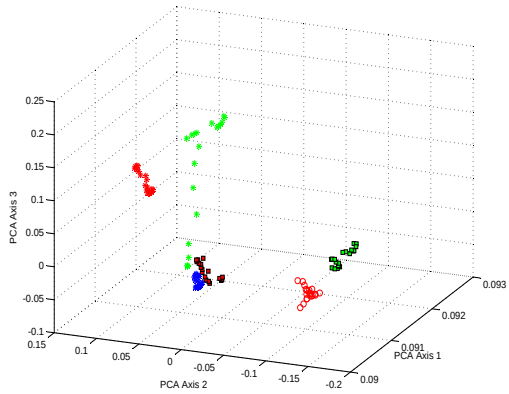

(c) PCA

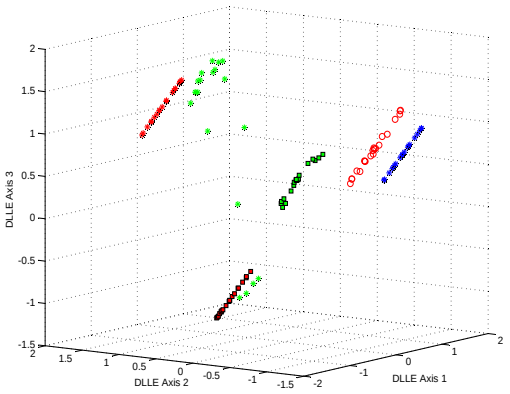

(d) DLLE

Figure 7.4: 3D projection using different NDR methods.

only one sequence for each expression. When the data set contains many image sequences for the same kind of expression, it is very hard to catch the first kind of variation using a small number of nearest neighbors. But with the increased number of nearest neighbors, the images of different expressions are more prone to be mixed up.

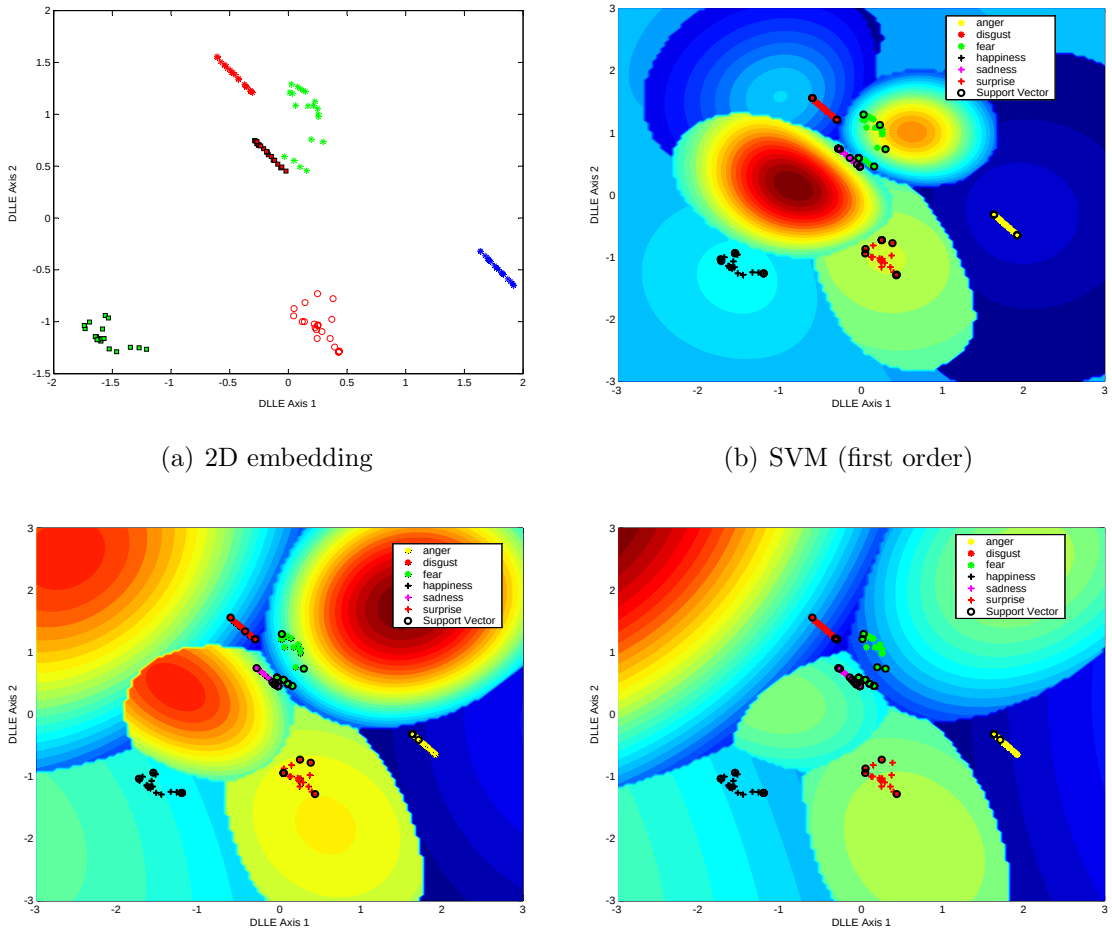

(a) 2D embedding

(b) SVM (first order)

(c) SVM (third order)

(d) SVM (fifth order)

Figure 7.5: The SVM classification results according to the 2D embedding

7.2.2 SVM classification

Fig. 7.5 demonstrates the classification algorithms on the 2D embedding of the original data. The original data set are of 320×240 dimension, and the goal is to classify the class of these expression images. To visualize the problem we restrict ourselves to the two features(2D embedding) that contain the most information about the class. The distribution of the data is illustrated in Fig. 7.5(a).

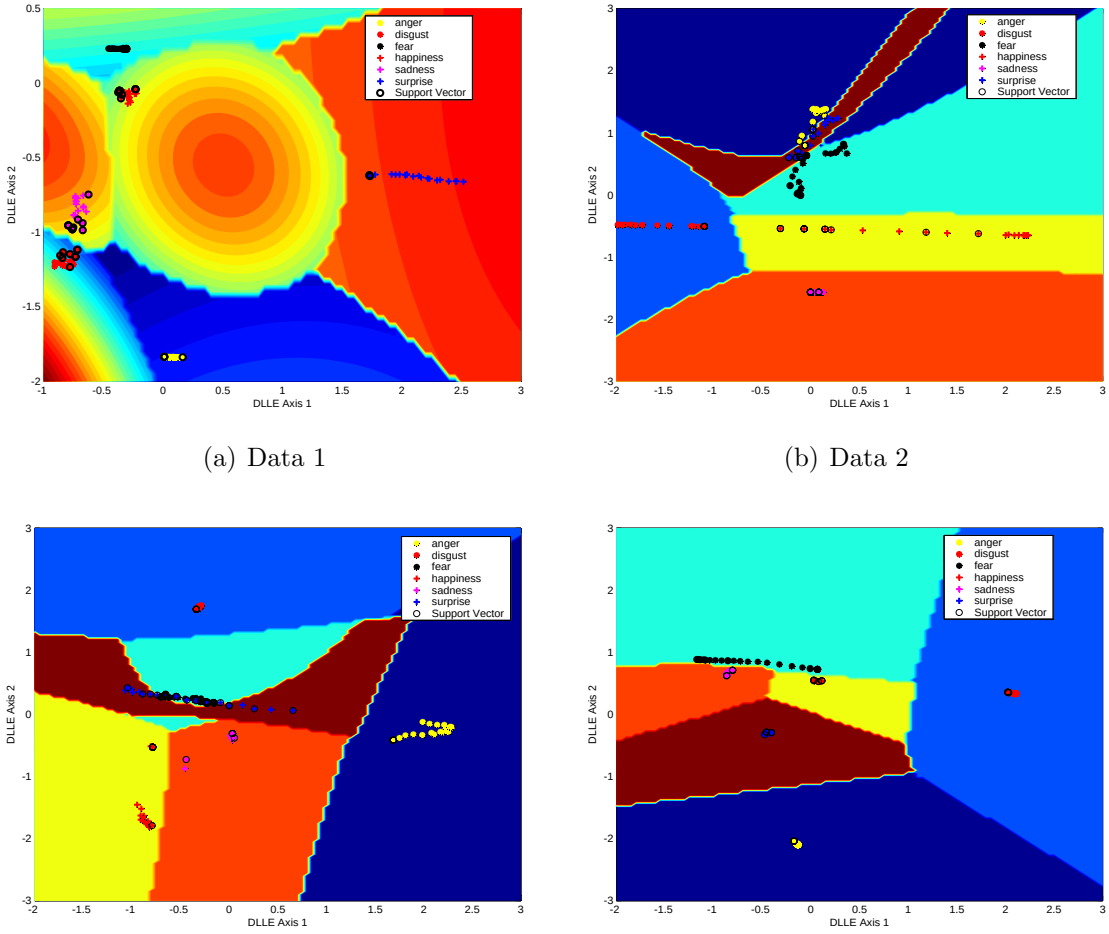

(a) Data 1

(b) Data 2

(c) Data 3

(d) Data 4

Figure 7.6: The SVM classification results according to the 2D embedding of Fig. 7.3(d)

The kernel was chosen to be the polynomial. The polynomial mapping is a popular method for non-linear modeling. The penalty parameter is set 1000 (C=1000). Fig. 7.5(b), Fig. 7.5(c) and Fig. 7.5(d) illustrate the SVC solution obtained using a degree 1, degree 3 and degree 5 polynomial for the classification. The circled points are the support vectors for each classes. It is clear that SVM can correctly classify the embedding of sample data sets.

Table 7.2: Recognition results using DLLE and SVM(1V1) for training data

Emotion	Happiness	Sadness	Fear	Disgust	Surprise	Anger	Rate
Happiness	80	0	0	0	0	0	100%
Sadness	0	80	0	0	0	0	100%
Fear	0	0	80	0	0	0	100%
Disgust	0	0	0	80	0	0	100%
Surprise	0	0	6	0	73	1	91.25%
Anger	0	0	0	0	1	79	98.75%

Table 7.3: Recognition results using DLLE and SVM(1V1) for testing data

Emotion	Happiness	Sadness	Fear	Disgust	Surprise	Anger	Rate
Happiness	18	2	0	0	0	0	90%
Sadness	0	20	0	0	0	0	100%
Fear	0	0	19	0	1	0	95%
Disgust	0	0	0	20	0	0	100%
Surprise	0	0	0	0	20	0	100%
Anger	0	0	0	0	1	19	95%

Fig. 7.6 illustrates the classification results using the same parameters for different data samples. We can see that the solutions are with good expected generalization. Fig. 7.6(b) and Fig. 7.6(b) show the non-separable nature between some expression groups. Using the selected parameters, the SVM can generate proper classification results.

Tables 7.2 and 7.3 show the recognition results using DLLE and SVM(one against one algorithm) for the training and testing data. The database contains 480 images

of 6 different type of expressions for training. These samples are used for training the SVM. Apart from the training samples, there are another 120 samples of 6 expressions are employed to be tested.

The average recognition accuracy is over 95%. In Table 7.2, we can also see that some "Surprise" expressions are misclassified as "Fear". It is natural to understand that both emotions contain astonished reaction to the unexpected outside events. The rest of the expressions are correctly classified.

7.3 Person Independent Recognition Results

Initially, a front view image of the tester's neutral face is captured. This image is processed to detect the tester's face region, extract the eyebrows, eyes, nose and mouth features according to the methods described in chapter 2. In fact, this process is done in a flash. Our system is able to complete the process by just clicking a button on the interface. The features locations are then mapped to the real-time video according to the video's resolution. Once the initialization is completed, the tester can express his emotion freely. The feature points can be predicted and tracked frame by frame using Lucas-Kanade optical flow method. The displacement and velocity of each feature points are recorded at each frame. By analyzing the dynamic movement pattern of feature points, the expression potential energy and kinetic energy are computed out in real-time. Once an expression occur, the detection system will make a judgement using the method described in Chapter 4. The recognition result will be displayed at up-right corner of the video window. When one expression is over, the tester can express his following emotions or re-initialize the system if any tracker is lost.

In [22], the author use the average of two people making an expression as the motion-energy template images to conduct recognition test. This is static and hard to represent the general case. In our system, we adopt a dynamic process which takes every input expression into the average template after the test is conducted. The first initiation is composed by an average of two people making the same expression. Subsequently, each input image is taken into account and the template is composed by averaging these input images of the same expression.

Fig. 7.7 shows the expression recognition results under different environments. It can be seen from these figures that the system can robustly recognize the human's expression regardless the background.

The results of real-time person independent expression recognition are given in Fig. 7.8. Our system can reach 30 FPS(frame per second). The pictures are captured while the expression occurs. The recognition results are displayed in real-time in red at the up-left corner of the window. From these pictures, we can see that our proposed system can effectively detect the facial expressions.

(a) happiness

(b) sadness

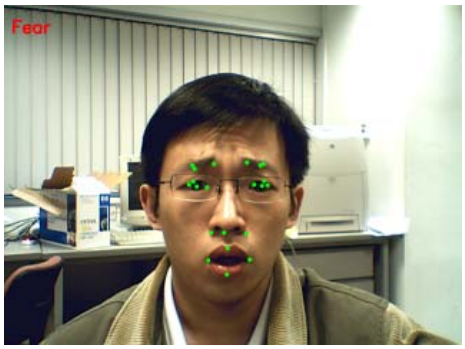

(c) fear

(d) disgust

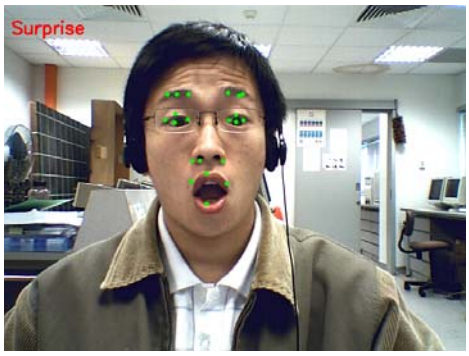

(e) surprise

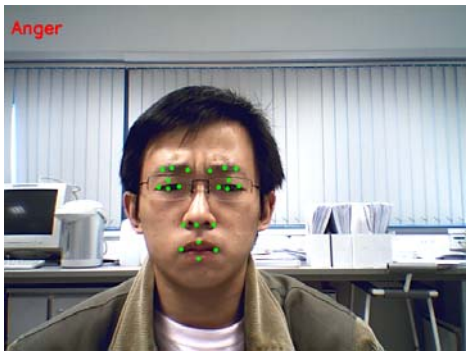

(f) anger

Figure 7.7: Real-time video tracking results in different environment.

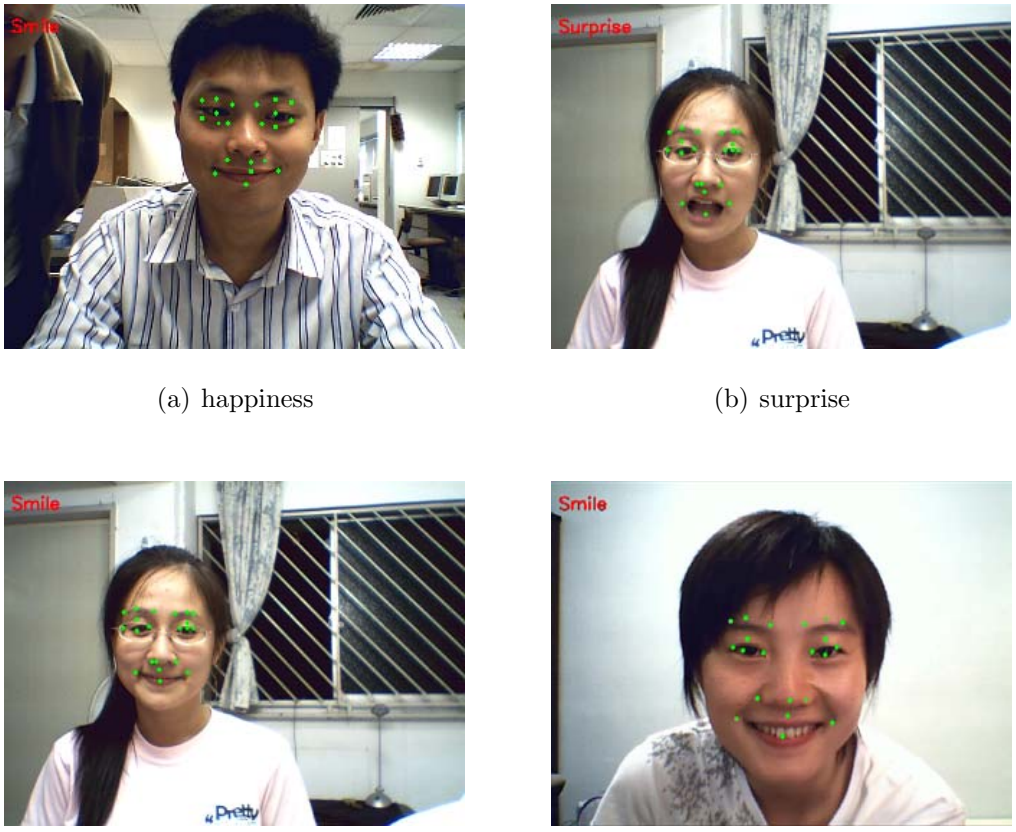

(a) happiness (b) surprise

(c) happiness (d) happiness

Figure 7.8: Real-time video tracking results for other testers.

Chapter 8

Conclusion

8.1 Summary

This thesis attempts to recognize the six emotions universally associated with unique facial expressions. Vision based capturing of expression has been a challenging problem due to the high degree of freedom of facial motions. In our work, two methods for person-dependent and person-independent recognition are presented. Our methods can successfully recognize the static, off-line captured facial expression images, track and identify dynamic on-line facial expressions of real-time video from one web camera. The face area is automatically detected and located by making using of face detection and skin hair color information. Our system utilizes a subset of Feature Points (FPs) for describing the facial expressions which is supported by the MPEG-4 standard. 21 facial features are extracted from the captured video and tracked by optical flow algorithm.

In this thesis, an unsupervised learning algorithm, DLLE, has been developed to discover the intrinsic structure of the data. These discovered properties are used to compute their corresponding low-dimensional embedding. It is conducted

by estimating the probability density function from the input data and using an exponential neighbor finding method to automatically obtain the embedding. Associated with SVM, a high recognition accuracy algorithm has been developed for static facial expression recognition. We also give out the test results by DLLE, NLE and LLE embedding from where we can see that our method is better in separating the high-dimensional data in low-dimensional space.

We also incorporate facial expression motion energy to describe the facial muscle's tension during the expressions for person-independent tracking. It is composed by the expression potential energy and kinetic energy. The potential energy is used as the description of the facial muscle's tension during the expression. Kinetic energy is the energy which a feature point possesses as a result of facial motion. For each facial expression pattern, the energy pattern is unique and it is utilized for the further classification. Combined with the rule based method, the recognition accuracy can be improved for real-time person-independent facial expression recognition.

A 3D realistic interactive expression model is integrated into our face recognition and tracking system which can derive multiple virtual character expressions according to the input expression in real-time.

8.2 Future Research

There are a number of directions which could be done for future work.

- One limitation of the current system is that it can detects only one front view face looking at the camera. Multiple face detection and feature extraction could be further improved. Since the current system can deal with some

degree of lighting and orientation variation, the resolution of the image would be the main problem to concur for multi-person expression analysis.

- One direction to advance our current work is to combine the human speech and make both virtual and real robotic talking head for human emotion understanding and intelligent human computer interface, and explore virtual human companion for learning and information seeking.

Bibliography

[1] C. Darwin, *The Expression of the Emotions in Man and Animals*. London: John Murray, Albemarle Street, 1872.

[2] C. Kotropoulos and I. Pitas, "Rule-based face detection in frontal views," in *Proc. of IEEE Int. Conf. on Acoustics, Speech and Signal Processing (ICASSP 97)*, vol. IV, pp. 2537–2540, April 1997.

[3] G. Yang and T. S. Huang, "Human face detection in a complex background," *Pattern Recognition*, vol. 27, pp. 53–63, 1994.

[4] M. Pantic and L. J. M. Rothkrantz, "An expert system for recognition of facial actions and their intensity," *Image and Vision Computing*, vol. 18, pp. 881–905, 2000.

[5] S. A. Sirohey, "Human face segmentation and identification," Tech. Rep. CS-TR-3176, 1993.

[6] H. Graf, T. Chen, E. Petajan, and E. Cosatto, "Locating faces and facial parts," in *Int. Workshop on Automatic Face and Gesture Recognition*, pp. 41–46, 1995.

[7] K. Sobottka and I. Pitas, "Face localization and facial feature extraction based on shape and color information," in *Proc. of IEEE Int. Conf. on Image Processing*, pp. 483–486, 1996.

[8] C. T. T. Cootes, D. Cooper and J. Graham, "Active shape models-their training and application," *Computer Vision and Image Understanding*, vol. 61, pp. 38–59, 1995.

[9] T. F. Cootes, G. J. Edwards, and C. J. Taylor, "Active appearance models," in *European Conf. on Computer Vision (ECCV)*, vol. 2, 1998.

[10] M. Turk and A. Pentland, "Eigenfaces for recognition," *Journal of Cognitive Neuroscience*, vol. 3, no. 1, p. 71C86, 1991.

[11] F. Fogelman Soulie, E. Viennet, and B. Lamy, "Multi-modular neural network architectures: applications in optical character and human face recognition.," *IEEE Trans. on Pattern Analysis and Machine Intelligence*, vol. 7, p. 721, 1993.

[12] P. Michel and R. E. Kaliouby, "Real time facial expression recognition in video using support vector machines," in *5th Int. Conf. on Multimodal interfaces table of contents*, vol. 3, pp. 258 – 264, 2003.

[13] S. Y. Kang, K. H. Young, and R.-H. Park, "Hybrid approaches to frontal view face recognition using the hidden markov model and neural network.," *Pattern Recognition*, vol. 31, pp. 283–293, Mar. 1998.

[14] M. J. Lyons, S. Akamatsu, M. Kamachi, and J. Gyoba, "Coding facial expressions with gabor wavelets," in *Proc. of the Third IEEE Int. Conf. on Automatic Face and Gesture Recognition*, pp. 200–205, April 1998.

[15] R. Brunelli and T. Poggio, "Face recognition: Features versus templates," *IEEE Trans. on Pattern Analysis and Machine Intelligence*, vol. 15, no. 10, pp. 1042–1052, 1993.

[16] I. Craw, D. Tock, and A. Bennett, "Finding face features," in *European Conf. on Computer Vision (ECCV)*, pp. 92–96, 1992.

[17] K. Waters, "A muscle model for animating three-dimensional facial expression," *Computer Graphics*, vol. 21, July 1987.

[18] K. Scott, D. Kagels, S. Watson, H. Rom, J. Wright, M. Lee, and K. Hussey, "Synthesis of speaker facial movement to match selected speech sequences," in *In Proc. 5th Australian Conf. on Speech Science and Technology*, 1994.

[19] B. Horn and B. Schunck, "Determining optical flow," *Artificial Intelligence*, vol. 17, no. 1-3, pp. 185 – 203, 1981.

[20] M. N. Dailey and G. W. Cottrell, "PCA gabor for expression recognition," Tech. Rep. CS1999-0629, 26, 1999.

[21] M. Bartlett, *Face Image Analysis by Unsupervised Learning and Redundancy Reduction*. PhD thesis, University of California, San Diego, 1998.

[22] I. A. Essa and A. Pentland, "Facial expression recognition using a dynamic model and motion energy," in *Int. Conf. on Computer Vision (ICCV)*, pp. 360–367, 1995.

[23] P. Ekman and W. Friesen, *Facial Action Coding System: A Technique for the Measurement of Facial Movement*. Palo Alto, California, USA: Consulting Psychologists Press, 1978.

[24] *ISO/IEC IS 14496-2 Visual: A compression codec for visual data*. 1999.

[25] A. Young and H. E. Ellis, *Handbook of Research on Face Processing*. North-Holland,Amsterdam: Elsevier Science Publishers B.V., 1989.

[26] C. Padgett and G. Cottrell, *Representing face images for classifying emotions*, vol. 9. Cambridge, MA: MIT Press, 1997.

[27] C. Padgett, G. Cottrell, and B. Adolps, "Categorical perception in facial emotion classification," in *Proc. Cognitive Science Conf.*, vol. 18, pp. 249–253, 1996.

[28] Y. Yacoob and L. Davis, "Recognizing human facial expressions from long image sequences using optical flow," *IEEE Trans. on Pattern Analysis and Machine Intelligence*, vol. 18, pp. 636–642, June 1996.

[29] T. Otsuka and J. Ohya, "Recognition of facial expressions using HMM with continuous output probabilities," in *Proc. 5th IEEE Int. Workshop on Robot and Human Communication RO-MAN*, pp. 323–328, 1996.

[30] Y.-L. Tian, T. Kanade, and J. Cohn, "Recognizing action units for facial expression analysis," *IEEE Trans. on Pattern Analysis and Machine Intelligence*, vol. 23, pp. 97 – 115, February 2001.

[31] M. Pantic and J. Rothkrantz, "Facial action recognition for facial expression analysis from static face images," *IEEE Trans. on Systems, Man and Cybernetics-Part B*, vol. 34, June 2004.

[32] C. E. Izard, "Facial expressions and the regulation of emotions," *Journal of Personality and Social Psychology*, vol. 58, no. 3, pp. 487–498, 1990.

[33] I. Essa and A. Pentland, "Coding, analysis, interpretation, and recognition of facial expressions," *IEEE Trans. on Pattern Analysis and Machine Intelligence*, vol. 19, no. 7, 1997.

[34] P. Roivainen, H. Li, and R. Forcheimer, "3-D motion estimation in model-based facial image coding," *IEEE Trans. on Pattern Analysis and Machine Intelligence*, vol. 15, pp. 545–555, 1993.

[35] G. Donato, M. S. Bartlett, J. C. Hager, P. Ekman, and T. J. Sejnowski, "Classifying facial actions," *IEEE Trans. on Pattern Analysis and Machine Intelligence*, vol. 21, no. 10, pp. 974–989, 1999.

[36] K. Mase, "Recognition of facial expression from optical flow," *Institute of electronics information and communication engineers Trans.*, vol. E74, pp. 3474–3483, 1991.

[37] B. Lucas and T. Kanade, "An iterative image registration technique with an application to stereo vision," in *Proc. of the 7th Int. Joint Conf. on Artificial Intelligence (IJCAI '81)*, pp. 674–679, April 1981.

[38] J. Lien, *Automatic recognition of facial expression using hidden Markov models and estimation of expression intensity.* PhD thesis, The Robotics Institute, CMU, April 1998.

[39] X. Zhou, X. S. Huang, and Y. S. Wang, "Real-time facial expression recognition in the interactive game based on embedded hidden markov model," in *Proc. of the Int. Conf. on Computer Graphics, Imaging and Visualization*, pp. 144–148, 2004.

[40] P. Ekman and R. J. Davidson, *The Nature of Emotion Fundamental Questions*. New York: Oxford Univ. Press, 1994.

[41] M. H. Yang, D. Kriegman, and N. Ahuja, "Detecting faces in images: A survey," *IEEE Trans. on Pattern Analysis and Machine Intelligence*, vol. 24, pp. 34–58, Jan. 2002.

[42] D. A. Forsyth and J. Ponce, *Computer Vision: A Modern Approach*. Upper Saddle River, New Jersey: Prentice Hall, 2002.

[43] M. Pantic and L. J. M. Rothkrantz, "Automatic analysis of facial expressions: The state of the art," *IEEE Trans. on Pattern Analysis and Machine Intelligence*, vol. 22, no. 12, pp. 1424–1445, 2000.

[44] S. McKenna, S. Gong, and Y. Raja, "Modelling facial colour and identity with gaussian mixtures," *Parttern Recognition*, vol. 31, pp. 1883–1892, December 1998.

[45] J. Yang, W. Lu, and A. Waibel, "Skin-color modeling and adaptation," in *Proc. of Asian Conference on Computer Vision*, pp. 687–694, 1998.

[46] J. Yang and A. Waibel, "A real-time face tracker," in *Proc. of the third IEEE Workshop on Applications of Computer Vision*, 1996.

[47] M. Jones and J. Rehg, "Statistical color models with application to skin detection," *International Journal of Computer Vision*, vol. 46, pp. 81–96, January 2002.

[48] C. Harris and M. Stephens, "A combined edge and corner detector," in *Proc. of the 4th Alvey Vision Conference*, pp. 147–151, 1988.

[49] D. Williams and M. Shah, "Edge characterization using normalized edge detector," *Computer Vision, Graphics and Image Processing*, vol. 55, pp. 311–318, July 1993.

[50] K. Hotta, "A robust face detection under partial occlusion," in *Proc. of Int. Conf. on Image Processing*, pp. 597–600, 2004.

[51] N. Tsapatsoulis, A. Raouzaiou, S. Kollias, R. Cowie, and E. Douglas-Cowie, *MPEG-4 Facial Animation*, ch. Emotion Recognition and Synthesis based on MPEG-4 FAPs. John Wiley & Sons, 2002.

[52] J. Bassili, "Emotion recognition: The role of facial movement and the relative importance of upper and lower areas of the face," *Journal of Personality Social Psychology*, vol. 37, pp. 2049–2059, 1979.

[53] J. Wang, Z. Changshui, and K. Zhongbao, "An analytical mapping for LLE and its application in multi-pose face synthesis," in *14th British Machine Vision Conference*, September.

[54] M. Bartlett and T. Sejnowski, "Independent components of face images: A representation for face recognition," in *Proc. of the 4th Annual Joint Symposium on Neural Computation*, 1997.

[55] I. Borg and P. Groenen, *Modern multidimensional scaling*. Springer-Verlag, 1997.

[56] P. N. Belhumeur, J. Hespanha, and D. J. Kriegman, "Eigenfaces vs. fisherfaces: Recognition using class specific linear projection," *IEEE Trans. on Pattern Analysis and Machine Intelligence*, vol. 19, no. 7, pp. 711–720, 1997.

[57] J. B. Tenenbaum, V. de Silva, and J. C. Langford, "A global geometric framework for nonlinear dimensionality reduction," *Science*, vol. 290, pp. 2319–2323, December, 2000.

[58] S. T. Roweis and L. K. Saul, "Nonlinear dimensionality reduction by locally linear embedding," *Science*, vol. 290, pp. 2323–2326, December, 2000.

[59] S. S. Ge, Y. Yang, and T. H. Lee, "Hand gesture recognition and tracking based on distributed locally linear embedding," in *Proc. of 2nd IEEE International Conference on Robotics, Automation and Mechatronics*, (Bangkok, Thailand), pp. 567–572, June 2006.

[60] S. S. Ge, F. Guan, A. P. Loh, and C. H. Fua, "Feature representation based on intrinsic discovery in high dimensional space," in *Proc. 2006 IEEE International Conference on Robotics and Automation*, pp. 3399–3404, May 2006.

[61] L. K. Saul and S. Roweis, "Think globally, fit locally: Unsupervised learning of low dimensional manifolds," *Journal of Machine Learning Research*, vol. 4, pp. 119–155, June, 2003.

[62] K. Matsuno and S. Tsuji, "Recognizing human facial expressions in a potential field," in *Proc. of Int. Conf. of Pattern Recognition*, pp. B:44–49, 1994.

[63] L. P. Nedel and D. Thalmann, "Real time muscle deformations using mass-spring systems," in *Proc. of the Computer Graphics International*, pp. 156–165, 1998.

[64] K. Kahler, J. Haber, and H. Seidel, "Geometry-based muscle modeling for facial animation," in *Proc. of Graphics Interface*, 2001.

[65] D. Terzopoulos and K. Waters, "Analysis and synthesis of facial image sequences using physical and anatomical models," *IEEE Trans. on Pattern Analysis and Machine Intelligence*, vol. 15, no. 6, pp. 569–579, 1993.

[66] K. Waters and J. Frisbie., "A coordinated muscle model for speech animation," in *Proc. of Graphics Interface*, pp. 163–170, 1995.

[67] G. Feng, P. Yuen, and J. Lai, "Virtual view face image synthesis using 3d spring-based face model from a single image," in *Automatic Face and Gesture Recognition, 2000. Proc. Fourth IEEE Int. Conf. on*, pp. 530–535, 2000.

[68] V. Vapnik, *The Nature of Statistical Learning Theory*. New York: Springer, 1995.

[69] C. J. C. Burges, "A tutorial on support vector machines for pattern recognition," *Data Mining and Knowledge Discovery*, vol. 2, no. 2, pp. 121–167, 1998.

[70] Y. Zhang and Q. Ji, "Active and dynamic information fusion for facial expression understanding from image sequences," *IEEE Trans. on Pattern Analysis and Machine Intelligence*, vol. 27, pp. 699–714, 2005.

[71] R. A. Clark, K. Richmond, and S. King, "Festival 2 – build your own general purpose unit selection speech synthesiser," in *Proc. 5th ISCA workshop on speech synthesis*, 2004.

[72] K. Balci, "Xface: MPEG-4 based open source toolkit for 3d facial animation," in *Proc. Advance Visual Interfaces*, pp. 399–402, 2004.

[73] Intel Corporation, *OpenCV Reference Manual*, 2001. `http://www.intel.com/technology/computing/opencv/index.htm`.

[74] F. Wallhoff, "Facial expressions and emotion database," http://www.mmk.ei.tum.de/~waf/fgnet/feedtum.html.